Universitetet i Stavanger

Faculty of Science and Technology

MASTER'S THESIS

Study program/Specialization: MSc Petroleum Geosciences Engineering	Spring semester, 2015 Open
Writer: Luis Alberto Rojo Moraleda	…… (Writer's signature)

Faculty supervisor: Dr. Alejandro Escalona, University of Stavanger

External supervisor(s): Lothar Schulte and Sultan Abdullah Sayghe, Schlumberger SIS

Thesis title:

Interpretation, modelling, and halokinetic evolution of salt diapirs in the Nordkapp Basin

Credits (ECTS): 30

Key words: Seismic attributes Halokinesis Salt restoration Nordkapp Basin	Pages: 105 + CD Stavanger,15th June 2015

Interpretation, modelling, and halokinetic evolution of salt diapirs in the Nordkapp Basin

by

Luis Alberto Rojo Moraleda

MSc Thesis

Presented to the Faculty of Science and Technology

University of Stavanger

University of Stavanger

2015

ACKNOWLEDGEMENTS

This master thesis is submitted in completion of the MSc in Petroleum Geosciences Engineering at the University of Stavanger.

I would like to express my gratitude to my thesis supervisors Alejandro Escalona, Lothar Schulte, and Sultan Abdullah Sayghe, for their outstanding guidance through salt tectonics and seismic attributes needed for the completion of this master thesis. In addition, I would like to thank the University of Stavanger for providing the dataset and workstation, and to Schlumberger and Midland Valley for providing Petrel and Move license.

Finally I would like to express my gratitude to my family and friends for their support and advices through this master thesis period.

Interpretation, modelling, and halokinetic evolution of salt diapirs in the Nordkapp Basin

Luis Alberto Rojo [1,*], Alejandro Escalona [2], Lothar Schulte [3], Sultan Abdullah Sayghe [4]

1, 2: Department of Petroleum Technology, University of Stavanger, 4036 Stavanger, Norway
3, 4: Schlumberger SIS, Risabergveien 3, 4068 Stavanger, Norway

ABSTRACT

The Nordkapp Basin provides one of the examples of salt diapirism in the southwestern Barents Sea, becoming an area of interest for hydrocarbon exploration during the last 30 years. Several exploration wells have been drilled close to salt structures, finding hydrocarbons shows but not commercial reservoirs. Consequently, it is of critical importance to get a better understating about salt kinematics, which plays an important role creating structural traps and controlling the distribution of reservoirs around salt structures. In this study, we use 3D seismic data and well data located in the southwestern sub-basin of the Nordkapp Basin. Different mapping attribute workflows are used with the aim of defining salt structures, salt-related structural elements, strata terminations, and halokinetic sequences. Therefore, the main objective is to improve mapping techniques and get a better understanding of salt geometries and movement through time, which can provide insights on basin infill. Preliminary work reveals that the salt was deposited during the Late Carboniferous-Early Permian and was remobilized several times during the Triassic, Late Cretaceous and Cenozoic. Seismic multi-trace attributes like Dip illumination and Variance seem to be very suitable for defining salt bodies. Dip illumination produces and excellent definition of the salt body, and Variance is used to identify locations where the salt flank locations are difficult to define. To identify salt-related structural elements, the attribute Ant tracking is applied on the Chaos volume attribute. The so-called Chaos attribute highlights areas where the seismic shows large variation in the locally estimated dip and azimuth. Ant tracking searches for high energy surfaces (fault planes) provided by attributes such as Variance or Chaos and consequently, is reducing the noise inherited to these volumes attributes. Attributes like Cosine of Phase and frequency filters enhances the continuity of reflectors in areas of uncertainty, and highlights the main strata relationships, being possible to define the periods of salt diapirism and the type of halokinetic sequences. Furthermore, the use of filters and cosine of phase has been crucial in this study to detect the presence of sedimentary wedges. The presence of these wedges indicates a complex salt-controlled sedimentation during the Triassic, ranging from marine to fluvio-deltaic environments of deposition. Uplifted or domed areas caused by diapirism, are interpreted to be the main sources of these wedges, which might act as potential reservoirs within the Nordkapp minibasins.

Contents

1. **Introduction** 1
   1.1 Study area and geological problem 1
   1.2 Objectives and motivation 5
   1.3 Background of seismic attributes used in salt-related basins 5
   .....
   1.4 Background of halokinetic models 7
2. **Geological Setting** 13
   2.1 Introduction 13
   2.2 Evolution 13
      Late Paleozoic 13
      Mesozoic 14
3. **Database and methodology** 17
   3.1 Data Base 17
   19
   3.2 Methodology 20
4. **Multi-trace seismic attributes workflows** 23
   4.1 Seismic conditioning 23
      Structural Smoothing 23
   4.2 Salt structures interpretation workflow 26
      Analysis of Structural Smoothed time slices 26
      Dip Illumination 26
      Variance 27
   4.3 Structural attribute workflow 34
      Analysis of Structural Smoothed time slices 34
      Chaos 34
      Ant-track 35
   4.4 Minibasin stratigraphy workflow 40
      Spectral Decomposition 40
      Cosine of Phase 41
5. **Observations and interpretations based on attribute workflows** 46

5.1 Salt structures 46
5.2 Minibasin stratigraphy 51
Megasequence 1 (MS1): Permian – Lower Early Triassic 51
Megasequence 2 (MS2): Upper Early Triassic – Middle Triassic 54
Megasequence 3 (MS3) – Middle-Late Triassic 60
Megasequence 4 (MS4) – Middle Jurassic - Cretaceous 64
Sequence 10 – Cenozoic 68
6. **Salt modelling, depth conversion, and salt restoration** 70
6.1 Salt modelling 70
6.2 Depth Conversion 72
6.3 Salt restoration 75
7. **Discussion** 80
7.1 The role of seismic attributes in salt-related basins. 80
7.2 Evolution 82
Pre-kinematic Permian – Lower Early Triassic 82
Main diapirism stage (Lower Early Triassic-Middle Triassic) 82
Late Stages of Diapirism (Middle Triassic-Late Triassc) 83
Quiescence period (Middle Jurassic-Late Cretaceous) 83
Reactivation (Cenozoic) 84
7.3 Implications of diapirism in the Triassic paleogeography 86
8. **Conclusions** 91
9. **References** 93

List of figures

Figure 1 .Location of the Nordkapp Basin in the southwestern Barents Sea. The presence of hydrocarbons within the basin is proved by the wells 7227/11-1 and 7228/7-1. 2
Figure 2. (A) Areas of uncertainty adjacent to salt structures in the Nordkapp Basin. (B) Drilling problems in the Gulf of Mexico due to the poor visualization of the trap geometry in areas of uncertainty represented by dashed lines (modified after (Swanston et al., 2011). The upper figure represents the pre-drilling interpretation and the lower figure the post drilling interpretation 3
Figure 3. Triassic paleogeography described by Glørstad-Clark et al. (2010). (A) Early Triassic shows continental environments of deposition without any influence of salt tectonics. (B) Middle Triassic has not been influenced by salt tectonics and shows continuous continental environments of deposition. 4
Figure 4. (A) Time slide of the salt structure. (B) Seismic textures identified around salt diapirs. (C) Seismic attributes as coherence improves the interpretation of the salt diapir (Berthelot et al., 2013). 5
Figure 5. (A) Spectral decomposition highlighting areas with broken reflectors defined as salt. (B) Chaos attribute results. Pink arrows indicate areas with salt (Ferguson et a.,2010). 6
Figure 6. (A) Structural oriented semblance highlights structural elements. (B) Attributes as Bedform enhance the continuity of reflectors in minibasins and improve the resolution of strata terminations such as downlap, onlap, and truncations (Ferguson et al., 2010). 7
Figure 7. (A) Salt structures classification (Fossen, 2010). (B) Dip of salt-sediment interface based on the relationship between sedimentation rate and salt growth rate (McGuinness and Hossack, 1993). (C) Evolution of salt diapirs and halokinetic sequences as a function of net sedimentation rate vs salt-supply rate (Giles and Lawton, 2002) 8
Figure 8. (A) Active diapirism followed by passive diapirism (Trusheim, 1960). (B) Reactive diapirism followed by passive diapirism (Fossen, 2010). (C) Contractional diapirism (Hudec and Jackson, 2007; Fossen, 2010). 10
Figure 9. (A) Generation of Tabular composited halokinetic sequences (CHS). (B) Generation of Tapered composite halokinetic sequences (CHS) (Giles and Rowan, 2012). 12
Figure 10. Structural elements of the southwestern Barents Sea with main focus on the Nordkapp Basin (modified after Nilsen et al.,1995 and Henriksen et al.,2011). 15
Figure 11. (Left) Regional seismic line through the Nordkapp Basin. (Right) Main tectonic events and environments of deposition of the Nordkapp Basin (modified after Henriksen et al.,2011). 16
Figure 12. (A) Dataset location. (B) Examples of seismic artifacts encountered in the seismic survey 18
Figure 13. (A) Seismic well tie correlation. (B)Well logs and synthetic seismogram correlation for the well 7228-7/1A. Arrows indicate good quality reservoirs located within the Jurassic and Triassic. Generally Jurassic reservoirs are water-wet. On the other hand, Triassic reservoirs contain hydrocarbons without economic values (NPD, 2003). 19
Figure 14. Methodology scheme 22
Figure 15. (A). Seismic noise associated with poor amplitude connection between traces due to sampling problems. (B). The attribute Structural Smoothing produces an aggressive noise cancellation and improves the continuity of the seismic events 24
Figure 16. (A) Plain Structural Smoothing does not improve the continuity of dipping reflectors, therefore, areas close to salt diapirs will remain noisy. (B) Dip-Guided Structural Smoothing provides better results enhancing the continuity of dipping reflections in areas close to salt flanks. 25

Figure 17. (A) Dip-Guided Structural Smoothing time slice analysis and seismic textures based on different seismic responses. (B) Interpretation based on seismic textures. Blue colours indicate areas of uncertainty (2km approx.) where the salt-sediment interface is not clear. 29
Figure 18. (A) Dip-Illumination time slice analysis and seismic textures. (B) Interpretation based on seismic textures. Blue colours indicate areas of uncertainty (between 1,5 and 1km) where the salt-sediment interface is not clear..... 30
Figure 19. (A) Directional filter of -45 from the cross line direction. (B) -90 degrees directional filter seems to be the more suitable, reducing the areas of uncertainty down to 200m. (C). Directional filter of -135 degrees. (D) Directional filter of -150 degrees. (E) Directional filter of -180 from the cross line direction 31
Figure 20. Results of Dip-Guided Variance. (A) Time slice analysis with seismic textures. (B) Interpretation based on seismic textures. This attribute is mainly use to refine the interpretation of salt boundaries from the Dip-Illumination cube. However, light blue areas appear poorly solved, being difficult to delineate salt boundaries. 32
Figure 21. Summary salt interpretation workflow 33
Figure 22. (A) Time slice analysis of the Dip-Guided structural smoothing cube. Notice the discontinuous seismic events caused by salt-induced faults. (B) Interpretation highlighting areas with salt (red), highly dipping reflectors (light blue), and areas with similar dip and azimuth (purple)..... 36
Figure 23. (A) Time slice analysis of the Chaos cube. Notice that the definition of radial faults has been improved. (B) Interpretation highlighting areas with salt (red), highly dipping reflectors (light blue), highly faulted areas (green), and areas with similar dip and azimuth (purple). 37
Figure 24. (A) Time slice analysis of the Ant-track cube. Notice that the definition of radial faults has been improved. (B) Interpretation highlighting areas with salt (red), highly dipping reflectors (light blue), highly faulted areas (green), and areas with similar dip and azimuth (purple) 38
Figure 25. Summary structural workflow 39
Figure 26. Spectral Decomposition. (A) Input seismic (cf=40 Hz). (b) Frequency filter (cf=50 Hz) displays a better resolution of strata terminations and the presence of growth strata. (C) Frequency filter (cf=60 Hz) displays higher resolution at shallower levels. Notice the loss of high frequencies at deeper levels. 43
Figure 27. Seismic facies table based on seismic responses and Gamma-ray information. (Base on Escalona and Mann, 2006)..... 44
Figure 28. (A) Frequency filter (cf=50 hz) displaying areas of low amplitude poorly solved seismic events. (B) Cosine of Phase enhances the continuity of the reflectors in those areas and provides a better resolution of the drape folding. 45
Figure 29. 3D configuration of Permian salt in the data set. Notice how the salt layer changes its geometry towards the NE. Three salt structures have been identified: salt wall, salt roller, and salt stock. 47
Figure 30. (Left) Cross-section of the input seismic through the salt wall. (Right) Cross-section of Cosine of Phase showing the salt wall and minibasin interpretations..... 48
Figure 31. (Left) Cross-section of the input seismic through the salt roller. (Right) Cross-section of Cosine of Phase showing the salt roller and minibasin interpretations..... 49
Figure 32. (A) Cross-section of the input seismic through the salt stock. (B) Cross-section of Cosine of Phase showing the salt stock and minibasin interpretations. 50

Figure 33.Seismic analysis results based on the combination of input seismic and Cosine of Phase. Seismic input provides the main information about seismic facies while Cosine of Phase enhanced the visualization of drape folding and helps the identification of sedimentary wedges. 52
Figure 34. (A) Ant-track results for MS1. (B) Ant-track results for MS2 53
Figure 35. (A) Thickness map of Megasequence 2 (MS2). (B) Thickness map of Megasequence 3 (MS3). 57
Figure 36. Vertical depocenter migration during the Triassic period. 58
Figure 37. (A) Thickness map of sedimentary wedge 1. (B) Thickness of sedimentary wedge 2 59
Figure 38. Thickness map of sedimentary wedge 3 62
Figure 39. (A) Ant-track results of sequence 5 . (B) Ant- track results of sequence 6. (C) Ant-track results of sequence 7 displaying small evidences of radial faulting represented by black arrows. 63
Figure 40. Seismic analysis of Megasequence 4 (MS4) (Middle Jurassic-Cretaceous) and Sequence 10 (Cenozoic)..... 65
Figure 41. (A) Thickness map of Megasequence 4 (MS4)- (Middle Jurassic-Cretaceous) . (B) Thickness map of Sequence 10 (S10) – (Cenozoic). 66
Figure 42. . (A) Ant-rack results for Sequence 8 (Jurassic). (B) Results for Sequence 9 (Cretaceous). (C) Results for Sequence 10 (Cenozoic). Salt-related structural elements are highlighted with black arrows. 67
Figure 43. Thickness map of sedimentary wedge 4 (Cenozoic) 69
Figure 44. (A) Structural modelling of the salt wall, roller, and stock using curved faults. (B) Pillar gridding process showing the creation of upper, middle, and lower skeleton. (C) Creation of 3 segments for future velocity model: segment 1 (minibasin sediments), segment 2 (salt wall) and segment 3 (salt stock)..... 71
Figure 45. (Left) Interval velocities vs depth from the well 7228/7-1A. (Right) Average velocities vs depth from the well 7228/7-1A. 73
Figure 46. (Above) Salt roller interpretation in TWT (ms). (Below) Salt roller interpretation in depth (m) 74
Figure 47. Retrodeformation of salt roller from Cenozoic to Base Middle Jurassic..... 77
Figure 48. Retrodeformation of the salt roller from Base Middle Jurassic- Base Ansinian 78
Figure 49. Observations summary of the Nordkapp Basin 79
Figure 50. Characterization of halokinetic sequences based on input seismic and Cosine of Phase. Main stages of diapirism are characterized by the presence of Tapered composite halokinetic sequences. On the other hand , late stages of diapirism are characterized by Tabular composite halokinetic sequences. 81
Figure 51. Halokinetic conceptual model for the study area in the Nordkapp basin 85
Figure 52.Conceptual model of depositional environments of sequence 3 (S3). 87
Figure 53. Conceptual model of depositional environments of sequence (S4). 88
Figure 54. Conceptual model of depositional environments of sequences 5, 6, and 7. 90

1. Introduction

1.1 Study area and geological problem

The Barents Sea is a continental shelf located between Norway and Russia in the south, Svalbard towards the northwest, and Novaya Semlja towards the east (Fig.1). The study area is located in the southwestern Barents Sea, specifically in the Nordkapp Basin. The Nordkapp Basin provides one of the examples of salt diapirism in the southwestern Barents Sea, being an attractive area for petroleum exploration during the last 30 years. Several exploration wells have been drilled close to salt structures, finding hydrocarbons shows but not commercial reservoirs (Stadtler et al., 2014). As in any other important salt-related basins such as the North Sea, Santos Basin, Gulf of Mexico etc.., halokinetic movements play an important role producing different tectonic styles, creating structural traps, and controlling the distribution of reservoirs around salt structures. Therefore, an understanding of salt's behavior is essential for future exploration purposes in the Nordkapp Basin.

Salt has special properties that differ from other rocks encountered in salt-related sedimentary basins. This material is mainly composed by halite (NaCl), however it is often accompanied by another evaporitic minerals as anhydrite ($CaSO_4$) and gypsum ($2H_2OCaSO_4$), and might be interbedded by carbonates and fine grain siliciclastics. Salt exhibits low densities around 2,160 g/cm^2 and is an almost incompressible material respect to the surrounding overburden. Therefore, at certain depth, density inversion occurs, being salt less dense than the surrounding rocks, and producing salt flow or halokinetic movements towards the surface. Furthermore, its viscous behavior creates wide areas of deformation with the main detachments located within salt layers. In terms of hydrocarbon exploration, halokinetic movement plays a significant role, developing top and side seals due to the impermeability of this material (Fossen, 2010). Additionally, salt is characterized by its high heat conductivity, producing cooling of the underlying sediments and keeping favorable conditions for source rock maturation, even at depths greater than 5 Km in the Gulf of Mexico (Archer et al., 2012).

However, seismic imaging of salt-related basins as the Nordkapp Basin, becomes challenging due to the exceptional geomechanical properties of this material. Firstly, high velocities and low densities produce large reflection coefficients, and large amount of source energy is lost in the sediment-salt boundary. Consequently, pre-salt and sub-salt petroleum plays manifest this problem, and become challenging targets due to the poor information obtained from the layers located beneath allochthonous or autochthonous salt bodies. Secondly, due to the vertical geometry of salt structures, few reflections can be observed, creating areas of noise and uncertainty in salt flanks, and avoiding a clear image of the trap morphology adjacent to the diapir (Haugen et al., 2009; Hokstad et al., 2011; Stadtler et al., 2014) (Fig.2A). Risking a prospect in these areas of uncertainty can be a tedious job. The risk of missing the structural trap increases dramatically and the well can drill unexpectedly through salt resulting in salt-related drilling problems (Swanston et al., 2011)(Fig.2B). Additionally, this phase is followed by the development of side-tracks which will increase considerably the project budget. Finding out periods of salt mobilization, is another challenge in salt-related basins. Passive diapirism controls the sedimentation creating successions of growth strata, which are bounded at the top and base by angular unconformities (Giles and Lawton, 2002; Giles and Rowan, 2012). The influence of these halokinetic movements in the

Triassic paleogeography of the Nordkapp Basin is still poorly understood and continues to be debated. According to previous studies by Glørstad-Clark et al. (2010), the Early-Middle Triassic clinoforms prograde towards the west and northwest through the Nordkapp Basin showing continental environments of deposition (Fig.3). However, Triassic period in the Nordkapp basin is characterized by halokinetic movements, which formed large depocenters that might have influenced the migration of clinoforms creating a complex paleogeography (Jensen and Søresen, 1992; Koyi et al., 1995; Nilsen et al., 1995; Glørstad-Clark et al., 2010). Uplifted areas formed by diapirism, might have acted as local sediment sources. On the contrary, depletion of salt might have caused restricted sub-basins, being favorable for organic-rich deposition (Bugge et al., 2002).

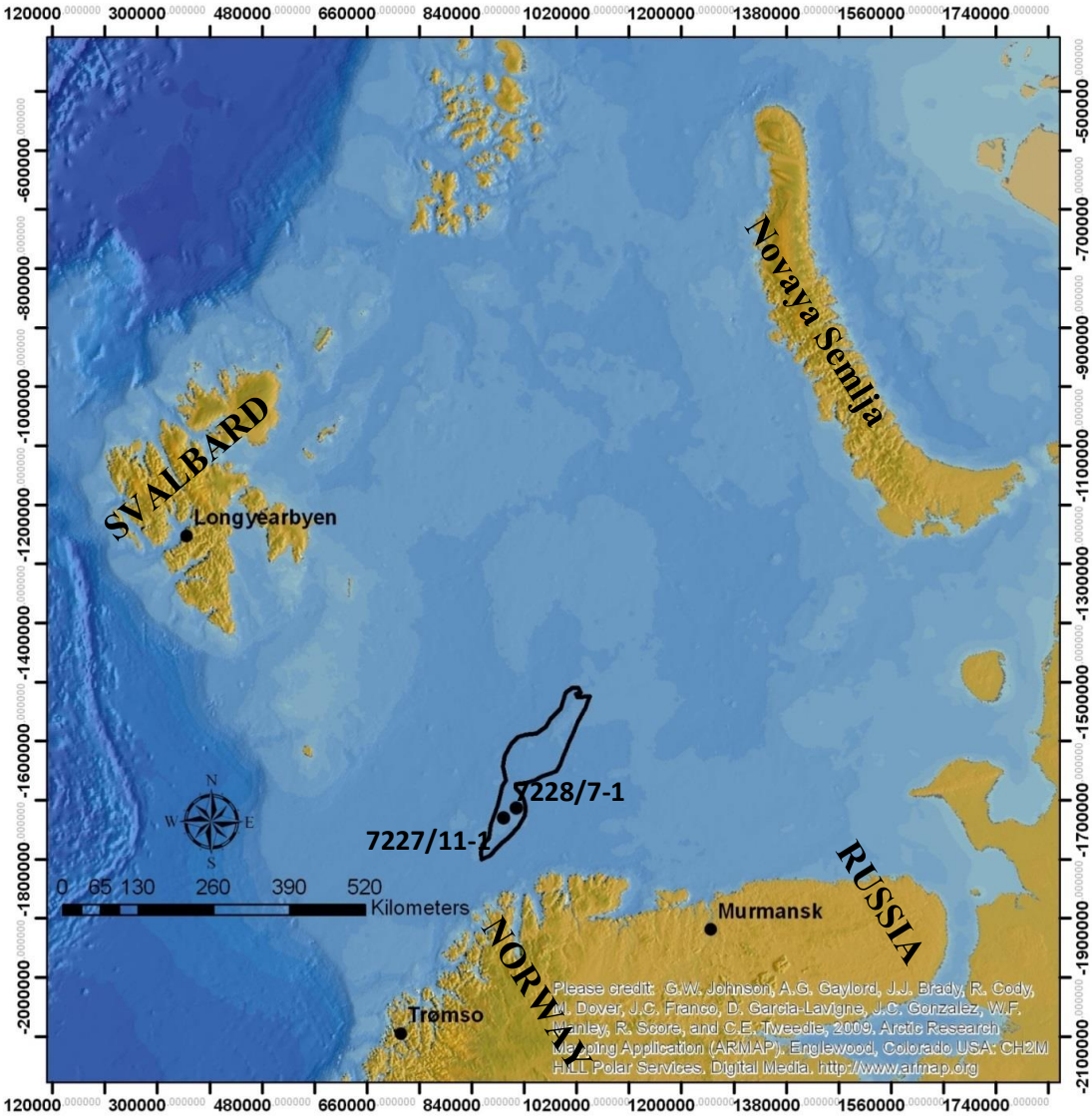

Figure 1 .Location of the Nordkapp Basin in the southwestern Barents Sea. The presence of hydrocarbons within the basin is proved by the wells 7227/11-1 and 7228/7-1.

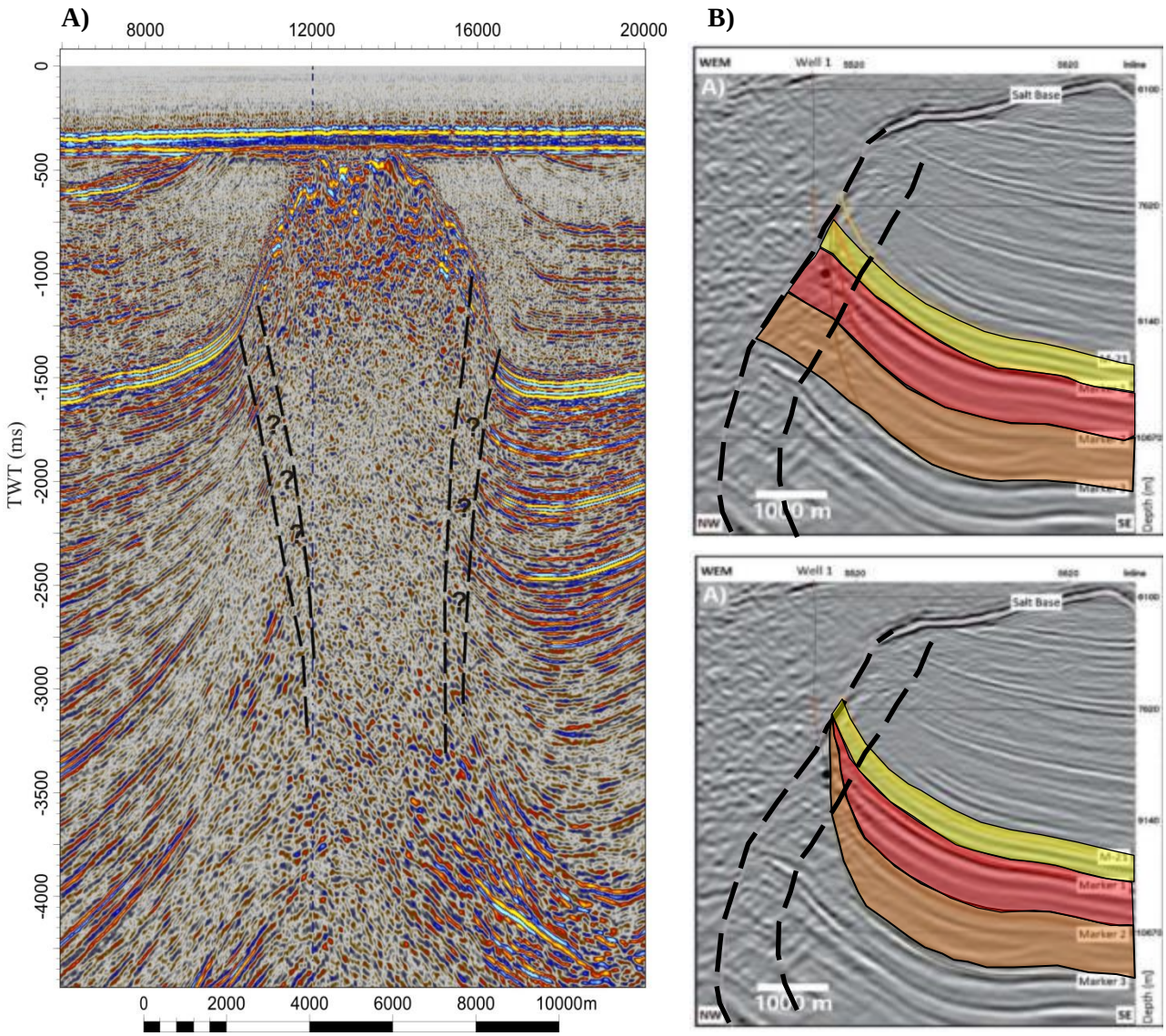

Figure 2. (A) Areas of uncertainty adjacent to salt structures in the Nordkapp Basin. (B) Drilling problems in the Gulf of Mexico due to the poor visualization of the trap geometry in areas of uncertainty represented by dashed lines (modified after (Swanston et al., 2011). The upper figure represents the pre-drilling interpretation and the lower figure the post drilling interpretation

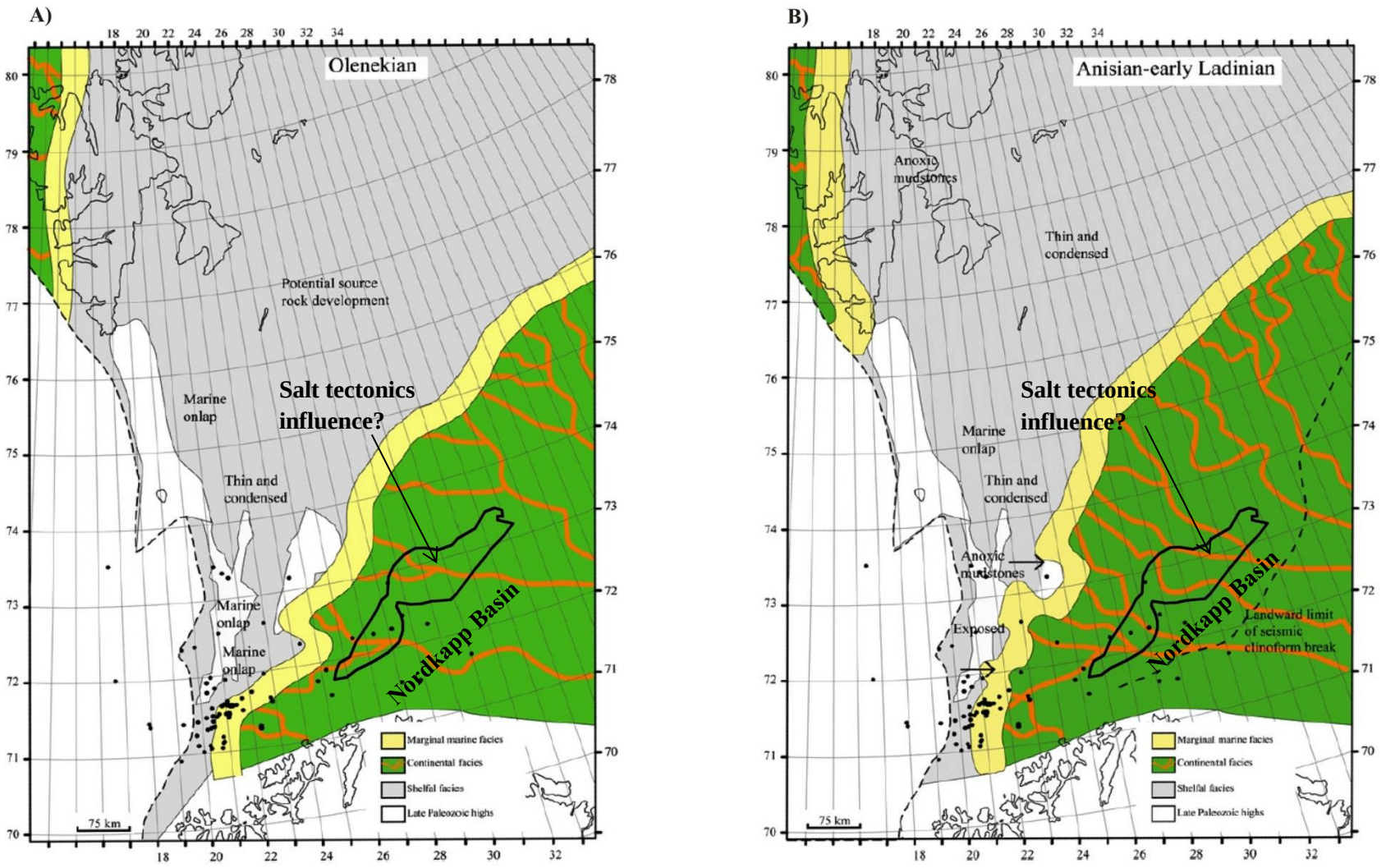

Figure 3. Triassic paleogeography described by Glørstad-Clark et al. (2010). (A) Early Triassic shows continental environments of deposition without any influence of salt tectonics. (B) Middle Triassic has not been influenced by salt tectonics and shows continuous continental environments of deposition.

1.2 Objectives and motivation

Today, few published studies are focused on the halokinetic basin infill evolution of the Nordkapp Basin, and consequently, there is a poor understanding and characterization of areas of uncertainty adjacent to salt diapir flanks, which might provide information about halokinetic movements and trap morphology. In addition, the Triassic variation of environments of deposition influenced by salt tectonics remains unknown. The poor published work in the Nordkapp, together with confirmation of hydrocarbons by exploration wells, caused the motivation and interest of this study. Therefore, the main objective is to develop suitable interpretation attribute workflows applied to observed salt structures, in order to refine the interpretation of areas of uncertainty along diapir rims, and get a better understanding about the influence of halokinesis in the Triassic paleogeography.

1.3 Background of seismic attributes used in salt-related basins

The development of new seismic processing techniques has improved considerably the characterization of subsalt strata. However, the detailed interpretation of sediments adjacent to salt structures is still challenging due to the high angle reflectors at salt margins and overhangs, which decrease the resolution of minibasin strata (Ferguson et al., 2010). In order to reduce the uncertainty in these areas, a wide range of seismic attributes have been used to improve the interpretation of salt structures and salt-related structural elements.

Previous studies conducted by Berthelot et al. (2013), analyze the different seismic textures around the diapir and applied attributes as GLCM (gray level co-ocurrence matrix), frequency-based attributes, and dip and similarity attributes, to improve the definition of the salt flanks (Figures 4A, 4B, and 4C). Changes in gray level distribution between pixels along a selected direction are measured by GLCM and it is useful to detect the different textures observed around salt structures. Dip and similarity attributes measure the dip variations between traces and detects vertical structures as salt diapirs.

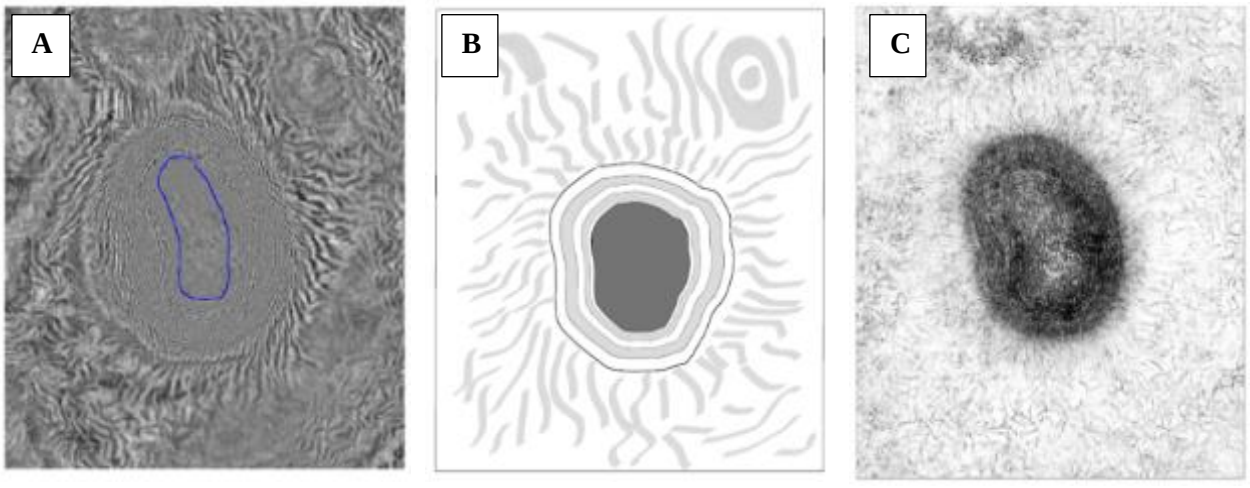

Figure 4. (A) Time slide of the salt structure. (B) Seismic textures identified around salt diapirs. (C) Seismic attributes as coherence improves the interpretation of the salt diapir (Berthelot et al., 2013).

RGB frequency decomposition is a relatively new tool included in most of the software and has been used in many studies in salt-related basins. Frequency decomposition generates 3 volumes with different narrow frequency bands within the seismic spectrum and assigns one colour (red, green or blue) to each frequency band. These technique provides responses from three frequencies, which makes it possible to acquire information about structural and stratigraphic boundaries, facies changes information, salt heterogeneities, and composition (Ferguson et al., 2010). Generally, the interface between low amplitude non-continuous reflectors of salt bodies and high amplitude strata of surrounding minibasins, is highlighted by RGB frequency decomposition, being possible to extract the salt structures from the surrounding minibasins (Fig.5A).

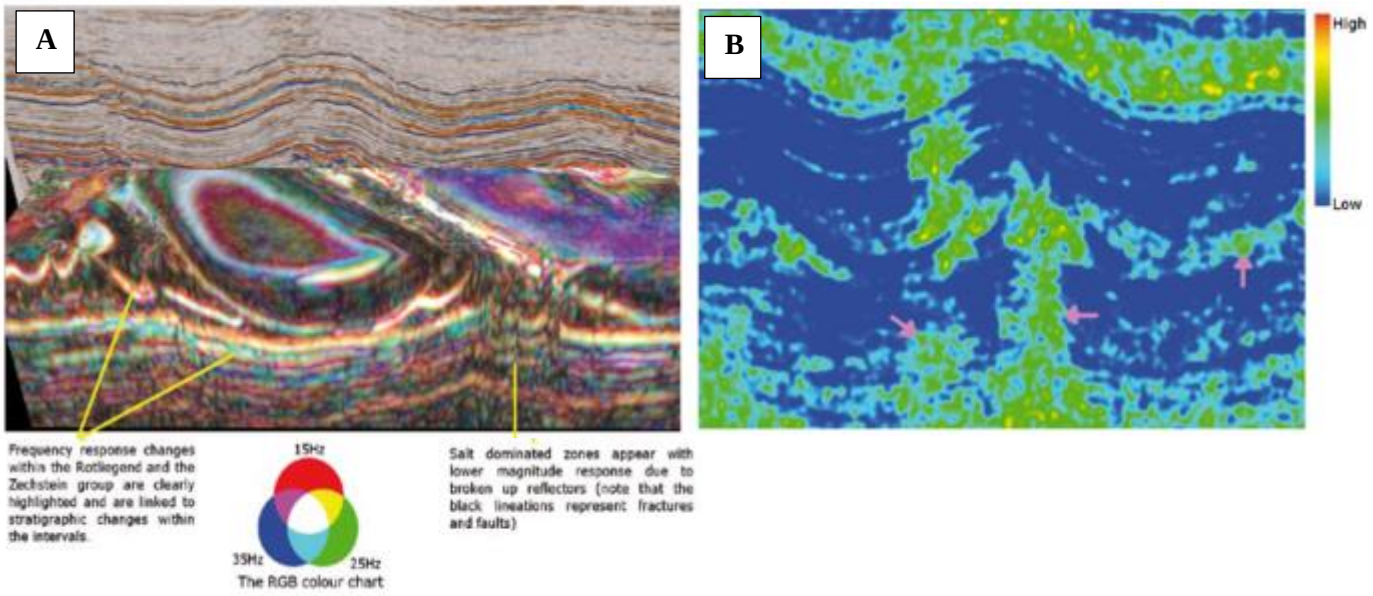

Figure 5. (A) Spectral decomposition highlighting areas with broken reflectors defined as salt. (B) Chaos attribute results. Pink arrows indicate areas with salt (Ferguson et a.,2010).

Research of fracture distribution related to halokinetic movements has become of interest for production purposes in salt related reservoirs (Jhonson and Bredeson, 1971; Davison et al., 2000a; Davison et al., 2000b; Quintà et al., 2012). Attributes like Chaos attribute highlight areas where the seismic shows large variation in the locally estimated dip and azimuth, being crucial to delineate areas with salt and associated structural elements (Fig.5B). Additionally, attributes like Structural Oriented Semblance and Ant-tracking detect high energy surfaces planes and are typically used in the industry to detect delineation of faults or small scale structures probably caused by the emplacement of salt (Fig. 6A)

Finally, attributes as Bedform extract thin lineation representing peaks and troughs, enhancing salt-sediments relationships such onlaps, truncations, pinch-outs which provided very valuable information for predicting trap geometries and reservoir distribution in uncertainty areas adjacent to salt structures (Ferguson et al., 2010) (Fig.6B).

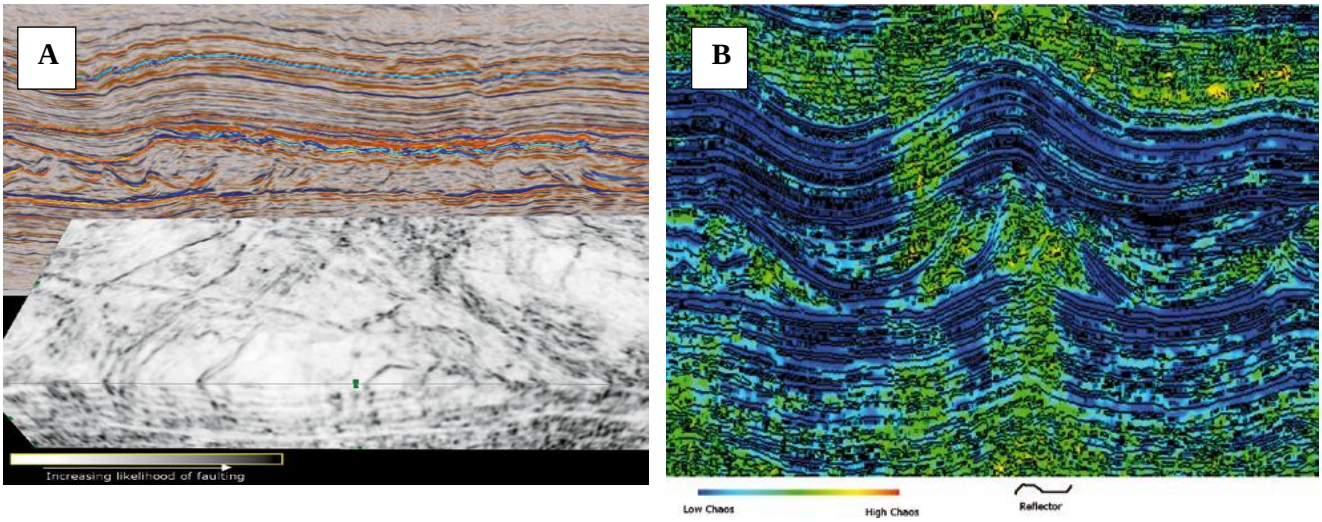

Figure 6. (A) Structural oriented semblance highlights structural elements. (B) Attributes as Bedform enhance the continuity of reflectors in minibasins and improve the resolution of strata terminations such as downlap, onlap, and truncations (Ferguson et al., 2010).

1.4 Background of halokinetic models

Several halokinetic models have been described in previous work to explain the geometry of salt structures, halokinetic movements, and halokinetic sequences.

Geometry of salt structures

Salt structures are characterized by a large geometrical variability, ranging from small salt anticlines, pillows and rollers, to large vertical salt walls, salt stocks, and horizontal salt canopies (Fig.7A). The morphology of these structures depends on factors such as: strength of the overburden, temperature of the salt, salt source layer thickness, tectonic regime, and sedimentation or erosion rate (Fossen, 2010). However, the most common factor used to explain the shape of salt diapirs is the net sedimentation rate vs net salt supply rate relationship, providing three different scenarios (McGuinness and Hossack, 1993; Giles and Lawton, 2002; Hudec and Jackson, 2007):

- High sedimentation rates vs salt supply rates tends to form salt structures with triangular shape as salt pillows and salt rollers (Fig.7B). Generally during this stage sediments onlap and overlap salt structures and, it is commonly observed a convergent vertical migration of depocenters towards salt structure apex. The halokinetic sequences deposited in this scenario display low-angle unconformities (Fig.7C).
- Equal net sedimentation rates vs net diapir growth rate develop vertical salt structures (Fig.7B). Halokinetic sequences deposited around the salt structure exhibits high angle unconformities. No depocenter migration is observed in this model and halokinetic sequences stack vertically (Fig.7C).
- Low sedimentation rates vs net diapir growth causes diapir widening with the subsequent divergent migration of depocenters (Fig. 7B and C). Due to the low sedimentation rates, this period likely develops salt glaciers or salt overhangs. Halokinetic sequences deposited in this scenario suffer large deformation, developing overturned beds.

A)

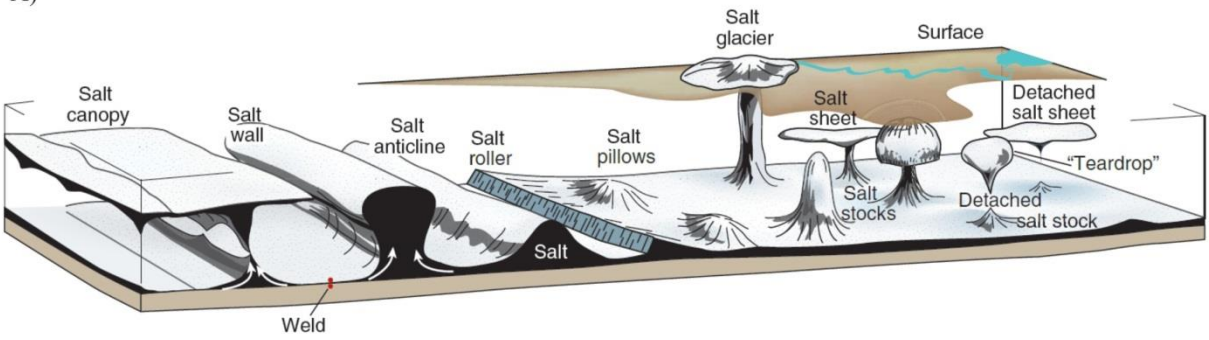

B)

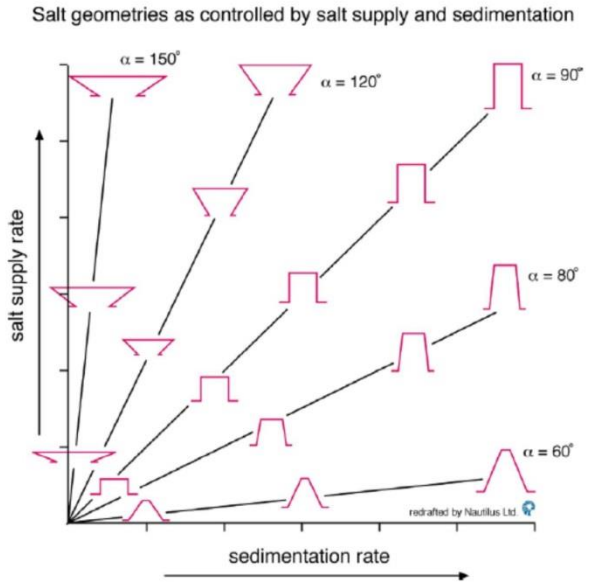

C)

Longterm Relative Rates	Characteristics	Fixed Reference Line
(A) expansion of diapir $R_{net} > A_{sed}$	Diapir expansion, flaring Potential surface glacial flow Overturned beds & repeated sections Offstepping halokinetic sequence stacking	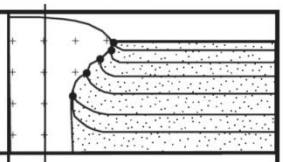
(B) vertical rise of diapir $R_{net} = A_{sed}$	Vertical diapiric rise Sediment aggradation and vertical beds High-angle angular unconformities Aggrading halokinetic sequence stacking	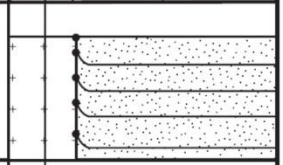
(C) reduction of diapir $R_{net} < A_{sed}$	Diapir contraction Sediments onlap and overlap the diapir Low-angle angular unconformities Onstepping halokinetic sequence stacking	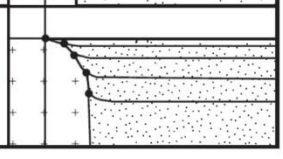

Figure 7. (A) Salt structures classification (Fossen, 2010). (B) Dip of salt-sediment interface based on the relationship between sedimentation rate and salt growth rate (McGuinness and Hossack, 1993). (C) Evolution of salt diapirs and halokinetic sequences as a function of net sedimentation rate vs salt-supply rate (Giles and Lawton, 2002)

Diapirism formation processes

Active diapirism and passive diapirism

During previous traditional models, upward movement of salt is caused by differential, thermal or displacement loading, starting the first stage of salt movement called active diapirism (Trusheim, 1960; Hudec and Jackson, 2007; Fossen, 2010). During this stage overburden layers are rotated upwards and eroded due to the doming caused by the salt pillow (Fig.8A2). As salt flows towards the salt pillow, the source layer is depleted, forming small minibasins called primary rim synclines. This process of salt depletion creating a minibasin is called downbuilding (Fossen, 2010).The mini-basin infill is mainly composed by growth strata, which get thinner towards the salt structure and thicker towards outside areas.

In the second stage, the diapir reaches the surface and rise at the same time that sedimentation is occurring (Fig.8.A3). This process is called passive diapirism (Hudec and Jackson, 2007; Fossen, 2010). The load produced by the minibasin infill induces salt movement towards the diapir and depletes the source layer, forming the second generation of rim-synclines. Secondary rim-synclines display larger dimensions and create the largest depocenters of growth strata around salt structures.

The third phase is characterized by a total depletion of the salt source layer, causing the third generation of rim-synclines (Fig.8A4).Third generation of rim-synclines creates small minibasins that will be filled by growth strata at the last stages of diapirism. After this stage, the diapirs are buried due to the lack of salt supply from the salt source layers.

Reactive or extensional diapirism

Generally, salt buoyancy forces associated with gravity inversion are not strong enough to break the overburden and produce active diapirism. Therefore, the only way to increase the influence of buoyancy forces and induce diapirism, is stretching the overburden by an extensional event. This process is called extensional diapirism or reactive diapirism and it has been registered in many salt-related basins (Hudec and Jackson, 2007; Fossen, 2010) (Fig.8B). The extensional event provides space for salt and develops triangular-shaped salt bodies defined as salt rollers. Reactive diapirism can be followed by a period of passive diapirism, developing vertical salt walls or stocks (Hudec and Jackson, 2007; Fossen, 2010).

Contractional diapirism

Vertical diapirs created normally under extensional events represent weak elements that might be affected by strong deformation under contractional events. During shortening, vertical salt diapirs are squeezed and salt moves towards the surface causing doming and subsequent syn-kinematic sedimentation (Fig.8C). This diapirism process is called contractional diapirism and is present in many basins that suffered contraction after extensional events (Hudec and Jackson, 2007; Fossen, 2010).

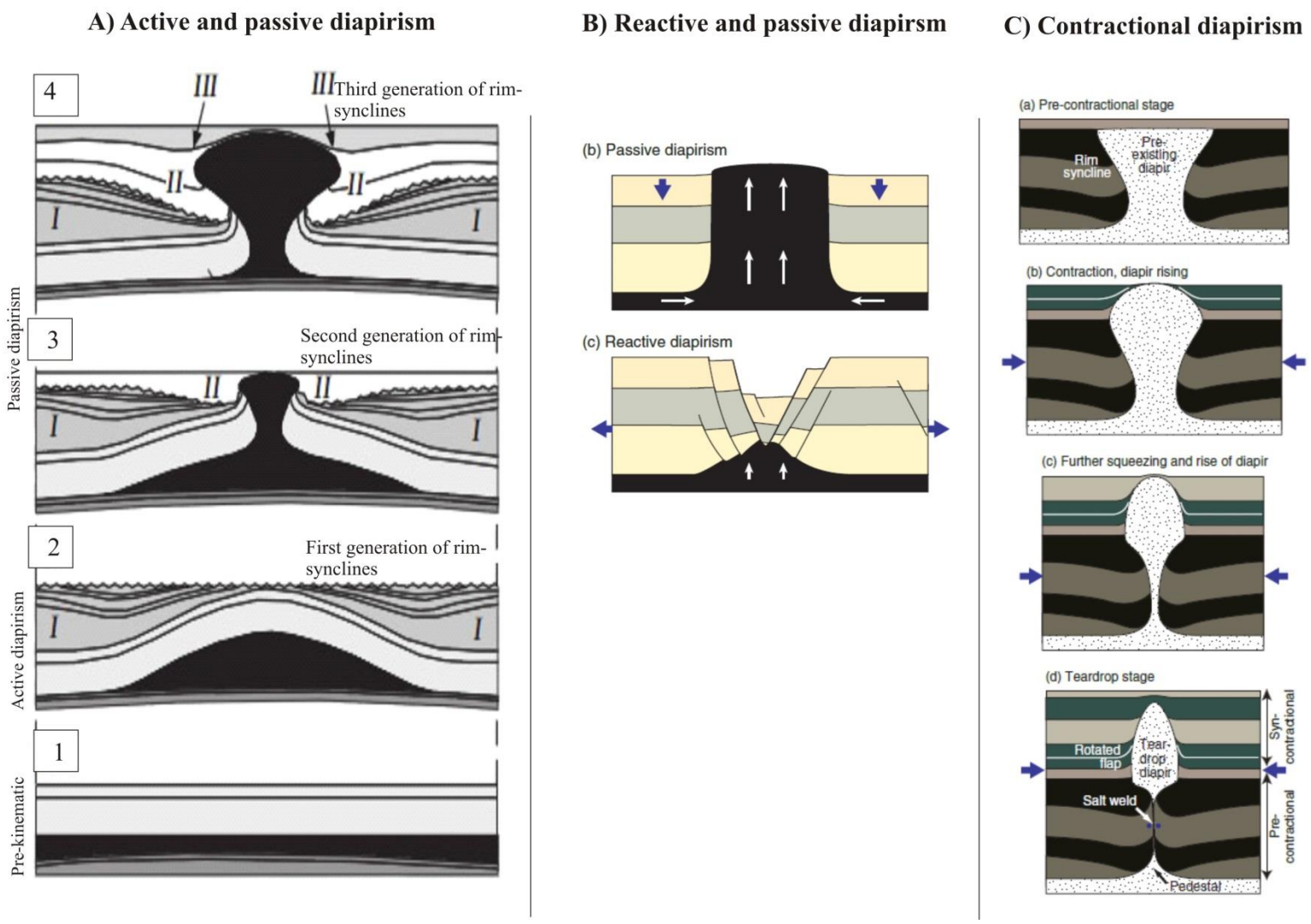

Figure 8. (A) Active diapirism followed by passive diapirism (Trusheim, 1960). (B) Reactive diapirism followed by passive diapirism (Fossen, 2010). (C) Contractional diapirism (Hudec and Jackson, 2007; Fossen, 2010).

Halokinetic Sequences

The presence of growth strata flanking salt structures has been extensively documented by previous work in surface and subsurface data (Bornhauser, 1969; Jhonson and Bredeson, 1971; Lemon, 1985; Davison et al., 2000a). These packages of growth strata are bounded at the top and the base by salt-related angular unconformities and, they are defined as halokinetic sequences (Giles and Lawton, 2002; Giles and Rowan, 2012). The folding of growth strata due to upward salt movement is called drape folding and, it produces high dips and even overturned layers adjacent to salt structures. The intensity of drape folding is controlled by the relationship net sedimentation rate vs net diapirism growth rate, being possible to divided halokinetic sequences into two types:

- Hook halokinetic sequences (Fig.9A). During the deposition of hook halokinetic sequences, net diapir growth is relatively higher than net sedimentation rate. This fact causes narrow areas of drape folding and thinning, ranging from 50 to 200 m, and develops 90 degrees angular unconformities. In addition, fast doming causes failures in the crest of the diapir, producing mass-wasted deposits at the beginning of each hook halokinetic sequence. The stack of hook halokinetic sequences is called tabular composite halokinetic sequences (CHS). Generally, tabular composite halokinetic sequences display several hundred of meters in thickness and are defined as third-order depositional sequences, covering from various thousand years to several million years (Giles and Rowan, 2012)
- Wedge halokinetic sequences (Fig.9B). This type of halokinetic sequences is deposited under high sedimentation rate vs salt growth rate, and the diapir is covered or overlapped by growth strata. Drape folding and thinning of growth strata occurs in a wider area, ranging from 300 m to 1000 m. In addition, minor bed rotation caused by drape folding generates <30 degrees angle truncations. The stack of wedge halokinetic sequences is called tapered composite halokinetic sequences and is considered as third-order depositional sequences as well (Giles and Rowan, 2012).

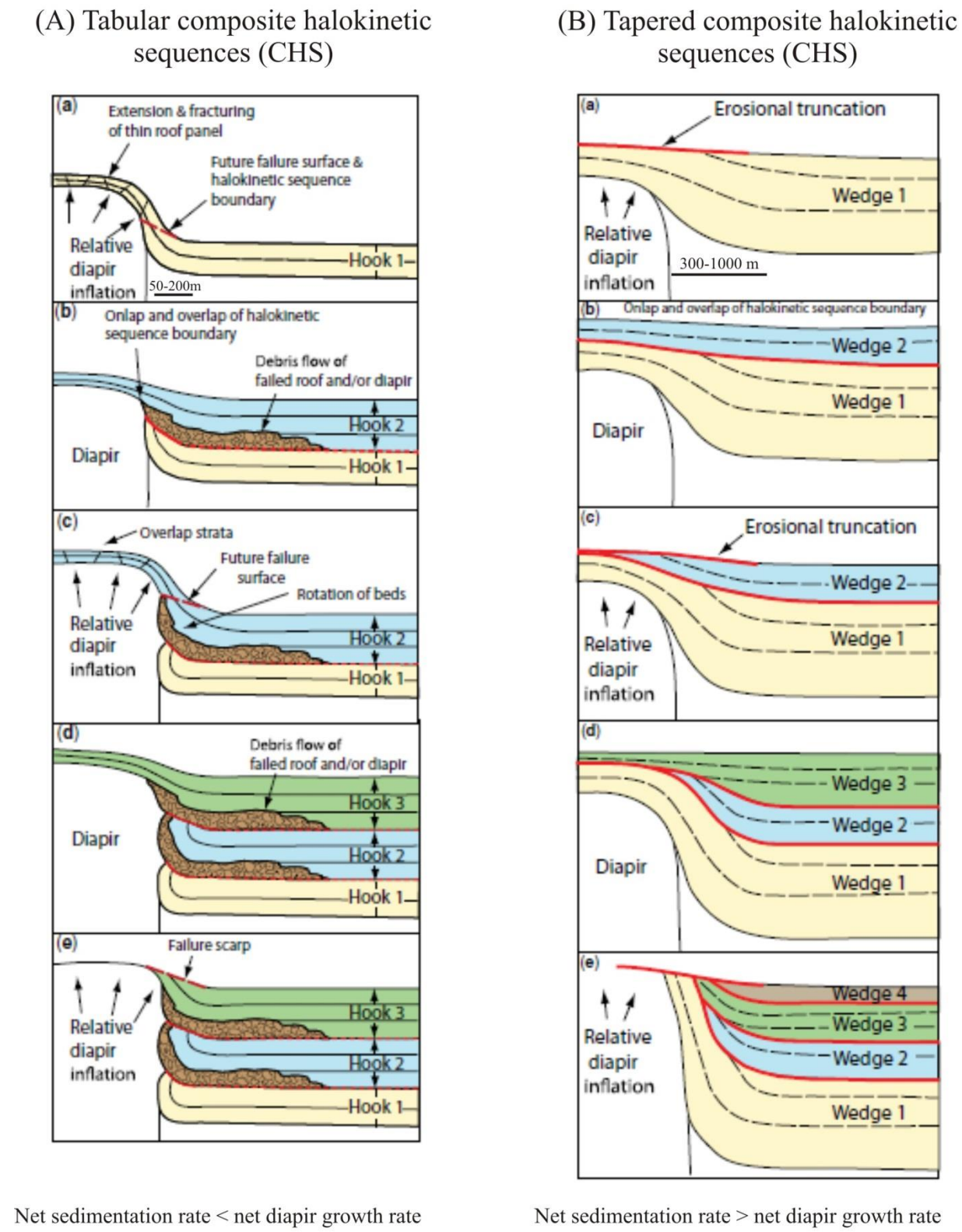

Figure 9. (A) Generation of Tabular composited halokinetic sequences (CHS). (B) Generation of Tapered composite halokinetic sequences (CHS) (Giles and Rowan, 2012).

2. Geological Setting

2.1 Introduction

The Nordkapp Basin is considered the main salt-related basin in the southwestern Barents Sea due to the presence of characteristic salt walls, stocks, and pillows encountered within the basin (Gabrielsen et al., 1990; Gabrielsen et al., 1992; Nilsen et al., 1995)(Fig.10). It is surrounded by the Bjarmeland Platform towards northeast, the Finnmark Platform towards southeast, and the Norsel High towards the southwest. The Nordkapp basin is divided into two sub-basins bounded by faults, as a result of Late Paleozoic rifting: (1) the northeastern sub-basin bounded by faults striking ENE-WSW and, (2) the southwestern sub-basin bounded by NE-SW faults (Rønnevik, 1982; Gabrielsen et al., 1990; Bugge et al., 2002).The basin infill of the Nordkapp Basin is composed by pre-salt strata and post-salt strata (Fig.11). Pre-salt strata ranges from Late Devonian – Late Carboniferous and is not well documented due to the poor drilling and reflection acquisition beneath the Late Carboniferous-Early Permian salt layer. Post-salt strata ranges from Permian to Quaternary, being the Triassic period the most dominant controlled by salt mobilization (Jensen and Søresen, 1992; Koyi et al., 1995; Nilsen et al., 1995).

2.2 Evolution

Late Paleozoic

The initial formation of the basin occurred during the Late Devonian–Early Carboniferous rifting, developing the subsequent NE-SW graben and half graben arquitecture observed in the Nordkapp, Trømso, Bjørnoya basins and onshore areas located in Svalbard (Dengo and Røssland, 1992). From Late Famennian (Late Devonian) to Viséan (Middle Missisippian), the southwestern Barents Sea was part of the northern Pangean margin, and it is believed that the incipient pre-salt basin infill in the Nordkapp Basin consists of non-marine gas prone coaly layers with alluvial-fluvial siliciclastics of the Billefjorden Group (Bugge et al., 2002; Worsley, 2008) (Fig.11). The ongoing rifting and regional uplift, was followed afterwards by a change in latitude resulting in arid conditions, and a regional sea-level rise, depositing the Gipsdalen Group from Bashkirian (Late Carboniferous) to Sakmarian (Early Permian) (Fig.11). The sedimentation during this period in the Nordkapp Basin was characterized by initial clastics from eroded footwalls, followed by warm-water carbonates intercalated by sabkha evaporites developed at basin boundaries. Salt thickness has been calculated in the basin axis, being 4 km in the northern sub-basin, and 2 km in the southwestern sub-basin, suggesting that Nordkapp was a large insolated basin with high evaporation rates during lowstand periods (Bergendhal, 1989; Jensen and Søresen, 1992). The end of the Gipsdalen Group is marked by a regional transgression that might be caused by the disappearance of the Gondwanan ice sheet (Worsley, 2008). This regional transgression was accompanied by an abrupt change in latitude, from warm waters to cold waters, allowing the deposition of cool carbonates of the Bjarmeland Group from Sakmarian to Kunguria (Fig.11). During the middle-upper Permian, the development of the Urals avoided the connection with warm waters from Tethys, producing cold water carbonate assemblages and spiculitic shale deposition of the Tempelfjorden Group (Worsley, 2008) (Fig.11)..

Mesozoic

The Nordkapp Basin exhibits large depocenters mainly caused by halokinetic movements active from the Early Triassic to Late Triassic (Jensen and Søresen, 1992; Koyi et al., 1995; Nilsen et al., 1995; Bugge et al., 2002)(Fig.11). The sedimentation during the Early Triassic in the Nordkapp was characterized by shallow – prodelta facies (Havert-Klappmyss fms), followed by Middle Triassic delta-front and shoreface deposits (Kobbe fm), and finally overlaid by Late Triassic fluvio-deltaic deposits (Snadd formation) (Henriksen et al., 2011) (Fig.11). Triassic sea level fluctuations together with salt tectonics, might have developed high reservoir quality and source potential, being the Triassic an attractive target for exploration purposes in the Nordkapp Basin (Bugge et al., 2002). The transition between Triassic and Jurassic is marked by the Bathonian regional transgression that cut off the input of coarse siliciclastics. Differences on thicknesses in the southwestern Barents Sea suggest the initiation of Upper Jurassic-Early Cretaceous extension, creating anoxia conditions and allowing the deposition of Upper Jurassic black shales (Hekkingen fm.) (Worsley, 2008) (Fig.11). This regional extension event had a very small influence in the Nordkapp Basin due to the presence of small faults affecting this interval (Jensen and Søresen, 1992). Base on characterization of Early Cretaceous clinoforms, most of the Nordkapp was characterized by deep water environments with deposition of fine silicilastics (Knurr/Kolmule fm). This episode is followed by a southwest prograding shelf with deltaic and fluvial environments of deposition (Marin et al., 2015). No active diapirism is registered from the Late Triassic due to the homogeneous thicknesses observed from Late Triassic to Late Cretaceous strata in the Nordkapp Basin (Jensen and Søresen, 1992; Koyi et al., 1995; Nilsen et al., 1995).

Cenozoic

The main salt reactivation occurred during the Cenozoic, being produced by salt buoyancy and density contrast, or external compressional events (Jensen and Søresen, 1992; Koyi et al., 1995; Nilsen et al., 1995). Cenozoic halokinesis and Late Cenozoic erosion created Early Cretaceous and Base Cenozoic truncations, exposing these rocks close to the sea floor, bellow 20 to 40 m of Quaternary sediments (Bugge et al., 2002).

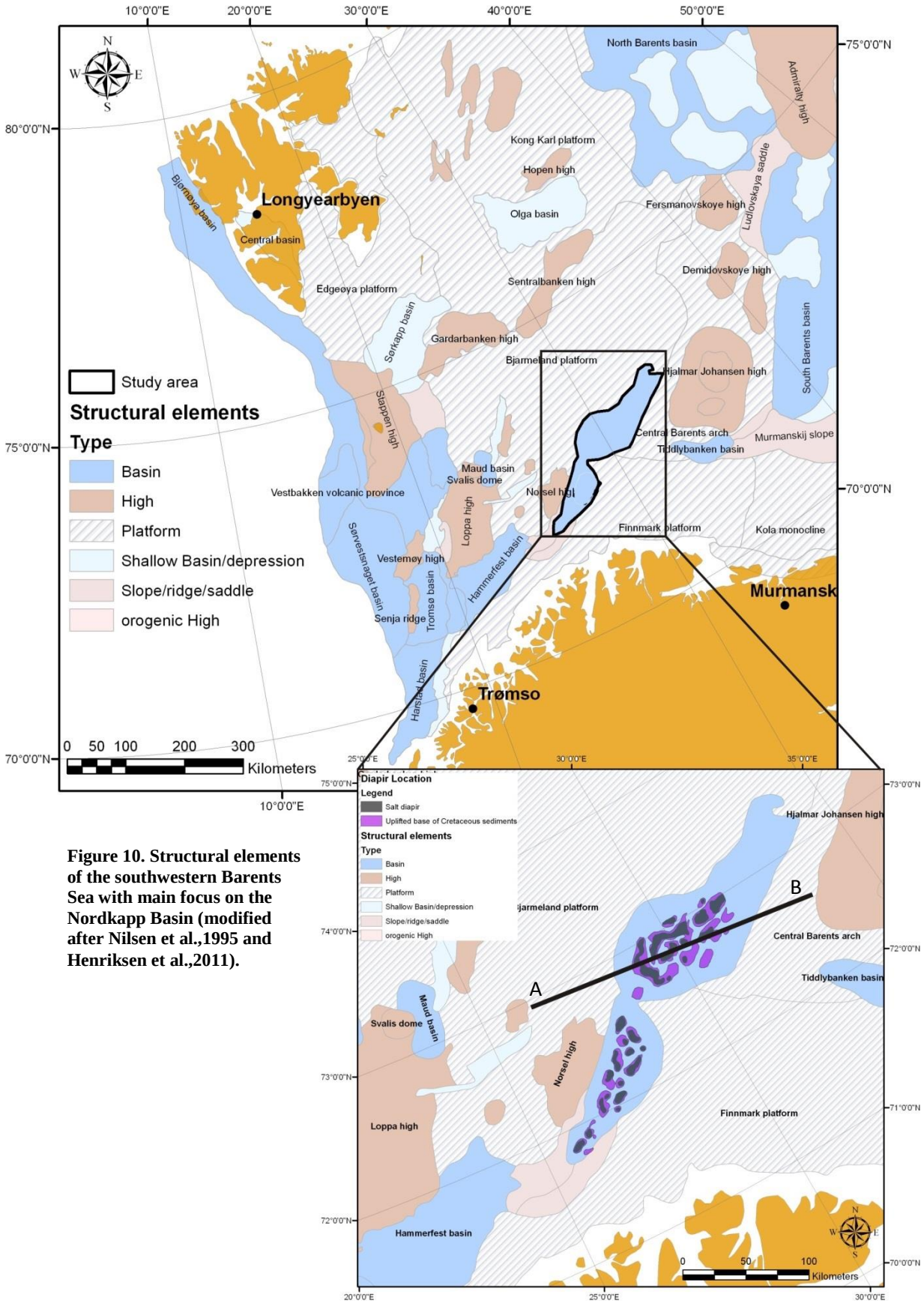

Figure 10. Structural elements of the southwestern Barents Sea with main focus on the Nordkapp Basin (modified after Nilsen et al.,1995 and Henriksen et al.,2011).

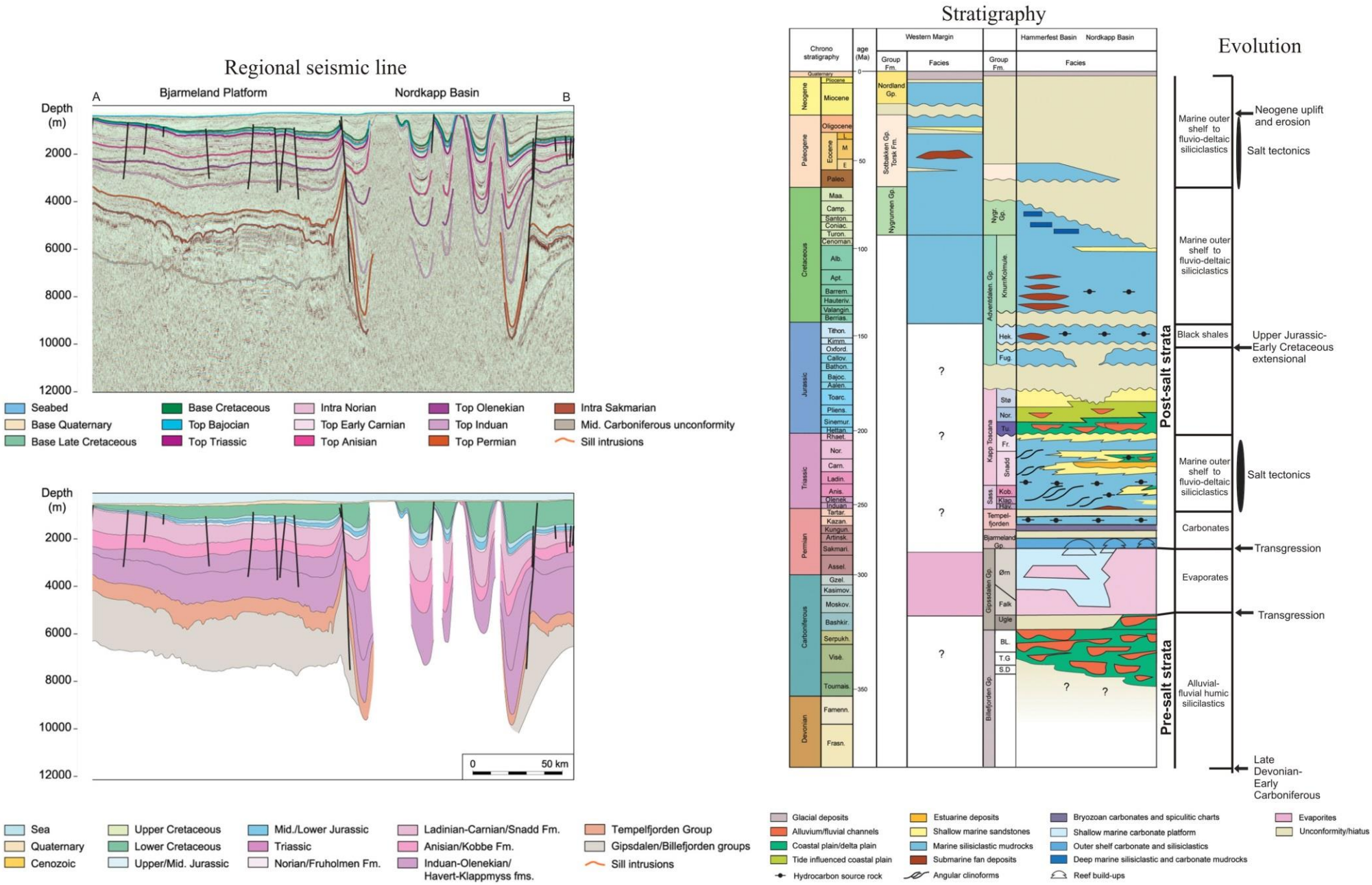

Figure 11. (Left) Regional seismic line through the Nordkapp Basin. (Right) Main tectonic events and environments of deposition of the Nordkapp Basin (modified after Henriksen et al.,2011).

3. Database and methodology

3.1 Database

The research area of this project is located in the southwestern sub-basin of the Nordkapp Basin (western Barents Sea) (Fig. 12A). The data set used in this project has been provided by the Norwegian Petroleum Directorate via Halliburton Norge Landmark and includes:

- ST9403 3D survey
- Well 7228/7-1A

3D survey ST9403

The 3D survey shows NE-SW inlines with a length of 44 Km, and NW-SE crosslines with a length of 25 Km. In total the 3D cube covers an area of 1010 Km^2 approximately (Fig.12A).. Maximum two way travel time is 4500 ms, being just possible to obtain information from post-salt sediments. Generally, the 3D cube shows good quality seismic due to the verticality of salt structures without the presence of salt overhangs. However, refraction and scattering of seismic raypaths travelling into and through the salt, creates random noise, increasing the interpretation uncertainty at salt boundaries (Fig.12B). Another issue is the high reflection coefficient observed at the sea floor and several reflectors beneath, which potentially can produce multiples at different levels (Fig.12B). Furthermore, certain areas of the 3D cube located towards the northeast, between inlines 498 and 98, do not provide any information, being probably associated with problems during data acquisition (Fig.12B).

Well 7228/7-1A

The Well 7228/7-1A is one of the two wildcats drilled in the southwestern part of the Nordkapp Basin, and it is located in the 3D ST 9403 survey, at inline 378, crossline 1557. The total depth of the well is 2848 m, reaching the Klappmyss Formation (Early Triassic) (Fig.13A). Previous to Early Triassic intervals, the well penetrated several good quality water wet reservoirs within the Jurassic, specifically the Stø Formation, the Nordmela Formation and the Tubåen Formation (Fig.13B). Furthermore this well proved the presence of hydrocarbons, penetrating a first HC level in the Snadd Formation (Late Triassic), and an additional HC second level located in the Klappmyss Formation (Early Triassic). However, the calculated hydrocarbons in place did not show economic volumes for exploitation (NPD, 2003).

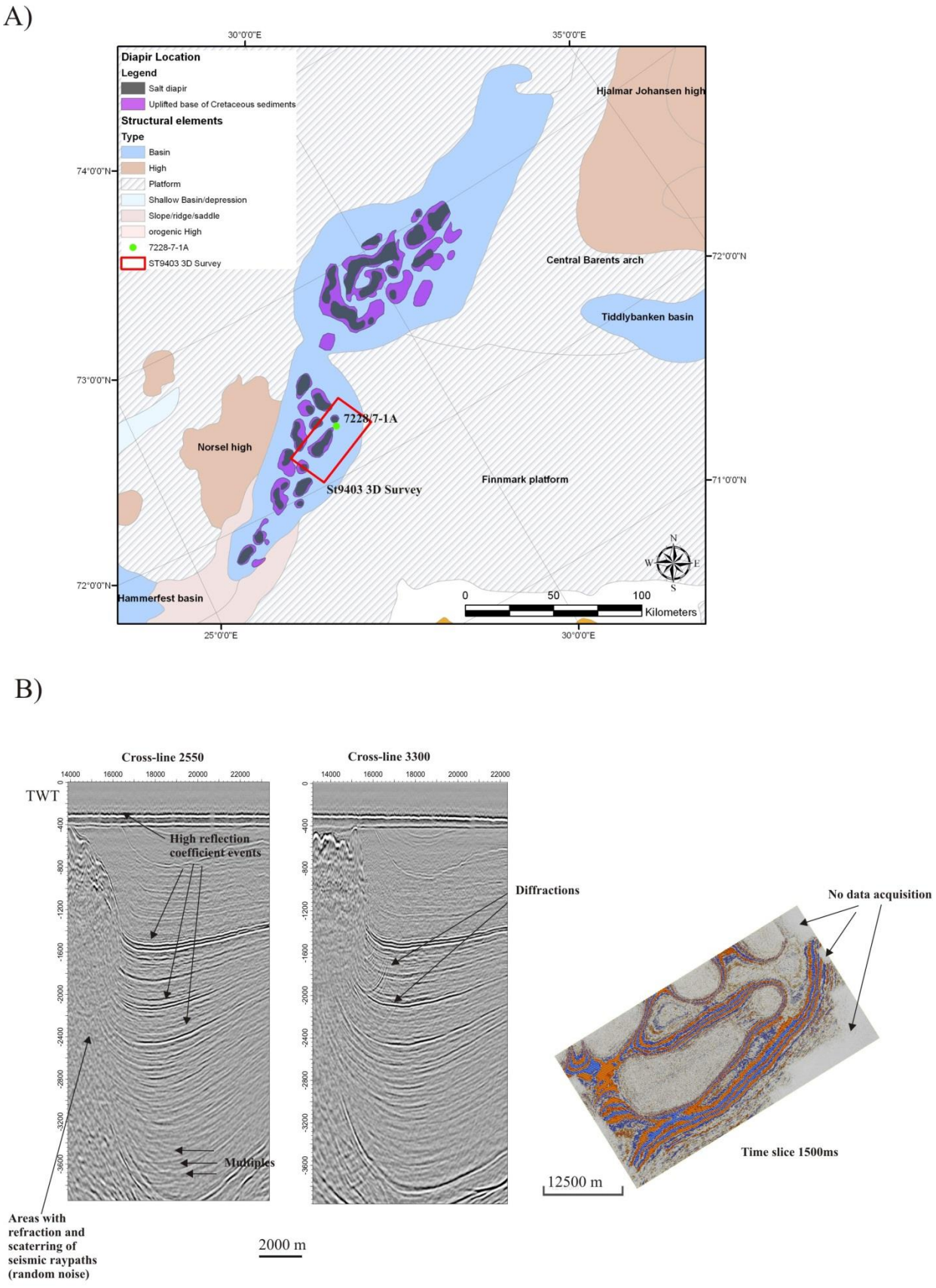

Figure 12. (A) Dataset location. (B) Examples of seismic artifacts encountered in the seismic survey

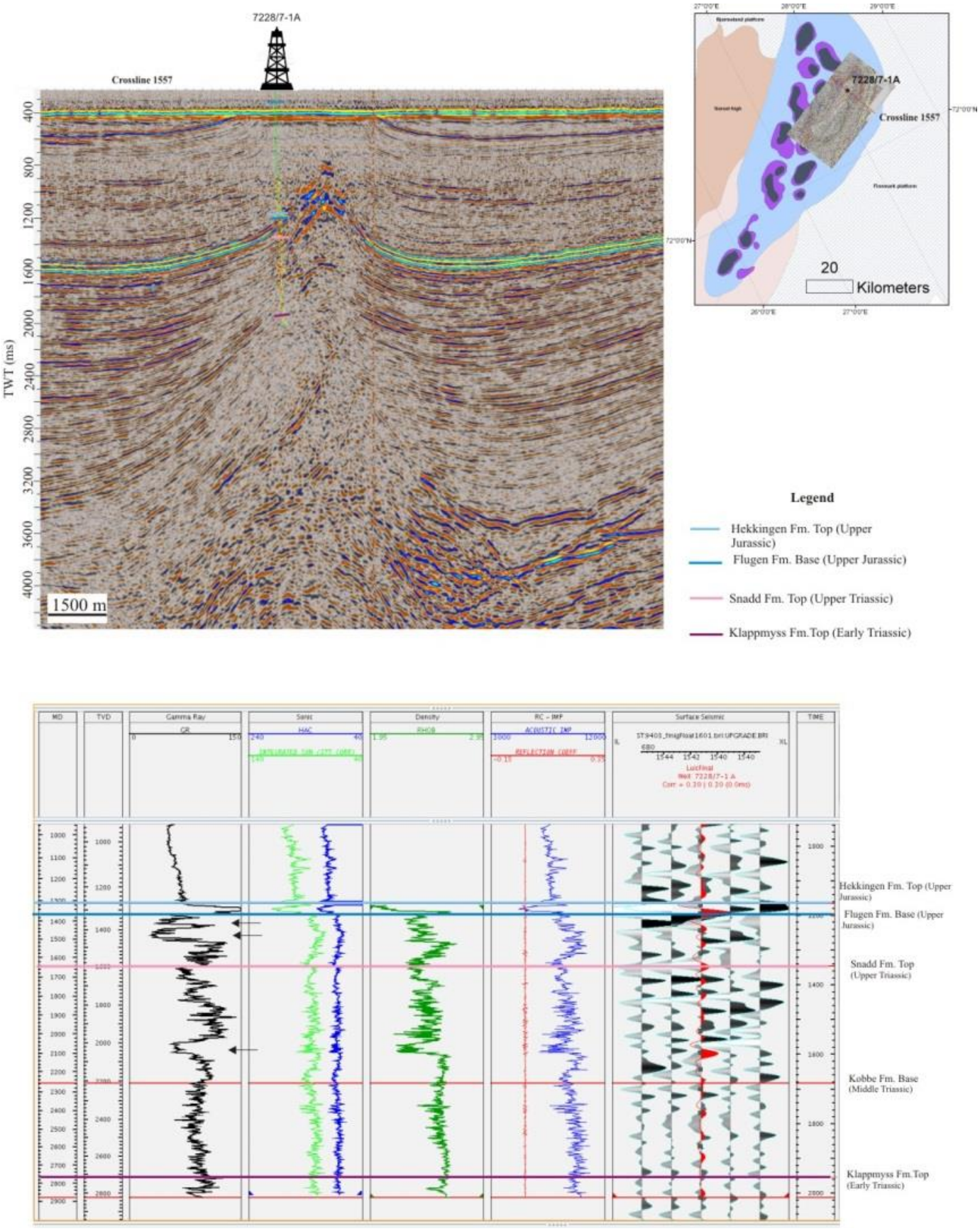

Figure 13. (A) Seismic well tie correlation. (B)Well logs and synthetic seismogram correlation for the well 7228-7/1A. Arrows indicate good quality reservoirs located within the Jurassic and Triassic. Generally Jurassic reservoirs are water-wet. On the other hand, Triassic reservoirs contain hydrocarbons without economic values (NPD, 2003).

3.2 Methodology

This study has been carried out using E&P Petrel and Move Software, which has been essential to provide a complete minibasin and salt structure characterization and evolution. Four steps were needed to complete this achievement (Fig.14)

Seismic multi-trace attribute workflows

Seismic conditioning

The seismic data contains a significant amount of noise and acquisition/processing-related artifacts that reduce the quality of the image for the interpretation. Thus, the first step consists of using appropriate seismic attributes which improve the signal to noise ratio, and enhances the continuity of the seismic events. After this step, algorithms like 3D auto-tracking will be more efficient mapping the main seismic events and detecting the complex areas that requires manual interpretation, for example, in areas close to salt structures.

Salt attribute workflow

Low amplitudes and dipping broken reflectors encountered in areas close to salt flanks, produce wide areas of noise, being difficult to define the interface between salt and sediments. Thus, it is crucial to understand the theory behind structural and complex attributes and select those attributes more suitable to define the location of the salt-sediment interface. Some of the attributes used in this study have a directional parameter which can be modified to efficiently highlight salt bodies. Although, the use of attribute is beneficial for mapping salt bodies, there are also several disadvantages that the interpreter should take into account. Therefore, recommendations will be attached to each attribute to avoid mistakes and highlight the more suitable directional muting with the aim of mapping salt bodies.

Salt-structural elements attribute workflow

Following the interpretation of salt structures, the detection of salt related structural elements is the next step in this study. Salt-related structural elements provide valuable information about halokinetic movements along the geological development of the basin. Therefore, the use of multi-trace seismic attributes to detect the different families of faults is crucial for this purpose. As in the previous section, it is necessary to get an understanding of the theory behind each structural attribute, highlighting the advantages and disadvantages, and giving recommendations to the interpreter.

Minibasin stratigraphy attribute workflow

Salt diapirism episodes are characterized by the presence of growth strata and angular unconformities. These characteristics occur in areas of uncertainty in salt flanks and most of the time coincides with areas of noise. Thus, the aim of this section is to provide seismic attributes and spectral filters which highlight the relationship between seismic events such as truncations, onlaps, and pinchouts located adjacent to salt structures. These relationships will allow the interpreter to identify the main episodes of salt diapirism.

Observations and interpretations base on previous attribute workflows

This chapter offers a full description of salt structures and minibasin stratigraphy based on the previous attribute workflows. Salt structures have been mapped using Multi-z tool in Petrel, which offers a three-dimensional view of salt distribution in the dataset. A detail seismic analysis of the Nordkapp Basin infill is provided in this study to describe the different seismic facies, strata terminations, as well as identify the main unconformities. Due to the lack of well tops at deeper levels, it has not been possible to observe the formations bellow Klappmyss Formation (Early Triassic). Therefore, the age of the main unconformities at deeper areas will be based on previous work by Jensen and Søresen (1992); Koyi et al. (1995); Nilsen et al. (1995); Henriksen et al. (2011). Finally, surface, structural, and thickness maps have been made to represent the main depocenters and get a better understanding about salt-related structural elements distribution and salt mobilization along the geological history of the Nordkapp Basin.

Modelling, depth conversion, and salt restoration

A section about modelling of salt structures is included in this study, showing problems and recommendations regarding the creation of a structural model and 3D Grid, which is needed for building a velocity field used by depth conversion process. Following the depth conversion process, a cross-section salt restoration has been carried out using Move software. The salt restoration will provide information about the progressive evolution of the salt structure, main periods of diapirism, salt source layer depletion, and approximate sedimentation rates.

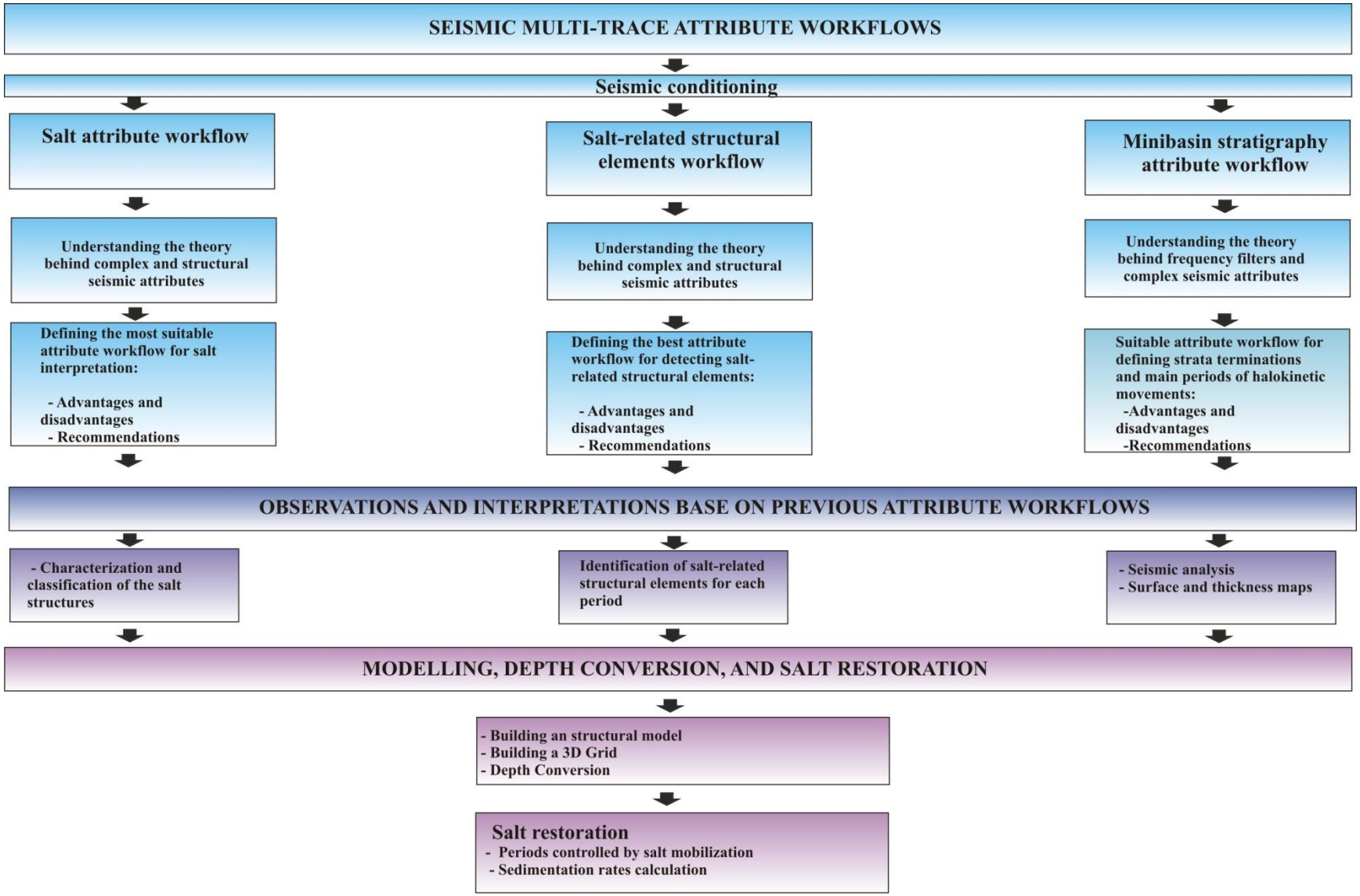

Figure 14. Methodology scheme

4. Multi-trace seismic attributes workflows

4.1 Seismic conditioning

The 3D volume used in this study shows many acquisition-processing issues that will interfere the interpretation, producing noise-related amplitude anomalies in the developed attribute workflows. Generally, cross-lines show good quality data with less noise, and seismic events can easily be followed. However, in-lines display very poor quality data. Reflectors exhibit small discontinuities in amplitude due to sample problems (Fig. 15A). This fact produces areas of noise that will affect negatively the results of algorithms like 3D Auto-tracking and other seismic attributes. Furthermore, seismic events located close to salt structures appear highly discontinuous due to poor reflection acquisition in those areas. Therefore, noise suppression is necessary to improve the signal to noise ratio and to better detect the seismic events close to salt bodies for further investigations.

Structural Smoothing

In order to enhance the continuity of seismic events close to salt structures, the attribute Structural Smoothing has been used. This attribute produces an aggressive noise cancellation, improving considerably the continuity of the reflectors (Fig.15B). Due to the small amount of faults and slightly dipping reflectors, 3D Gaussian smoothing could be used in this study. However, complex areas with highly dipping seismic events require the use of Dip-Guided Structural Smoothing, which will improve considerably the continuity of dipping reflectors adjacent to salt bodies (Fig.16B).

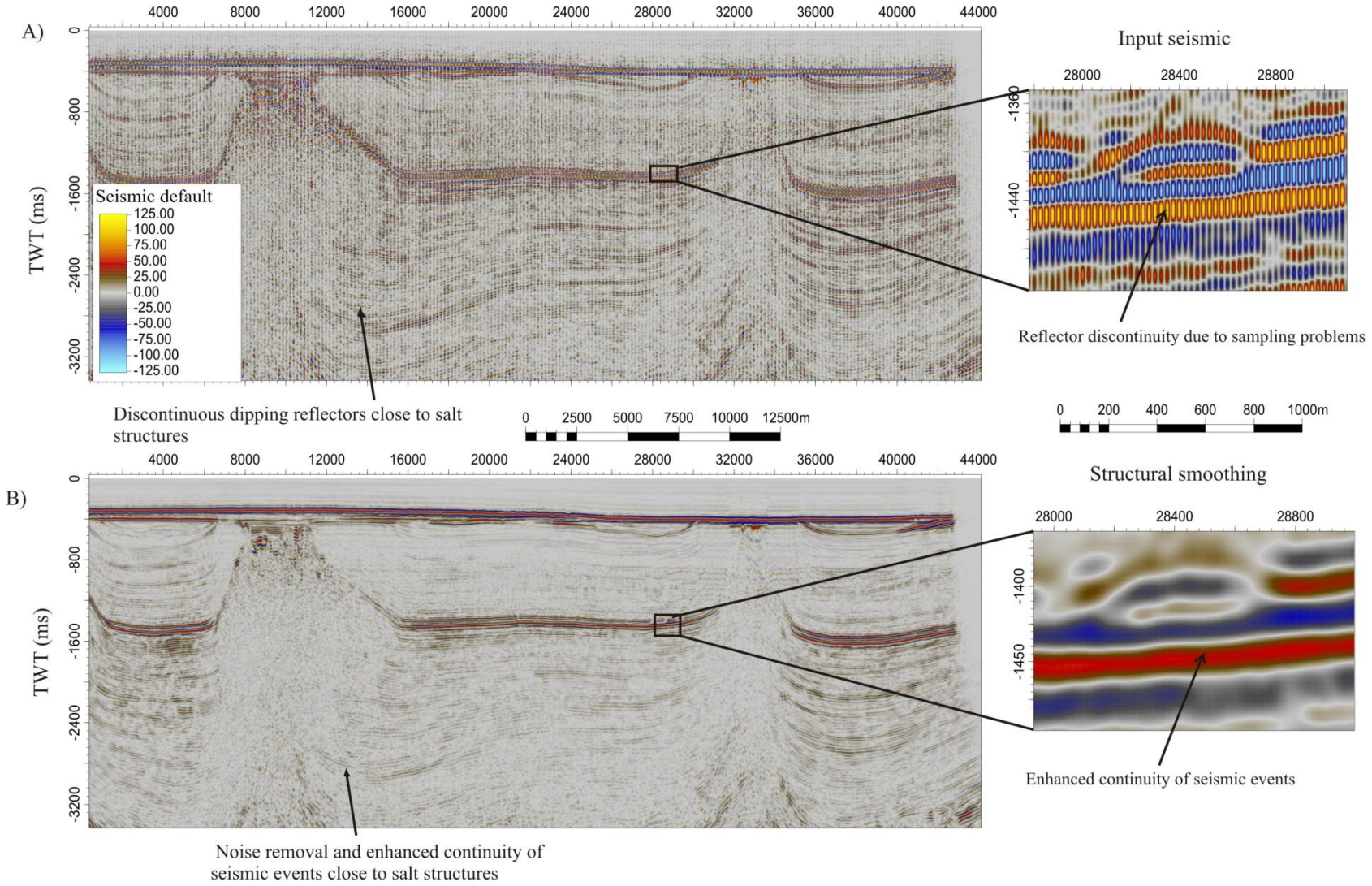

Figure 15. (A). Seismic noise associated with poor amplitude connection between traces due to sampling problems. (B). The attribute Structural Smoothing produces an aggressive noise cancellation and improves the continuity of the seismic events

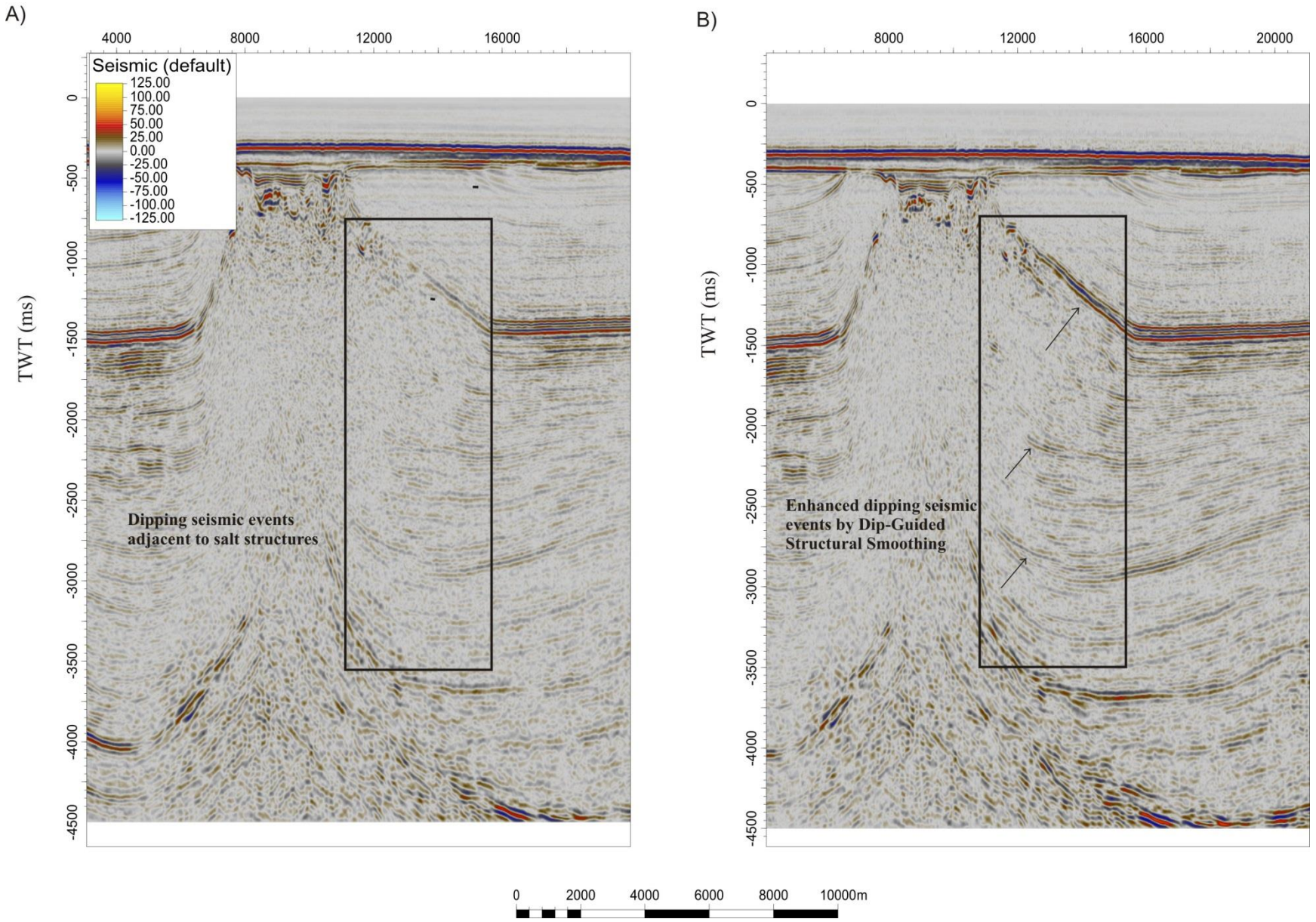

Figure 16. (A) Plain Structural Smoothing does not improve the continuity of dipping reflectors, therefore, areas close to salt diapirs will remain noisy. (B) Dip-Guided Structural Smoothing provides better results enhancing the continuity of dipping reflections in areas close to salt flanks.

4.2 Salt structures interpretation workflow

Analysis of Structural Smoothed time slices

Figure 17 displays a time slice of the Dip-Guided Structural Smoothing cube. Three types of seismic textures can be identified:

- (1) Homogeneous areas with no reflectors corresponding to salt diapirs.
- (2) Discontinuous, low amplitude, sub-vertical thin events located in the vicinity of salt diapirs.
- (3) Salt-related minibasins showing high amplitude dipping continuous events.

Although the morphology of the salt bodies is clearly represented in the time slice, there is still uncertainty regarding the location of the interface between salt and minibasins. Homogeneous areas interpreted as salt bodies still show high dipping thin events and therefore, this fact creates wider areas of approximately 2 km of uncertainty in which the interpreter has to choose the location of the salt-sediment interface.

Dip Illumination

The structural attribute Dip Illumination demonstrates to be suitable for highlighting salt edges in this study. Dip Illumination attribute developed by (Aqrawi et al., 2011), is based on structurally oriented filters which carry out a dip scan in a moving window of 5x5 traces . The combination of dip scan together with an Euler directional component is able to highlight salt edges and remove noise embedded in the seismic (Aqrawi et al., 2012)**.** As previously done, three seismic textures have been used to describe the results of dip illumination (Fig 18):

- (1) Homogeneous areas with no reflectors representing salt structures.
- (2) Areas highlighted in white and black representing areas of uncertainty with highly dipping reflectors.
- (3) Minibasins highlighted in gray.

The directional component of this filter plays an essential role highlighting salt edges in the applied direction and removing noise perpendicularly (Aqrawi et al., 2012). Consequently, different filter orientations are tested with the aim of improving the definition of salt boundaries and reducing areas of uncertainty (Figure 19):

- Directional filter of -45 degrees measured from cross-line direction (Figure 19A). The application of this filter shows good results, clearly displaying the shape of the salt body. Areas of uncertainty are displayed in white and black colours and are mainly associated with highly dipping events. Notice that areas of uncertainty have been reduced at least 1 km respect to the previous 3D Dip-Guided Structural Smoothing.
- Directional filter -90 degrees measured from cross-line direction (Figure 19B). In this case, -90 degrees directional filter seems to be the most suitable for interpreting salt. Areas of uncertainty around the diapir have been reduced considerably down to approximately 200 m, and the main salt structure has been divided into an elongate salt wall and a circular salt stock. Notice these two

salt structures are not distinguished applying any other angle and will remain highlighted as a unique salt wall.

- Directional filter from -135 to -180 measured from cross-line direction (Figure 19C, D, and E). The application of these filters shows similar results as the directional filter 0 to -45 degrees. However, areas of uncertainty increases up to 1,5-2 km.

It is recommended to apply the filter direction perpendicular to the main strike of faults or salt diapirs to obtain a general overview about the morphology. Afterwards, different filter direction angles can be tested with the aim of refining salt boundaries and reducing areas of uncertainty linked to sub-vertical layers at salt flanks. Once Dip- Illumination is applied, the color bar histogram might be stretched to highlight subtle changes in the data, which can increase positively the quality of the image. Furthermore, it is of great importance to take into account the noise muting occurring perpendicular to the filter direction. Perpendicular noise muting can remove data of interest as diapir-related radial faults. For this reason, the detection of salt-related structural elements has been evaluated in a separate workflow in this study.

Variance

Previous observations using Dip-Illumination on top of Dip-Guided Structural Smoothing, demonstrated the power of seismic attributes for delineating the salt-sediment interface. However, there are still areas of uncertainty ranging from 1 km to 200 m where salt identification is remains an issue.

In order to improve the interpretation of these areas, the structural attribute Variance has been applied in addition to the Dip-Illumination volume. The Variance attribute basically measures the horizontal continuity of the amplitude, in other words, the difference from the mean value within a gliding CMP window (Van Bemmel and Pepper, 2000). Thus, it is useful for detecting salt bodies due to the difference from broken reflectors (salt) to continuous reflectors (minibasins). However, in areas with highly dipping bedding, variance will deliver misleading results if the variation of the amplitudes is analyzed along time lines. This might lead to interpretation of layered areas as salt. Therefore, Dip-Guided Variance is used in this study to highlight areas of salt embedded in highly dipping bedding. Figure 20 shows the results of Dip-Guided Variance with the corresponding three seismic textures obtained from the image:

- (1) Values of variance close to 1. These areas are regarded as salt structures. Values of variance are close to one due to the verticality of the structures respect to surrounding dipping seismic events.
- (2) Mixture of values from 1 to 0,5. These areas still deliver uncertainty in the interpretation due to the unclear location of the salt-sediment interface.
- (3) Values of 0,50. These values are produced by differences in dip angle due to small faults.
- (4) Values close to 0. These are represented by highly dipping beds close to diapir flanks. The variance is calculated along the seismic horizons which only show small amplitude variations. Consequently the variance is close to zero.

To summarize, first tests indicated that Variance is an additional attribute for refining the interpretation in unsolved areas from the Dip-Illumination cube (Fig.21). However, areas with highly dipping reflectors adjacent to salt might produce high variance values, which may lead to wrong salt-sediment interface location. Therefore, it is recommended not to base the interpretation just on the Variance cube and always

compare the results with previous developed attributes such as Dip Illumination or Dip-Guided Structural Smoothing.

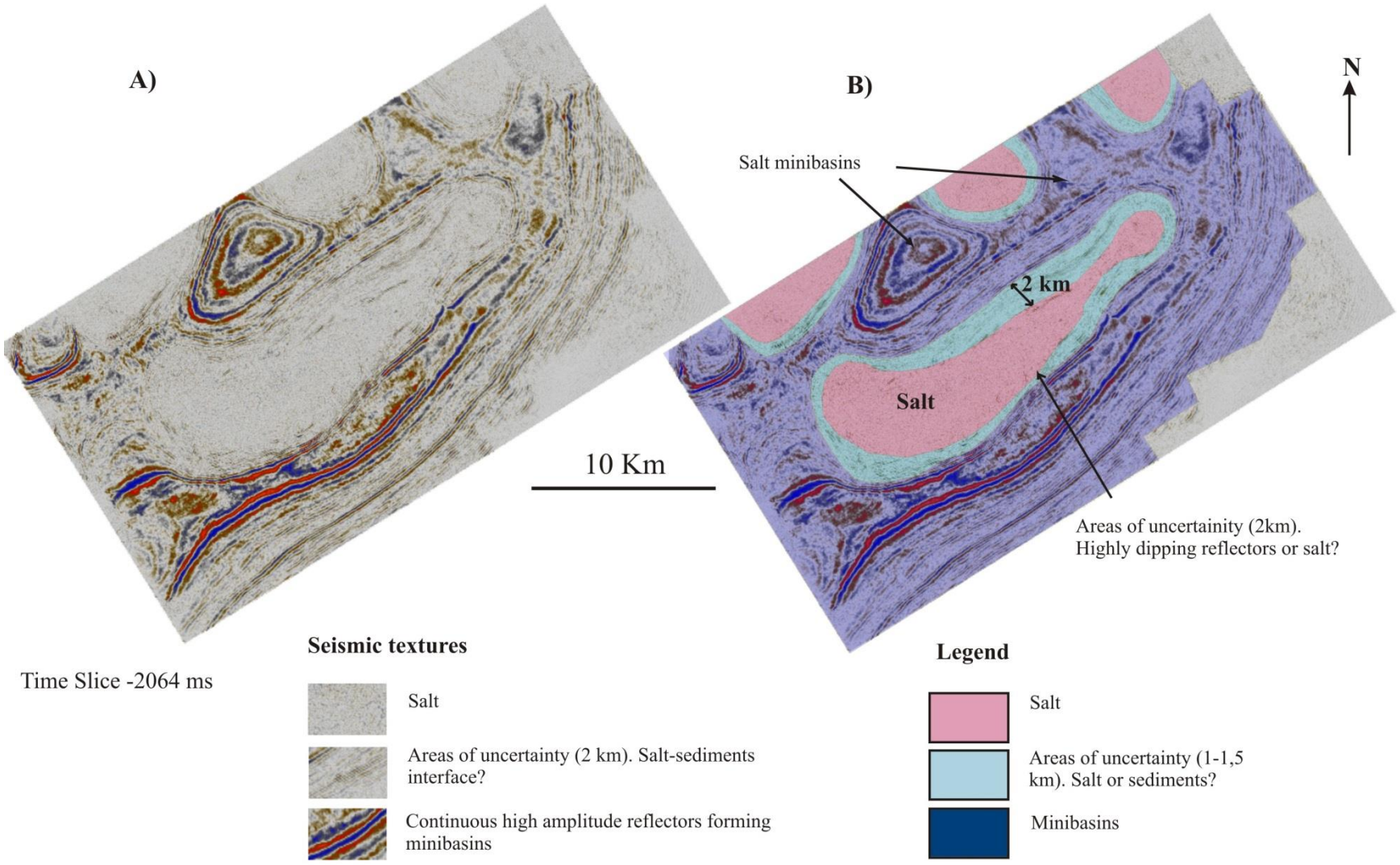

Figure 17. (A) Dip-Guided Structural Smoothing time slice analysis and seismic textures based on different seismic responses. (B) Interpretation based on seismic textures. Blue colours indicate areas of uncertainty (2km approx.) where the salt-sediment interface is not clear.

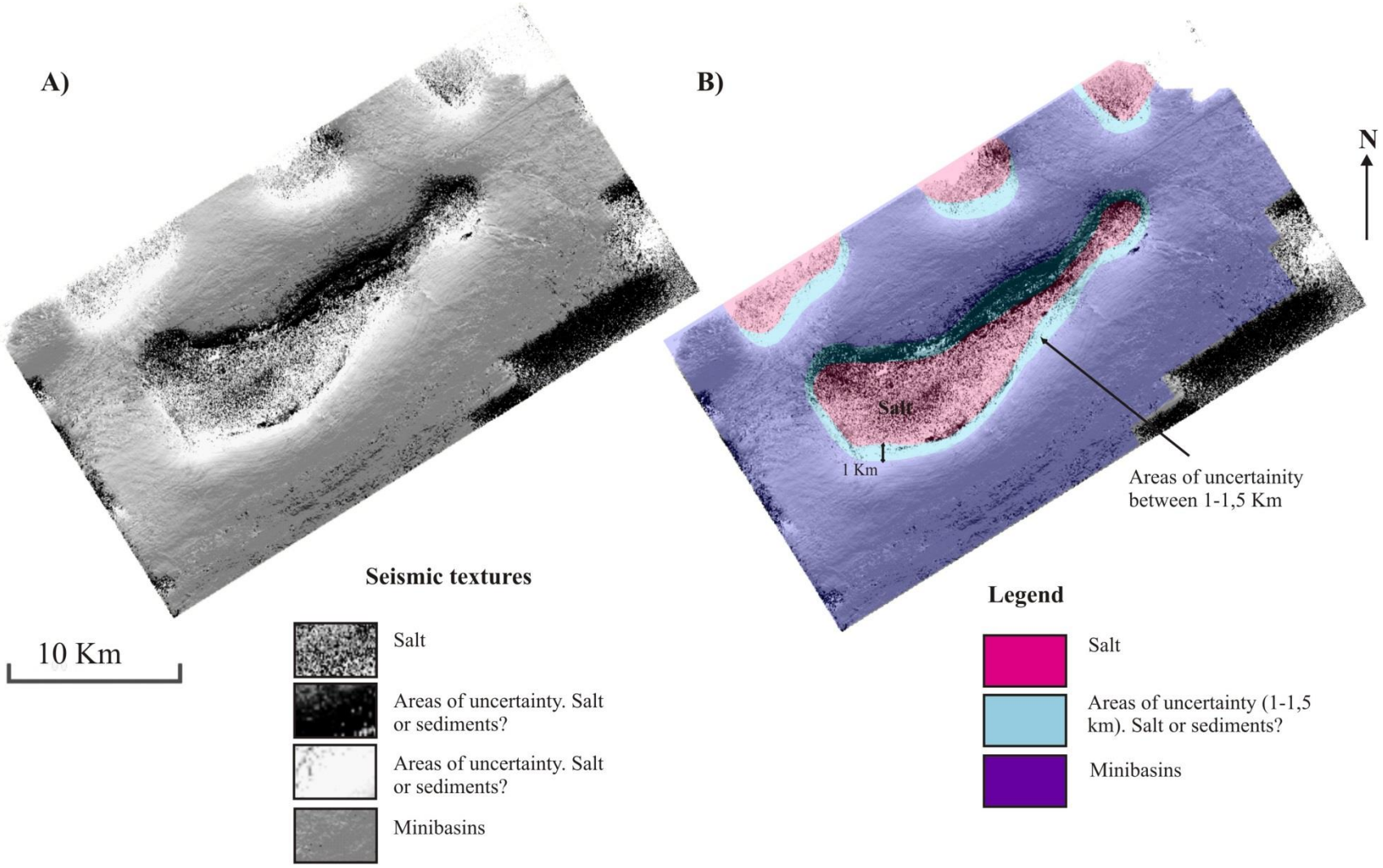

Figure 18. (A) Dip-Illumination time slice analysis and seismic textures. (B) Interpretation based on seismic textures. Blue colours indicate areas of uncertainty (between 1,5 and 1km) where the salt-sediment interface is not clear.

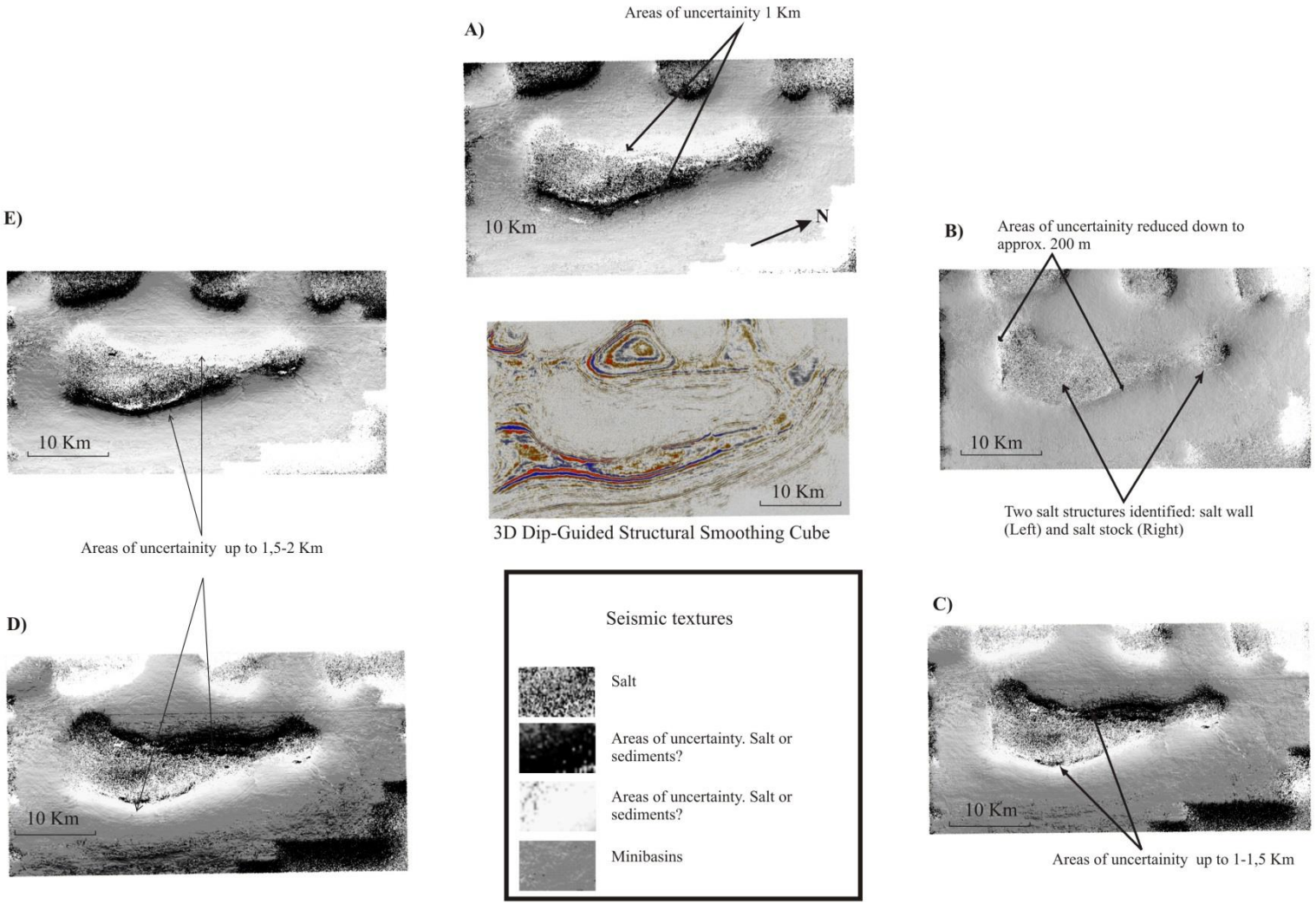

Figure 19. (A) Directional filter of -45 from the cross line direction. (B) -90 degrees directional filter seems to be the more suitable, reducing the areas of uncertainty down to 200m. (C). Directional filter of -135 degrees. (D) Directional filter of -150 degrees. (E) Directional filter of -180 from the cross line direction

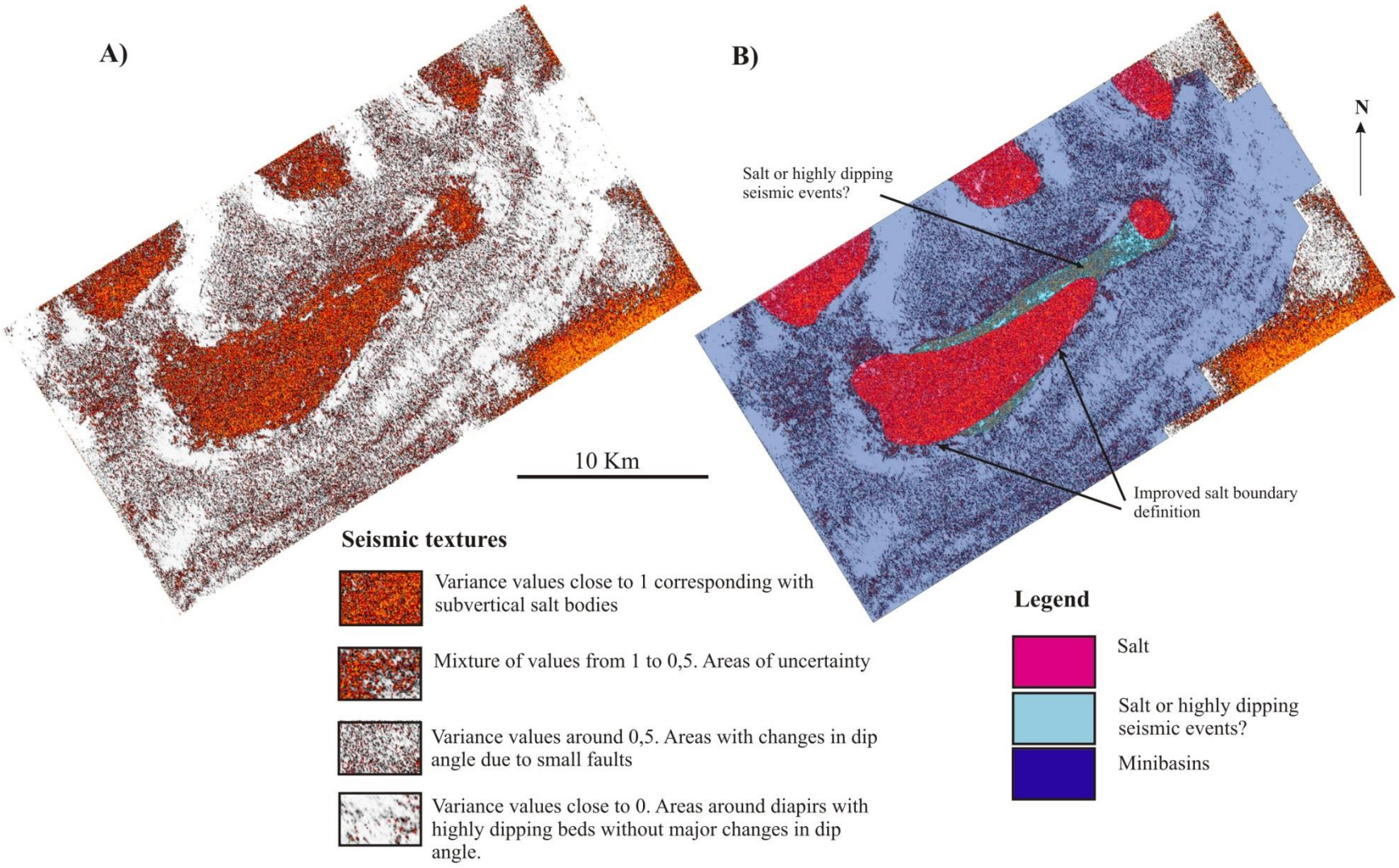

Figure 20. Results of Dip-Guided Variance. (A) Time slice analysis with seismic textures. (B) Interpretation based on seismic textures. This attribute is mainly use to refine the interpretation of salt boundaries from the Dip-Illumination cube. However, light blue areas appear poorly solved, being difficult to delineate salt boundaries.

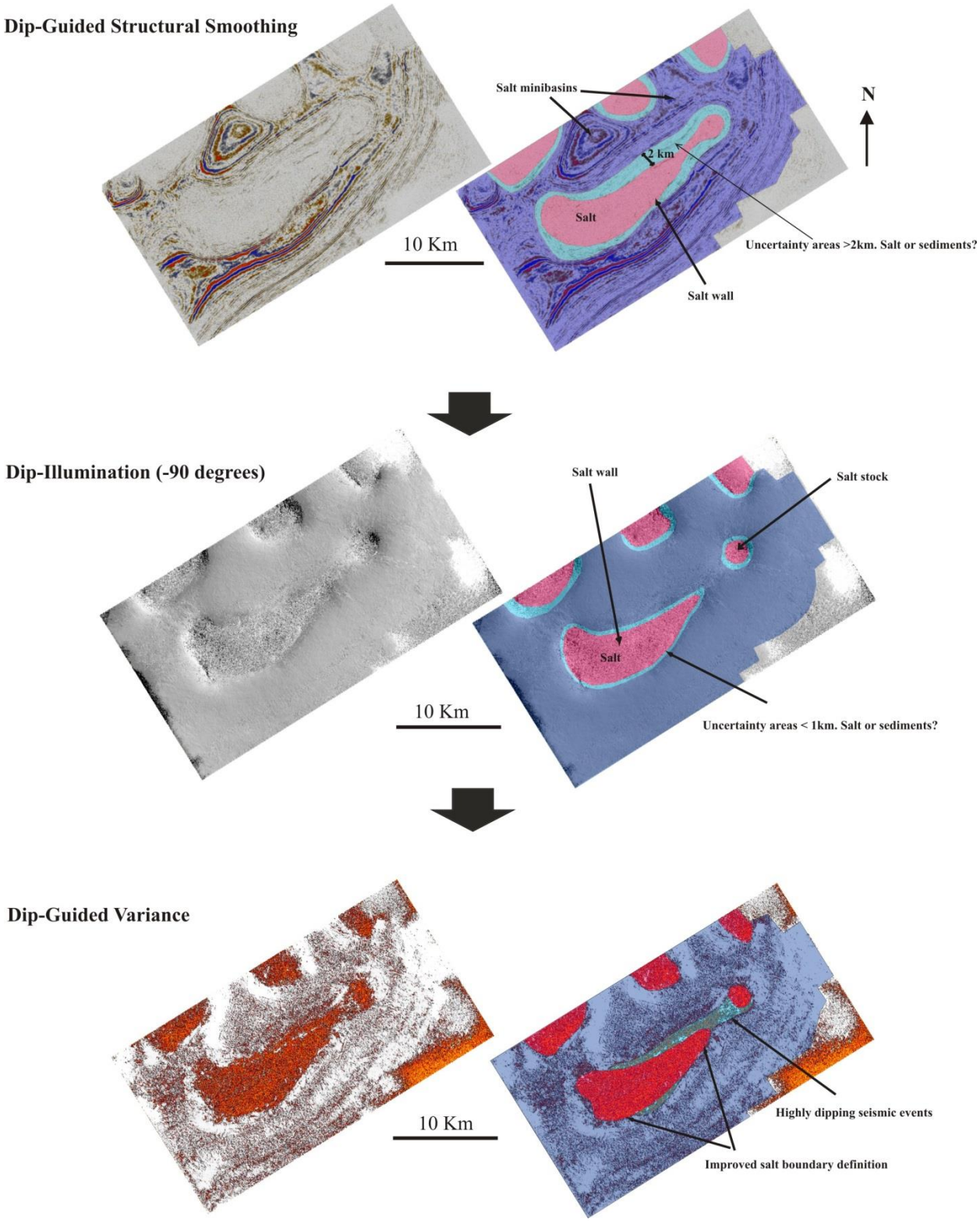

Figure 21. Summary salt interpretation workflow

4.3 Structural attribute workflow

The analysis of fracture generation adjacent to salt diapir provides information about diapir kinematics and structural trap generation being important for hydrocarbon exploration (Quintà et al., 2012). Therefore, in this section, a separated attribute workflow is provided with the aim of detecting salt-related structural elements along the geological history of the Nordkapp Basin.

Analysis of Structural Smoothed time slices

Figure 22 displays a time slice of the previous Dip-Guided Structural Smoothing cube created during the seismic conditioning step. Similar to the previous workflow, three seismic textures have been identified:

- (1) Areas with chaotic seismic events representing salt bodies.
- (2) Areas of highly dipping reflectors around salt diapirs.
- (3) Areas of gently dipping reflectors located further from salt structures.

Notice that some of the seismic events seem to be discontinuous around salt structures being interrupted by faults. Therefore, Dip-Guided Structural Smoothing provides a preliminary view of the location of salt-related structural elements displaying areas where the algorithm could not enhance the continuity of the reflectors.

Chaos

Seismic multi-trace structural attributes like Chaos seem to be very suitable for defining salt-related structural elements as radial faults (Fig.23). First, the attribute is applied on the Dip-Guided Structural Smoothing cube that previously removed noise and enhanced the continuity of the seismic events. Afterwards, the Chaos volume attribute highlights areas where the seismic shows large variation in the locally estimated dip and azimuth. These variations might be caused by salt structures, gas migration paths, reef textures, channel infill etc….(Ferguson et al., 2010). The Chaos attribute is scaled from 0 to 1, showing the following seismic textures:

- (1) Values > 0,60. These values are represented by red colors and are mainly caused by strong variation in dip and azimuth. These variations are mainly produced in the data set by salt structures, highly dipping seismic events, or highly faulted areas.
- (2) Values from 0,30 to 0,60. This range of values are represented by grey/red colors and indicates small variations of dip and azimuth mainly caused by salt-related radial faults or faulted areas
- (3) Values from 0,30 to 0. This range of values is represented by white colors and corresponds to areas with no evidence of strong variation of estimated dip and azimuth. Normally, these areas are located further away from salt diapirs where there are not structural elements causing variations in the amplitudes of the seismic horizons.

Ant-track

Previous results demonstrated that Chaos is an excellent attribute for highlighting salt-related radial and circular fault patterns. However, the definition of these structural elements can be enhanced using the algorithm Ant-track (Fig.24). This attribute is applied on the previous Chaos cube and highlights considerably high energy surfaces represented as faults planes by removing noise and non-faulted seismic events. Ant-track algorithm provides directional filters that display the fault plains striking in a specific direction. This tool is useful when the main strike of the tectonic structures is well understood. However, the use of directional filters in areas with salt might not be a good idea. Salt diapirs generally produce radial patterns striking from 0 to 360 degrees and the use of directional filters might remove salt-related structural elements in a specific filter direction. Therefore, the algorithm Ant-track has to be run for all the directions due to the radial and circular fault patterns caused by salt intrusions in areas with salt tectonics. In this case, two seismic textures have been identified after applying the Ant-track algorithm

- (1) Highly faulted areas or salt;
- (2) Areas poorly faulted mainly located further from salt structures.

A summary of the structural analysis work flow based on multi-trace attributes is given in Fig.25.

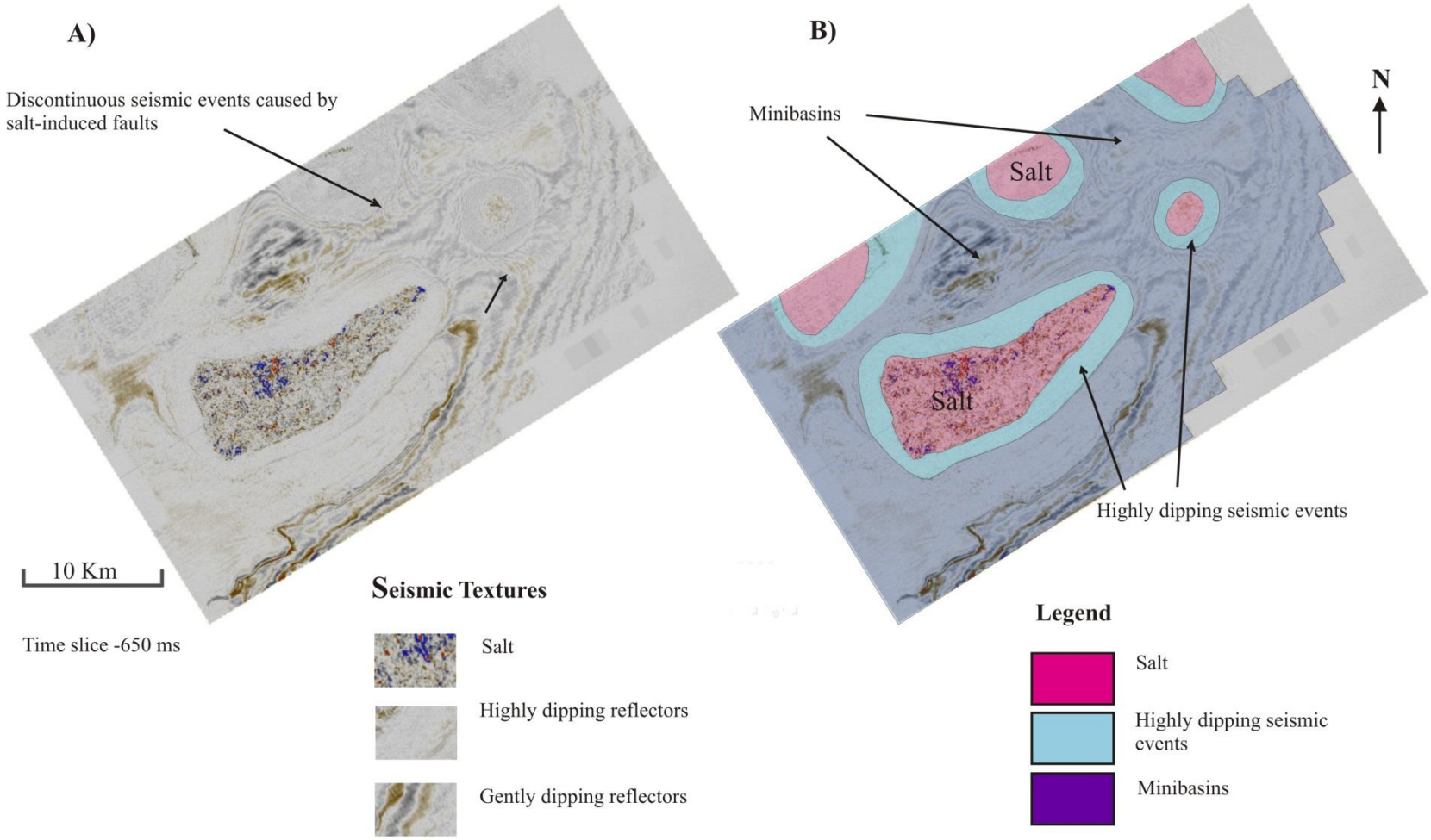

Figure 22. (A) Time slice analysis of the Dip-Guided structural smoothing cube. Notice the discontinuous seismic events caused by salt-induced faults. (B) Interpretation highlighting areas with salt (red), highly dipping reflectors (light blue), and areas with similar dip and azimuth (purple)

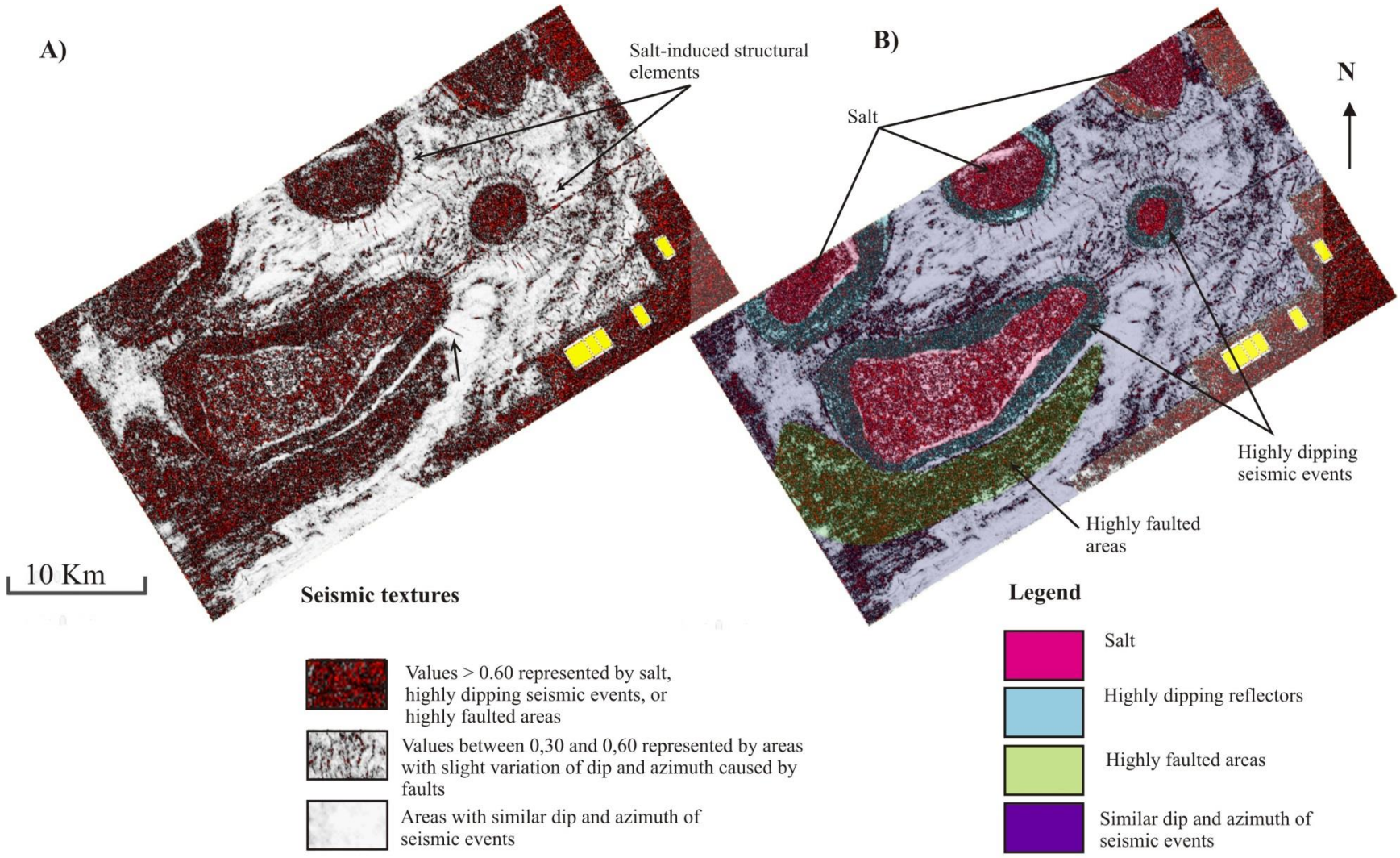

Figure 23. (A) Time slice analysis of the Chaos cube. Notice that the definition of radial faults has been improved. (B) Interpretation highlighting areas with salt (red), highly dipping reflectors (light blue), highly faulted areas (green), and areas with similar dip and azimuth (purple).

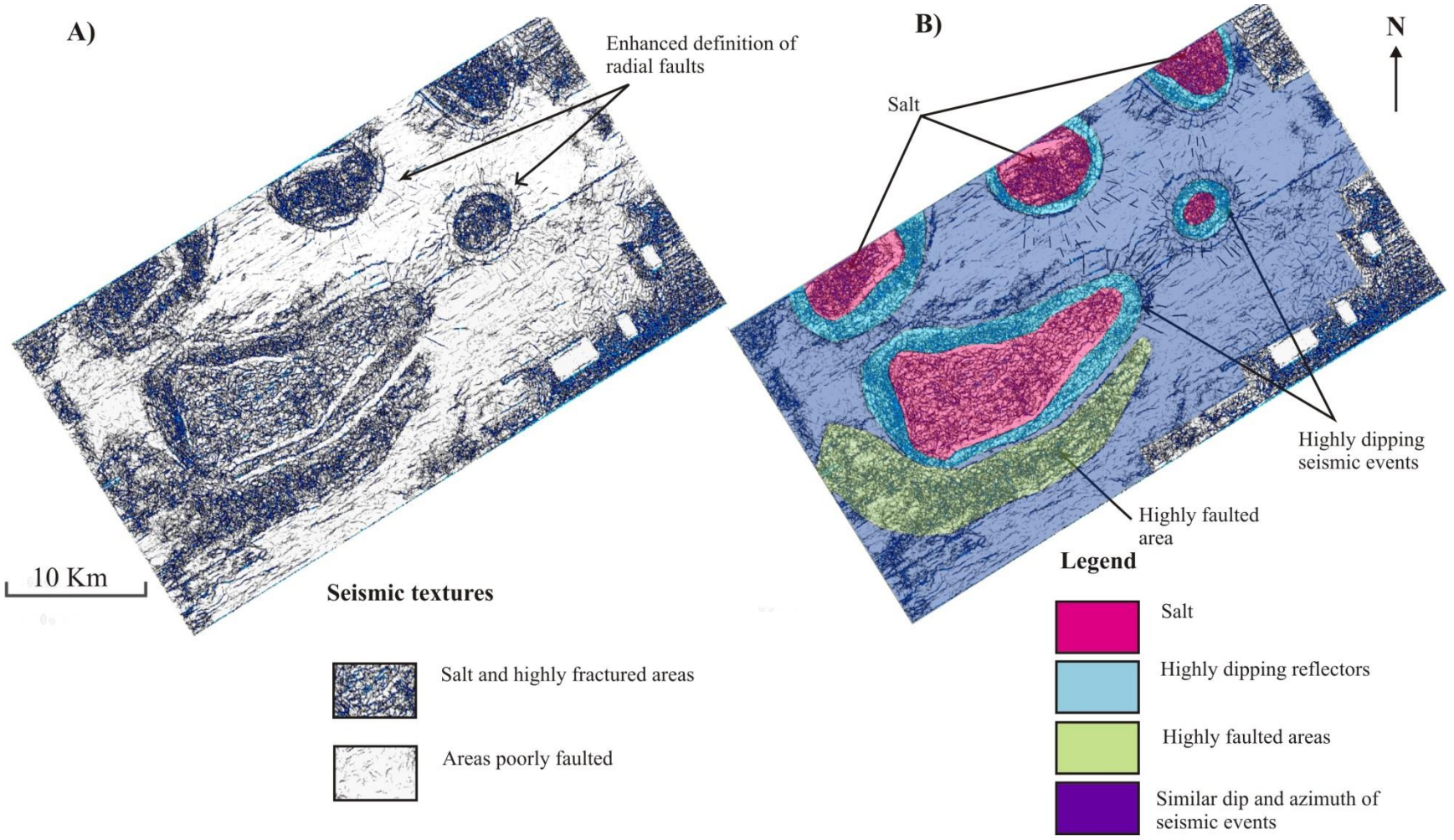

Figure 24. (A) Time slice analysis of the Ant-track cube. Notice that the definition of radial faults has been improved. (B) Interpretation highlighting areas with salt (red), highly dipping reflectors (light blue), highly faulted areas (green), and areas with similar dip and azimuth (purple)

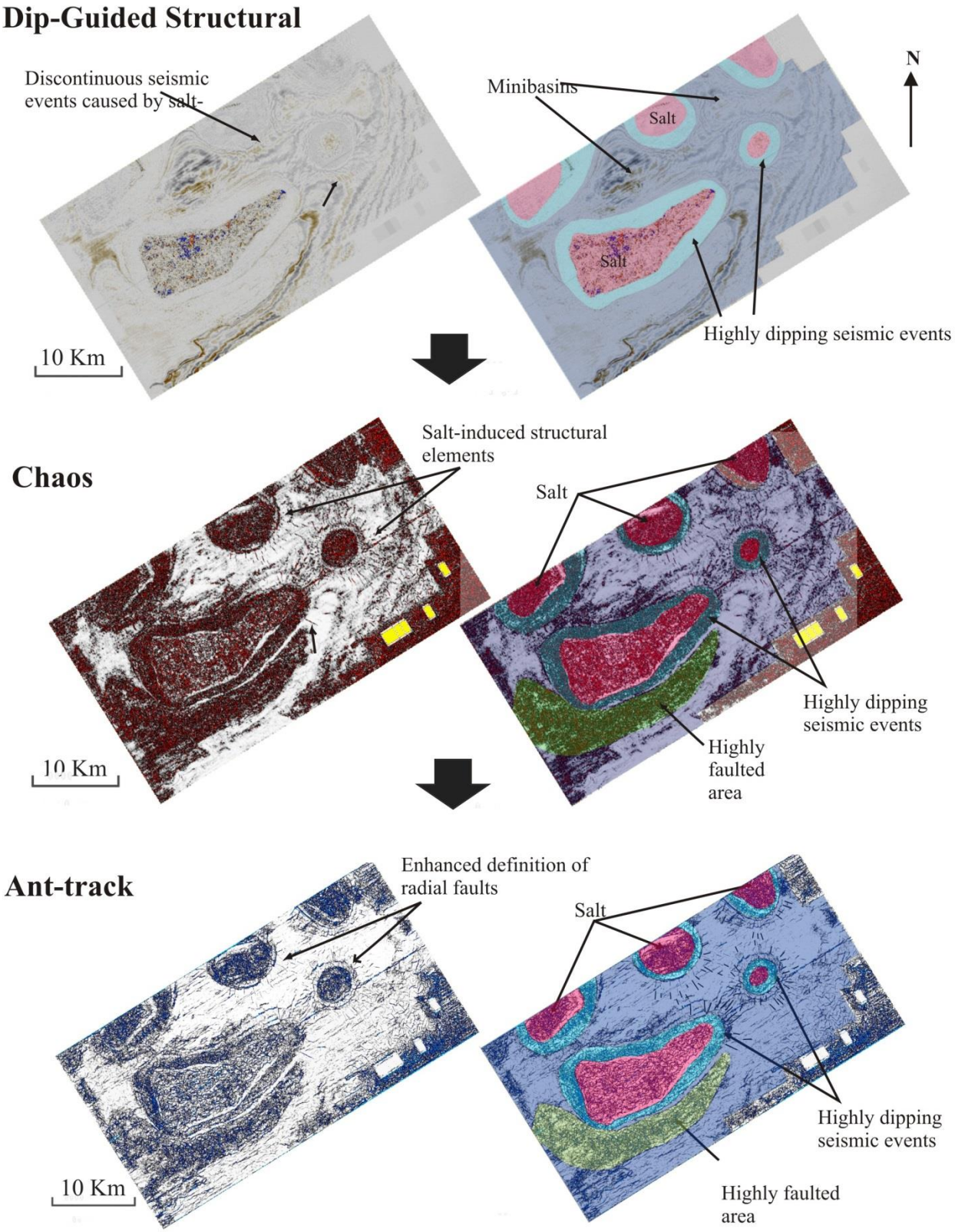

Figure 25. Summary structural workflow

4.4 Minibasin stratigraphy workflow

The stratigraphical analysis of salt minibasins provides valuable information about timing of salt movement and also describes the morphology of the structural and stratigraphic traps located adjacent to salt structures. Periods of salt diapirism are characterized by successions of growth strata bounded by unconformities at top and base. The analysis of the different strata terminations such as: onlaps, downlaps, and truncations, provides evidences of periods of diapirism well known as halokinetic sequences (Giles and Lawton, 2002; Giles and Rowan, 2012). However, these relationships between seismic events are located in areas of noise produced by poor reflection information acquired in areas close to salt. Therefore, the aim of this workflow is to provide the necessary seismic attributes that improve the detection of strata terminations and guide the interpretation in areas of uncertainty located close to salt structures.

Spectral Decomposition

In this process, the 3D cube is band-pass filtered using different frequency ranges. Each range of frequencies provides different seismic responses and therefore, this may help in terms of defining the main stratigraphic relationships. For this purpose, the seismic cube has been filtered using Ricker wavelets with different central frequencies (Cf): 40 Hz, 50 Hz, 60 Hz. The characteristics observed for each frequency are cited as follows (Fig.26):

Input Seismic (Cf=40 Hz) (Fig.26A). The first feature observable in the input seismic is the variability of reflection coefficient of the seismic events. This fact offers a general overview of the location of the main unconformities and the distribution of seismic facies. In total, eight different seismic facies have been identified based on different seismic and gamma ray (GR) responses (Escalona and Mann, 2006). Due to the lack of well data at deeper levels, the interpretation regarding depositional environments has been done using information from the regional geology of the southwestern Barents Sea (Worsley, 2008; Glørstad-Clark et al., 2010; Henriksen et al., 2011) (Fig. 27):

- Facies 1 (F1) composed by dominant semi-continuous, parallel, low amplitude seismic events with spontaneous intercalation of seismic events with higher amplitudes. GR character is defined as erratic for these facies. These seismic and GR responses correspond to marine homogeneous deposition of fine silicilastics with interruptions of sandstones bodies.
- Facies 2 (F2) composed by discontinuous, chaotic, inclined low amplitude seismic events with downlap strata terminations above unconformities. These chaotic bodies are onlapped and overlapped by continuous seismic events with higher reflection amplitudes. The GR ray response for these facies is defined as erratic as well. These characteristic seismic and GR responses are interpreted as wedge-shaped marine gravity flows such as debris flows, slumps, which are afterwards onlapped and overlapped by parallel marine sedimentation.
- Facies 3 (F3) characterized by inclined semi-continuous medium amplitude seismic events and a blocky and fining upwards GR signature. These facies are interpreted as wedge-shaped deltaic deposits developing high angle foresets
- Facies 4 (F4) is composed by continuous, irregular, medium-high amplitude seismic events, which laterally change to low amplitude seismic events. GR ray signature is defined as blocky with a fining upwards tendency. These characteristic seismic and GR responses correspond to fluvial or fluvio-

deltaic environments of deposition, where erosional surfaces are common and the deposition is very heterogeneous with sand and shale.

- Facies 5 (F5) is composed by high amplitude, continuous, and irregular parallel seismic events than become inclined at distal parts, developing downlap strata terminations above unconformities. They are interpreted as wedge-shaped alluvial fans or fandeltas that includes debris flows, sheet flows and channels.
- Facies 6 (F6) is composed by extremely high amplitude continuous and parallel seismic events. On the other hand, GR results display very high values. This high reflective pattern is typical of organic-rich shales encountered in the Barents Sea.
- Facies 7 (F7) is characterized by chaotic and broken seismic events with very high amplitudes that correspond to the presence of evaporates such us halite, anhydrite, gypsum, and intercalated carbonates.
- Facies 8 (F8) is composed by chaotic low amplitude seismic events at top and base by very high amplitude seismic events. This seismic response is interpreted to be typical from carbonates.

Dip-Guided Structural Smoothing + Frequency filter (Cf=50 Hz) (Fig. 26B). To improve the detection of truncations, Dip-Guided Structural Smoothing has been used to improve the continuity of dipping reflectors and remove noise. Afterwards, a Ricker wavelet of central frequency (Cf) of 50 Hz has been applied to obtain information from higher frequencies. The results display higher resolution of the seismic events, being possible to identify growth strata strongly truncated by angular unconformities, and the presence of downlap strata terminations.

Dip-Guided Structural Smoothing + Frequency filter (Cf=60 Hz) (Fig.26C). A Ricker wavelet of a higher center frequency (Cf) of 60 Hz can be used to refine the interpretation due to higher resolution of strata terminations at shallow levels. However, the information decreases from -2400 ms due to the attenuation of frequencies energy with depth. Therefore, this filter should be used for the interpretation at shallower levels.

Cosine of Phase

As shown in the previous section spectral filters are an appropriate tool for identifying the main strata terminations encountered in minibasins. However, there are areas adjacent to salt structures that still remain unsolved after the use of frequency filters. Figure (28A) displays the spectral filter result and highlights an area approximately 800 m wide characterized by sub-vertical seismic events with weak amplitudes. The stratigraphy in these areas is unsolved and to predict areas of drape folding where growth strata is strongly folded by diapirism, becomes the main challenge. To improve the interpretation in these areas, the attribute Cosine of Phase has been used in this study (Fig 28B). Cosine of phase is also called Normalized Amplitude because this attribute is insensitive to amplitude variations. Therefore, this attribute enhances the continuity of seismic events in these poorly solved areas of uncertainty located in the vicinity of salt structures. Consequently, it may provide evidences of drape folding of growth strata commonly located at 1km from salt structures (Giles and Rowan, 2012) .In addition, Cosine of Phase is an excellent indicator of seismic facies changes and strata terminations. Generally, three types of seismic facies have been encountered within the data set (Fig.28B):

- (1) Chaotic. This type is characterized by chaotic seismic events without any kind of continuity. Thus, it might be related to chaotic deposits without layering as salt, marine debris flows or alluvial fans
- (2) Semi-continuous or faulted. The continuity of the seismic events is continuously interrupted by probably small faults
- (3) Continuous. The seismic events do not show any disturbance and can be easily followed.

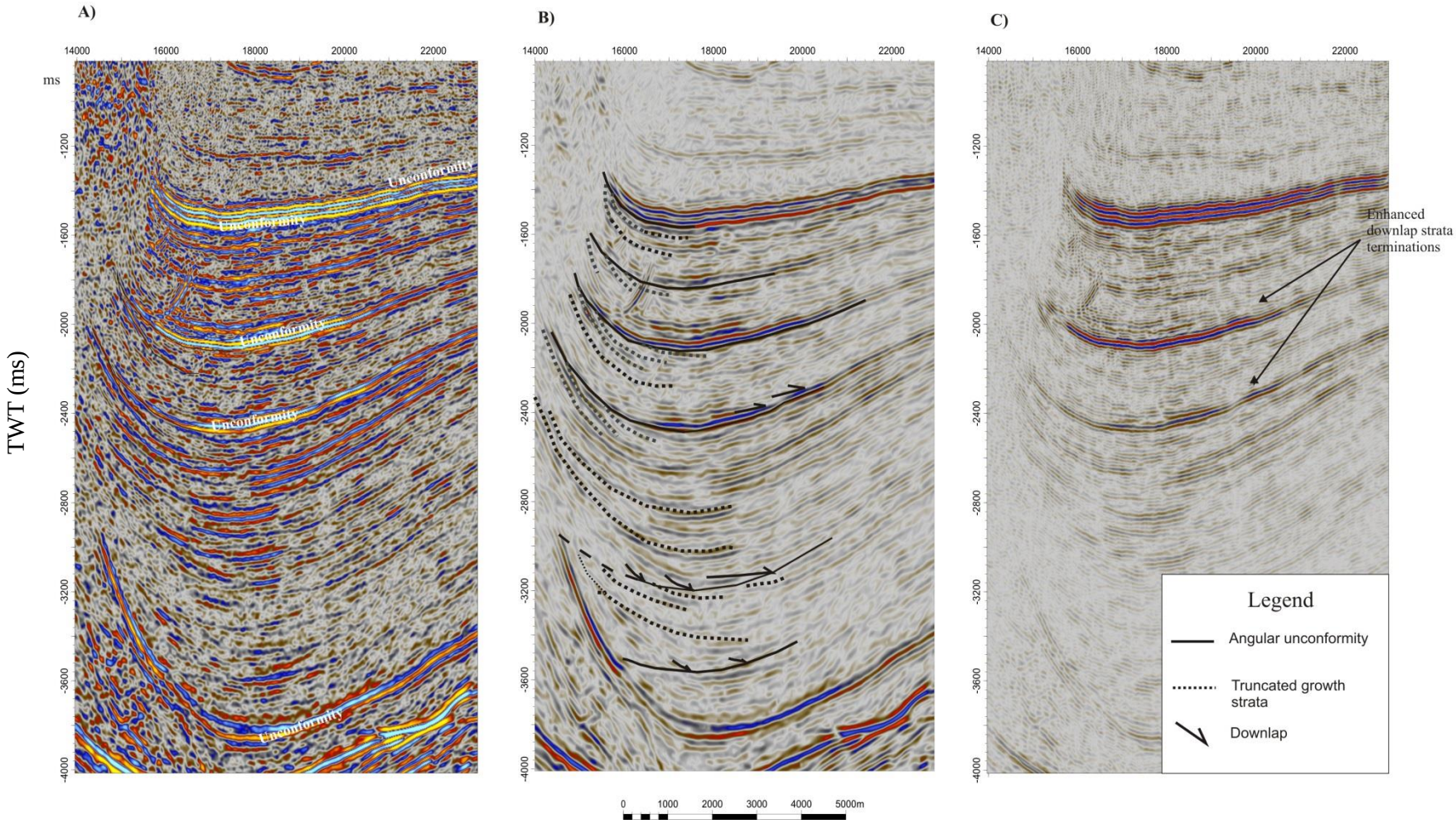

Figure 26. Spectral Decomposition. (A) Input seismic (cf=40 Hz). (b) Frequency filter (cf=50 Hz) displays a better resolution of strata terminations and the presence of growth strata. (C) Frequency filter (cf=60 Hz) displays higher resolution at shallower levels. Notice the loss of high frequencies at deeper levels.

Seismic Facies	Seismic reflection characteristics	Gamma-ray (GR) log pattern from well 7228/7-1A	Gamma-ray (GR) description	Interpretation	Examples of seismic facies in the Nordkapp Basin
F1	Dominant semi-continuous parallel low amplitude seismic events with spontaneous intercalations of medium to high amplitude seismic events		Erratic	Deep marine environment with a homogeneous dominant deposition of shales causing low reflection amplitudes. Medium to high amplitude might be produced by the presence of sandstone bodies embedded within shales.	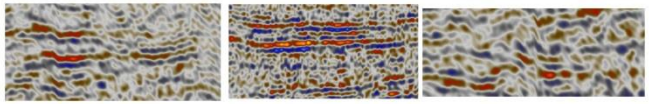
F2	Discontinuos, chaotic, inclined low amplitude seismic seismic events producing downlaps. Presence of higher amplitude seismic events onlaping the previous chaotic low amplitude seismic events.			Wedge-shaped marine gravity flows, debris flows, slumps onlaped by parallel marine sedimentation.	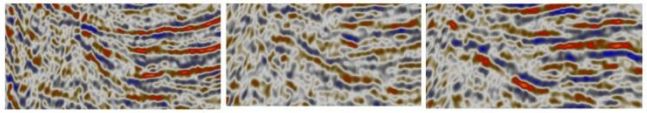
F3	Inclined semi-continuous middle amplitude seismic events . Presence of higher amplitude seismic events onlaping the previous chaotic middle amplitude seismic events.	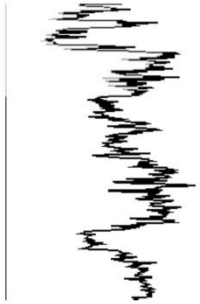	Blocky and fining upward	Wedge-shaped deltaic deposits develping high angle foresets	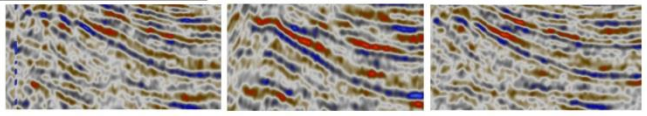
F4	Continuous, irregular, medium-high amplitude seismic events. They can gradually change to continuous low amplitude seismic events			Fluvio-delatic environment of deposition with commonly formed erosional surfaces and heterogeneous sand and shale sedimentation. It can laterally changes to areas with homogeneous shale sedimentation causing lower amplitudes.	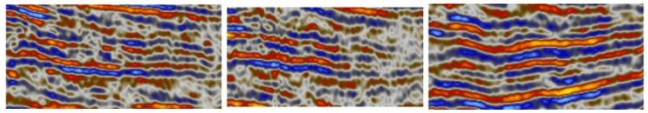
F5	High amplitude, continuous, and irregular incline seismic events developing downlaps and being onlapped and overlapped by lower amplitude seismic events. The base is normally a very high amplitude event			Wedge-shaped aluvial fans or fan deltas that includes debris flows, sheet floods, and channels	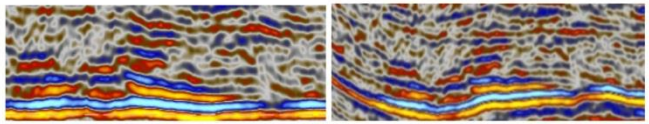
F6	Very high amplitude continuous and parallel seismic events		Insolated large spikes	Marine organic-rich shales	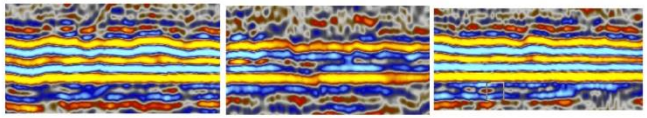
F7	Chaotic, discontinuous seismic events with very high amplitudes	Lack of well data		Salt probably composed by anhydrite, halite, gypsum, and intercalated carbonates.	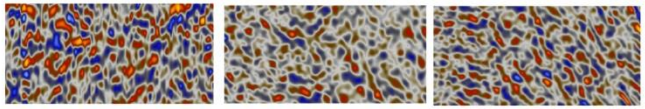
F8	Chaotic seismic events bounded by high amplitude seismic events at the top and base.	Lack of well data		Carbonates.	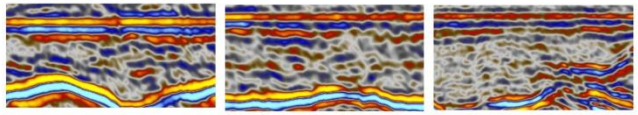

Figure 27. Seismic facies table based on seismic responses and Gamma-ray information. (Base on Escalona and Mann, 2006).

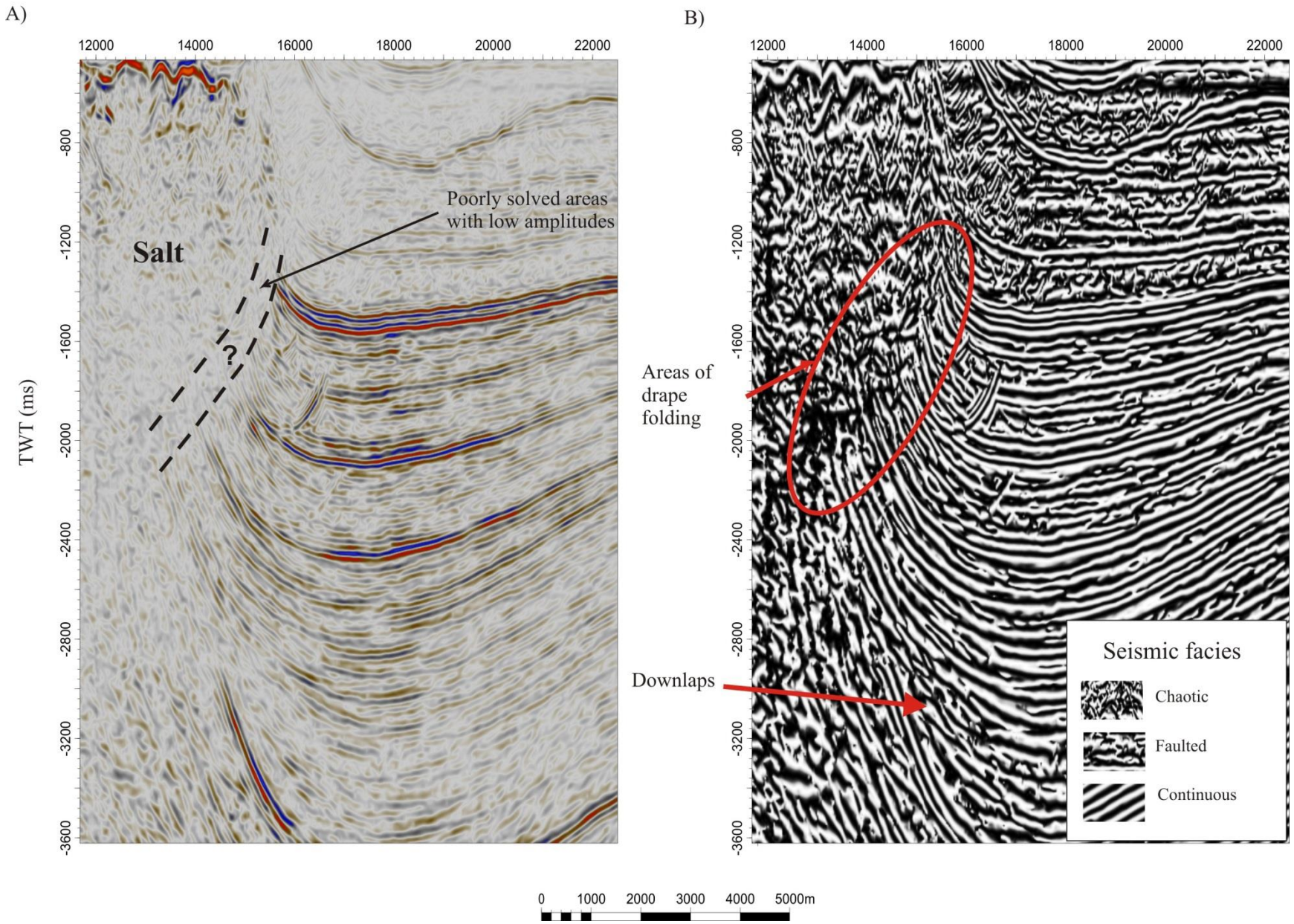

Figure 28. (A) Frequency filter (cf=50 hz) displaying areas of low amplitude poorly solved seismic events. (B) Cosine of Phase enhances the continuity of the reflectors in those areas and provides a better resolution of the drape folding.

5. Observations and interpretations based on attribute workflows

5.1 Salt structures

The mapping of salt structures has been carrying out by the previously discussed attribute workflow Dip Guided Structural Smoothing, Dip-Illumination, and Variance. Salt mapping results display the 3D configuration of the Permian salt, striking towards the NE and changing its geometry along that direction (Fig.29). Three types of salt structures have been identified:

- **Salt wall** is the largest salt structure of the data set, being approximately 14 km long and 6 km wide (Fig.29 and 30). Generally, the salt wall shows a triangular base that reduces its width from 10 km to an area of 2 km width called the neck. Areas located above the neck increase their width considerably until reaching almost the sea floor. Salt widening occurs normally at shallow areas approximately from 2500 ms and it is mainly observed towards the southwest (Fig.29).
- **Salt roller**. The salt wall develops laterally to a salt roller (Fig. 29 and 31). This structure shows triangular shape and the steepest flank works as a normal fault. In this case, salt was not able to migrate upwards and is being covered by approximately 2000 ms of sediments.
- **Salt sock**. The salt roller converts laterally to a salt stock (Fig.29 and 32). This structure shows a triangular base located between 2500 ms and 3500ms. Upwards, the structure develops an elongate and constant neck of approximately 2 km width. The main widening of the salt occurs from 1500 ms, reaching widths of 3,5 km.

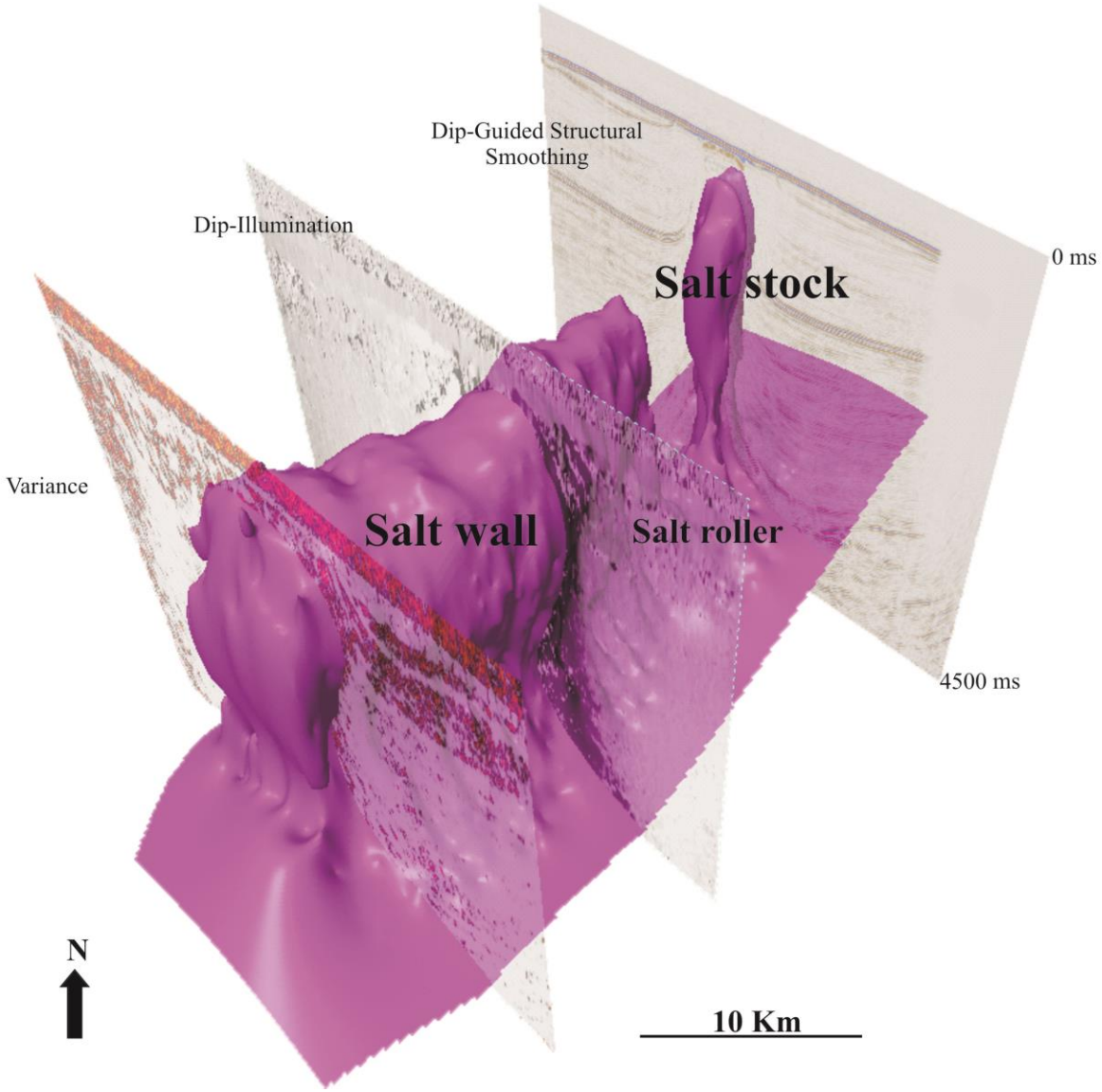

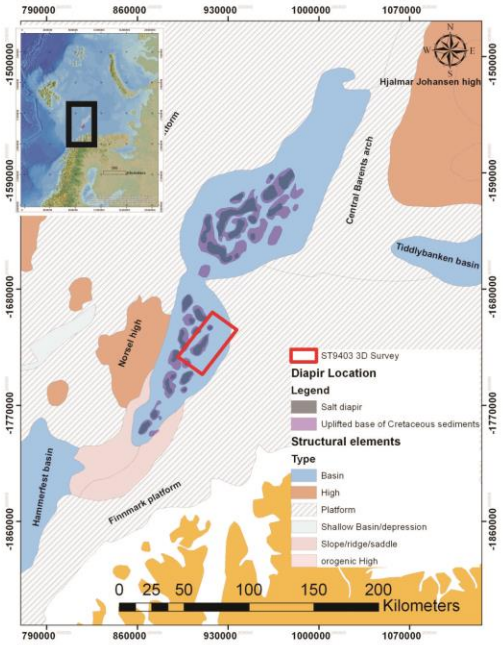

Figure 29. 3D configuration of Permian salt in the data set. Notice how the salt layer changes its geometry towards the NE. Three salt structures have been identified: salt wall, salt roller, and salt stock.

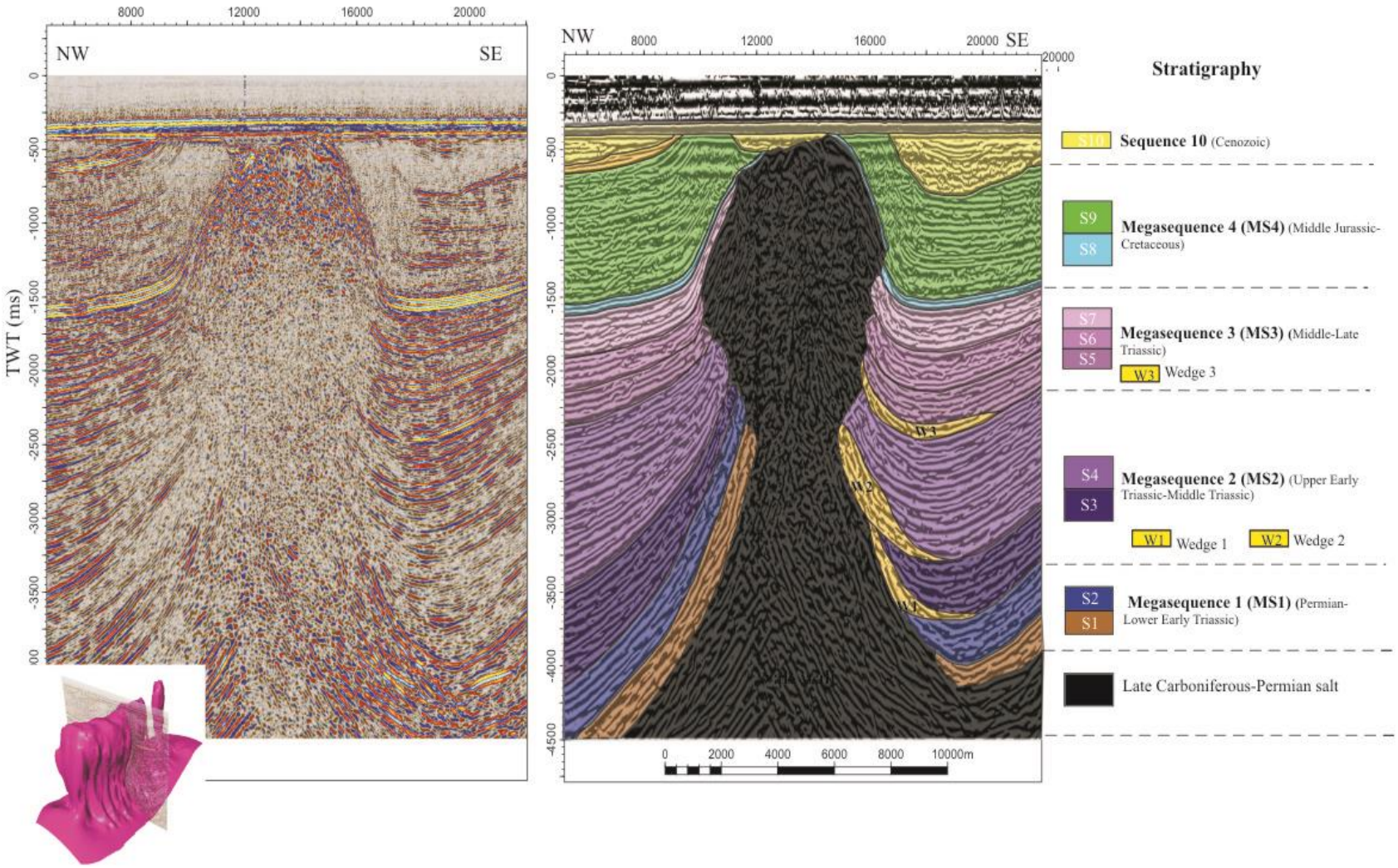

Figure 30. (Left) Cross-section of the input seismic through the salt wall. (Right) Cross-section of Cosine of Phase showing the salt wall and minibasin interpretations.

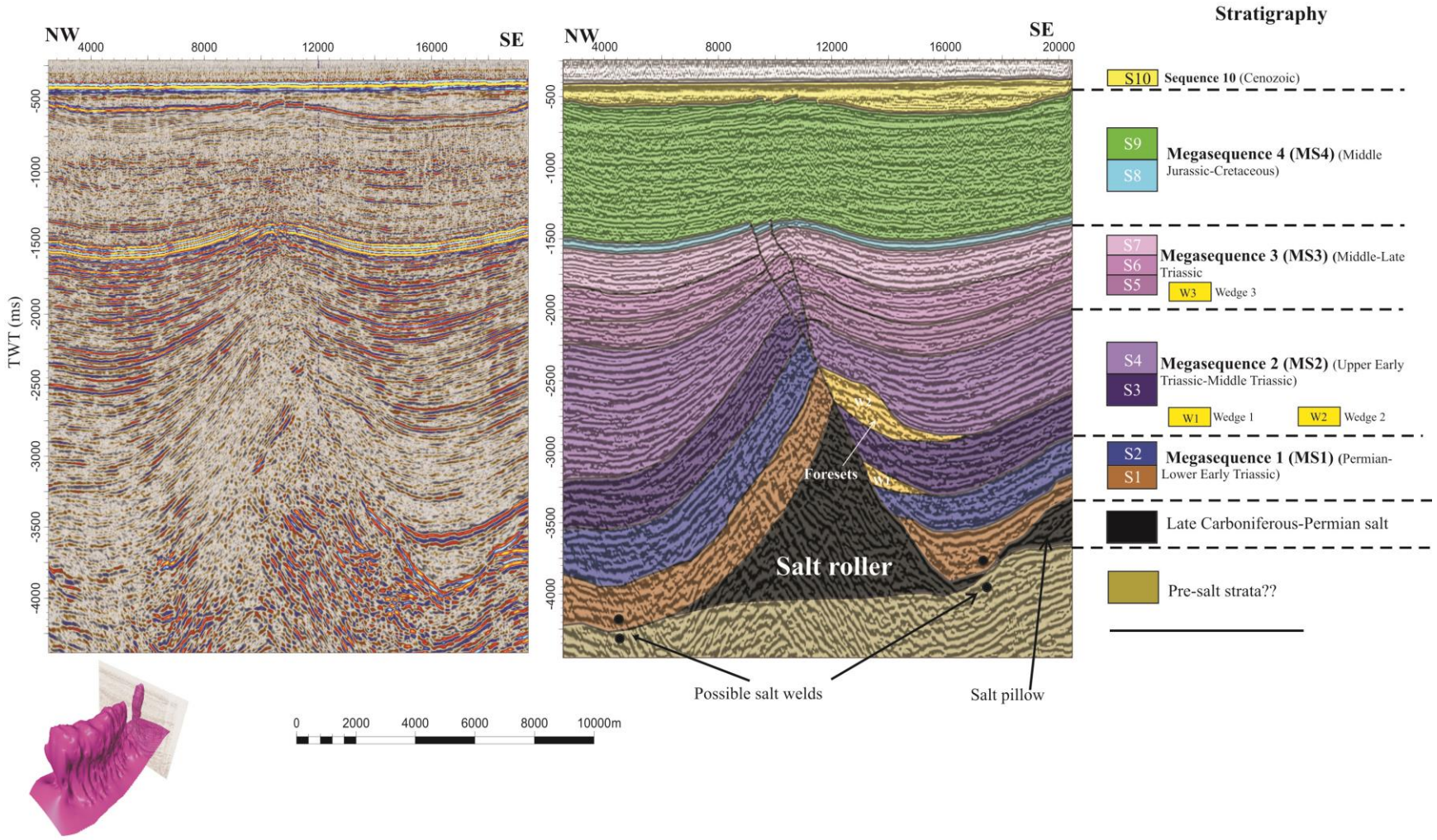

Figure 31. (Left) Cross-section of the input seismic through the salt roller. (Right) Cross-section of Cosine of Phase showing the salt roller and minibasin interpretations

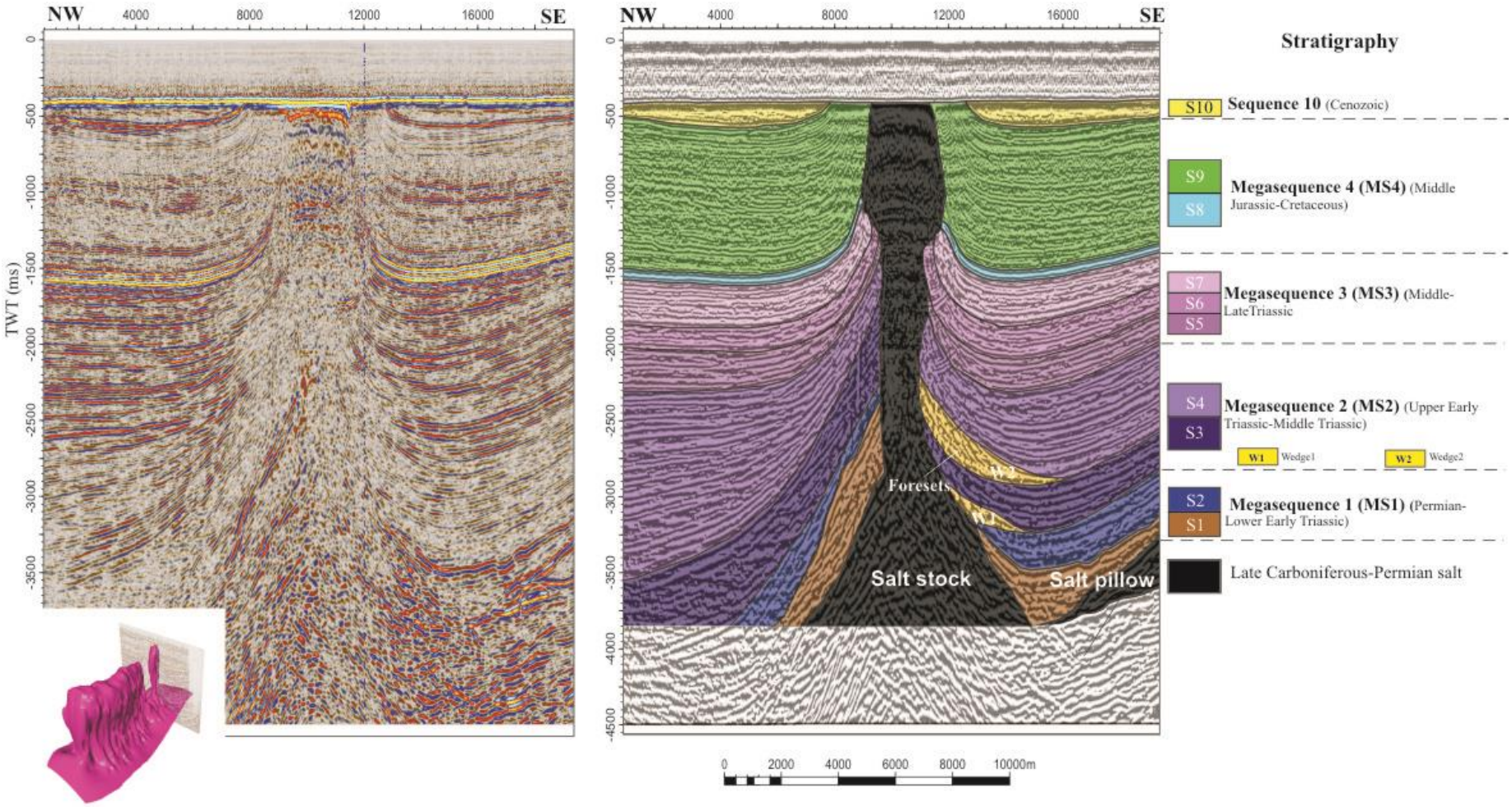

Figure 32. (A) Cross-section of the input seismic through the salt stock. (B) Cross-section of Cosine of Phase showing the salt stock and minibasin interpretations.

5.2 Minibasin stratigraphy

The used of frequency filters and Cosine of phase have demonstrated to be important tools to identify the main strata terminations and unconformities in the dataset. In total, ten post-salt sequences have been identified in the surrounding minibasins. The sequences that show similar stratigraphic and structural characteristics such as thickness variations, presence of growth strata, and structural elements, have been grouped into megasequences, reaching a total of four. The distribution of the four megasequences and their corresponding sequences around the different salt structures are mainly shown by the Figures 30, 31, and 32.

Megasequence 1 (MS1): Permian – Lower Early Triassic

General

The MS1 represents the oldest post-salt megasequence and is bounded by two strong seismic events defined as unconformities. The basal unconformity represents the Early Permian salt and the top unconformity is defined as the top of the Lower Early Triassic. Two main sequences have been identified within Megasequence 1: sequence 1 (S1) and sequence 2 (S2). Each sequence is mainly characterized by small thickness variations and absence of growth strata (Fig.30, 31, and 32).

Seismic analysis

The Permian sequence (S1) is characterized by chaotic seismic events interpreted as Permian carbonates (Facies 8) (Fig.33). This period is bounded by two high impedance unconformities. The basal unconformity represents the interface between carbonates of Facies 8, and chaotic high amplitude seismic events that correspond to Permian salt (Facies 7). On the other hand, the top unconformity is represented by the interface between carbonates and semi-continuous, parallel, low amplitude events from the Early Triassic (Facies 1). Truncations associated with active tectonism are not identified in this period.

The Early Triassic sequence (S2) exhibits semi-continuous, parallel, low amplitude seismic events interpreted as deep marine environment with dominant fine grain siliciclastics and some embedded sandstones bodies represented as medium amplitude seismic events (Facies 1) (Fig.33). Truncations become dominant in areas adjacent to salt structures, providing possible evidences of salt tectonics at the end of this period.

Structural analysis

The basal unconformity of MS1 has been flattened to search for salt-related structural elements. Ant-track results display highly distorted areas located towards the northwest. However, areas located close to salt structures do not show the presence of salt-related structural elements (Fig.34A).

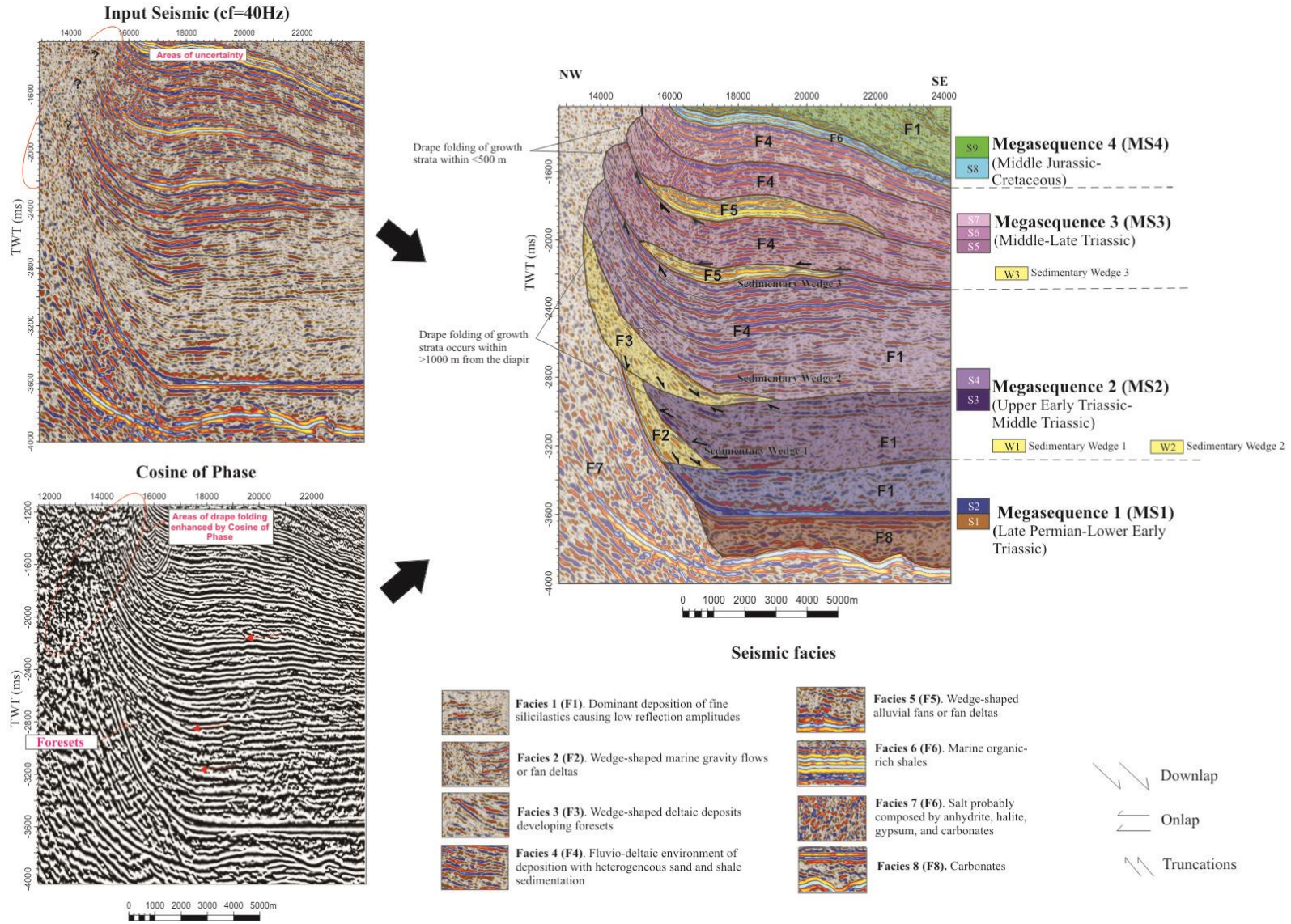

Figure 33.Seismic analysis results based on the combination of input seismic and Cosine of Phase. Seismic input provides the main information about seismic facies while Cosine of Phase enhanced the visualization of drape folding and helps the identification of sedimentary wedges.

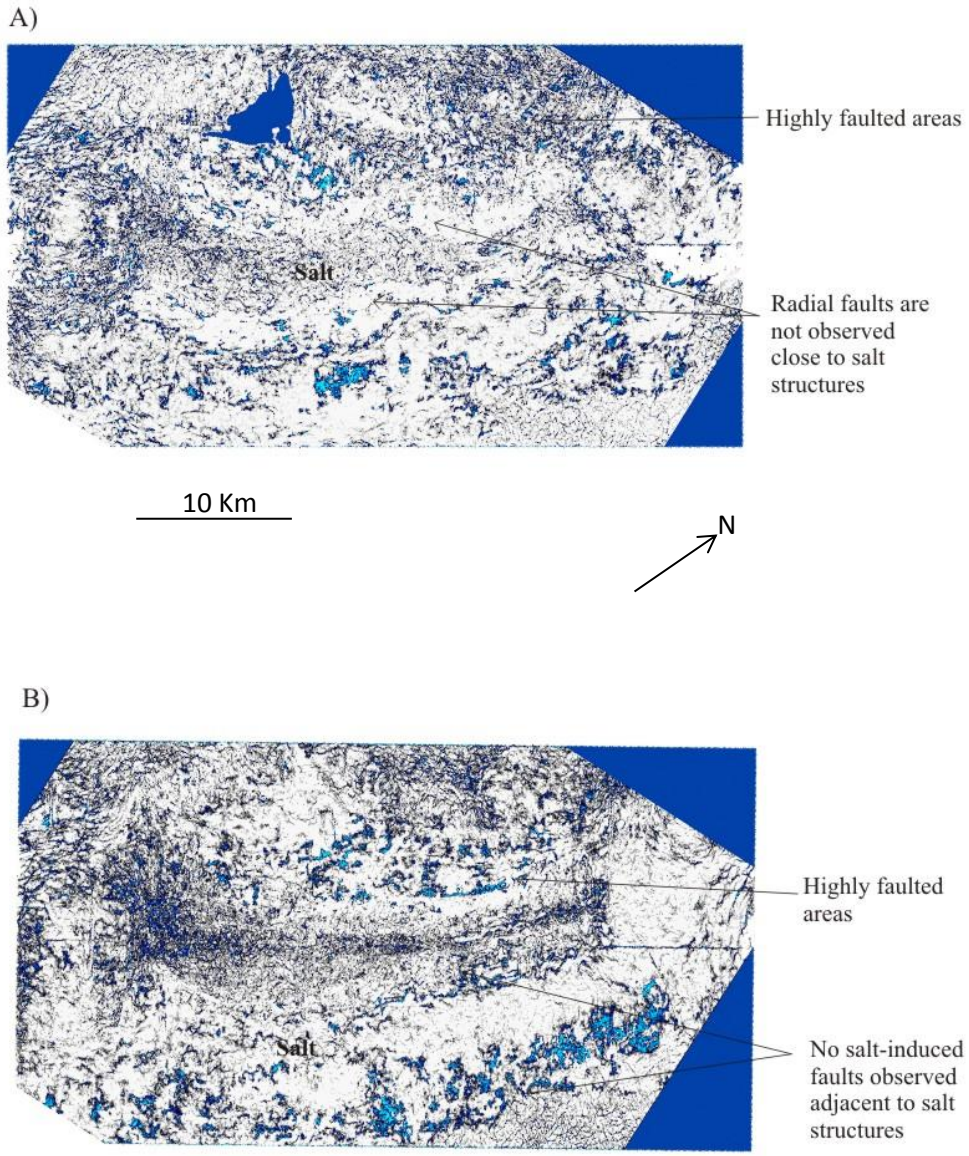

Figure 34. (A) Ant-track results for MS1. (B) Ant-track results for MS2

Megasequence 2 (MS2): Upper Early Triassic – Middle Triassic

General

Megasequence 2 (MS2) is bounded by two strong events located at the top and at the bottom. Base Landinian (Middle Triassic) represents the top unconformity, and the previous top lower Early Triassic is defined as the basal unconformity. Two main sequences have been identified within Megasequence 2: sequence 3 (S3) and sequence 4 (S4). Each sequence is characterized by strong thickness variations, presence of growth strata and sedimentary wedges, and abundance of truncated seismic events towards salt structures (Fig.30, 31, and 32).

Seismic Analysis

- Sequence 3 (S3) (Fig.33). This period is characterized by the presence of semi-continuous low amplitude reflectors (Facies 1) interpreted as marine fine silicilastics. The abundance of medium-high seismic events increases towards salt structures, indicating a more heterogeneous sedimentation. Facies 1 changes horizontally and towards the diapir to Facies 2. It consists of discontinuous, chaotic, inclined seismic events, which develop downlaps strata terminations at the basal unconformity. These characteristic seismic responses are interpreted as wedge-shaped marine gravity flows and it will be named as sedimentary wedge 1. This sedimentary wedge has been only identified in the southeastern flank of the salt structure, being important characteristics to take into consideration for the discussion. Finally, Cosine of Phase results display the drape folding of growth strata occurring approximately 1,5 km from the diapir, developing 50-30 degrees truncations.

- Sequence 4 (S4) (Fig.33). The basal part is represented by marine fine silicilastics of previous Facies 1. Laterally and towards salt structures, Facies 1 changes to Facies 3 defined as wedge-shaped deltaic deposits and named as sedimentary wedge 2. A difference with the previous wedge. Cosines of Phase results display the development of high angle foresets, being a characteristic feature of this wedge (Fig.32). It is important to notice that sedimentary wedge 2 is just encountered in the southeastern flank of the salt structures as well. Shallower levels in this sequence display medium-high continuous seismic events of Facies 4 interpreted as shallow marine or fluvio-delatic environments of deposition. Horizontally, the presence of Facies 4 increases towards salt structures and changes laterally to Facies 1 in areas further from salt. Cosine of phase results indicate that, drape folding of growth strata occurs within 1-1,5 Km, developing high angle truncations from 90 to 30 degrees.

Thickness analysis

Horizontal distribution of depocenters

Generally, the largest thicknesses and thickness variations are located in the northwestern flank, where growth strata is strongly thinned towards salt diapirs (Fig.35A):

- The first depocenter is located on the northwestern flank of the salt stock and shows a maximum thickness of 2100 ms, decreasing dramatically to 600 ms towards the salt stock. This depocenter is relatively small, extending approximately 5 km long and 5 km wide.
- The second depocenter is located on the northwestern flank of the salt wall and exhibits a maximum thickness of 2100 ms that decreases to 1200 ms towards the salt wall. This depocenter follows the same dimensions than the salt wall, extending around 10 km towards the NE and 5 Km towards the SE.
- The third depocenter is located in the frontal part of the salt wall. It shows a maximum thickness of 1900 ms that decreases rapidly within 1 km towards the east due to the presence of a normal fault striking NW-SE.
- The fourth depocenter is located in the southeastern part of the salt wall. It displays a maximum thickness of 1700 ms that decreases dramatically to 700 towards the salt wall. However, thickness decreases gradually towards the northeast. This depocenter follows the same dimensions of the salt wall, extending 12 km long and 5 km wide.

Vertical distribution of depocenters

During the deposition of Megasequence 2, a vertical migration of depocenters occurred between its sequences. It is observed that the depocenter of sequence 4 is slightly displaced towards the northwest respect to the depocenter of sequence 3 (Fig.36).

Sedimentary wedges 1 and 2

Two sedimentary wedges have been previously observed based on seismic facies characterization and strata terminations. Thickness maps have been carried out to localize the extension and the main depocenters of these sedimentary wedges:

The sedimentary wedge 1 located in Sequence 3 extends to approximately 20 km, being present just in the southeastern flank of the structures (Fig.37A). The main depocenters are located in the vicinity of the salt wall, where two fan-shape depocenters have been identified in the figure:

- The southwestern most depocenter extends 3 km along the salt wall and 2 Km perpendicularly. Maximum thicknesses ranges from 180 and 150 ms.
- The second depocenter displays larger dimensions, extending 10 km along the salt wall and 3 km in the perpendicular direction. Maximum thickness ranges from 180 to 150 ms, decreasing gradually to outside areas.

The sedimentary wedge 2 located in Sequence 4 extends approximately 20 km and is present just in the southeast flank of the salt structures (Fig.37B). It shows higher thickness than the previous wedge, displaying a maximum thickness of 480 ms in areas adjacent to salt structures. The thickness decreases gradually within a distance of 5 km towards the southeast. Additionally, three fan-shaped depocenters have been observed:

- The largest fan-shaped depocenter is located towards the south and follows the same dimensions as the salt wall, extending 12 km approximately. It displays a maximum thickness of 450 ms that decreases gradually towards the northeast and dramatically towards the southwest.

- The second fan-shaped depocenter is located at the end of the salt wall. It shows smaller dimensions than the previous one, being 2,5 km long and 2,5km wide. Maximum thickness ranges from 350 to 300 ms
- The third fan-shaped depocenter is located besides the salt stock. It extends 3 km long and 2,5 km wide. Maximum thickness ranges from 250 to 200 ms

Structural analysis

The basal unconformity of Megasequence 2 has been flattened to search for structural elements using Ant-track. As in the previous Megasequence 1, this period does not display mayor salt-related structural elements adjacent to salt structures (Fig.34B).

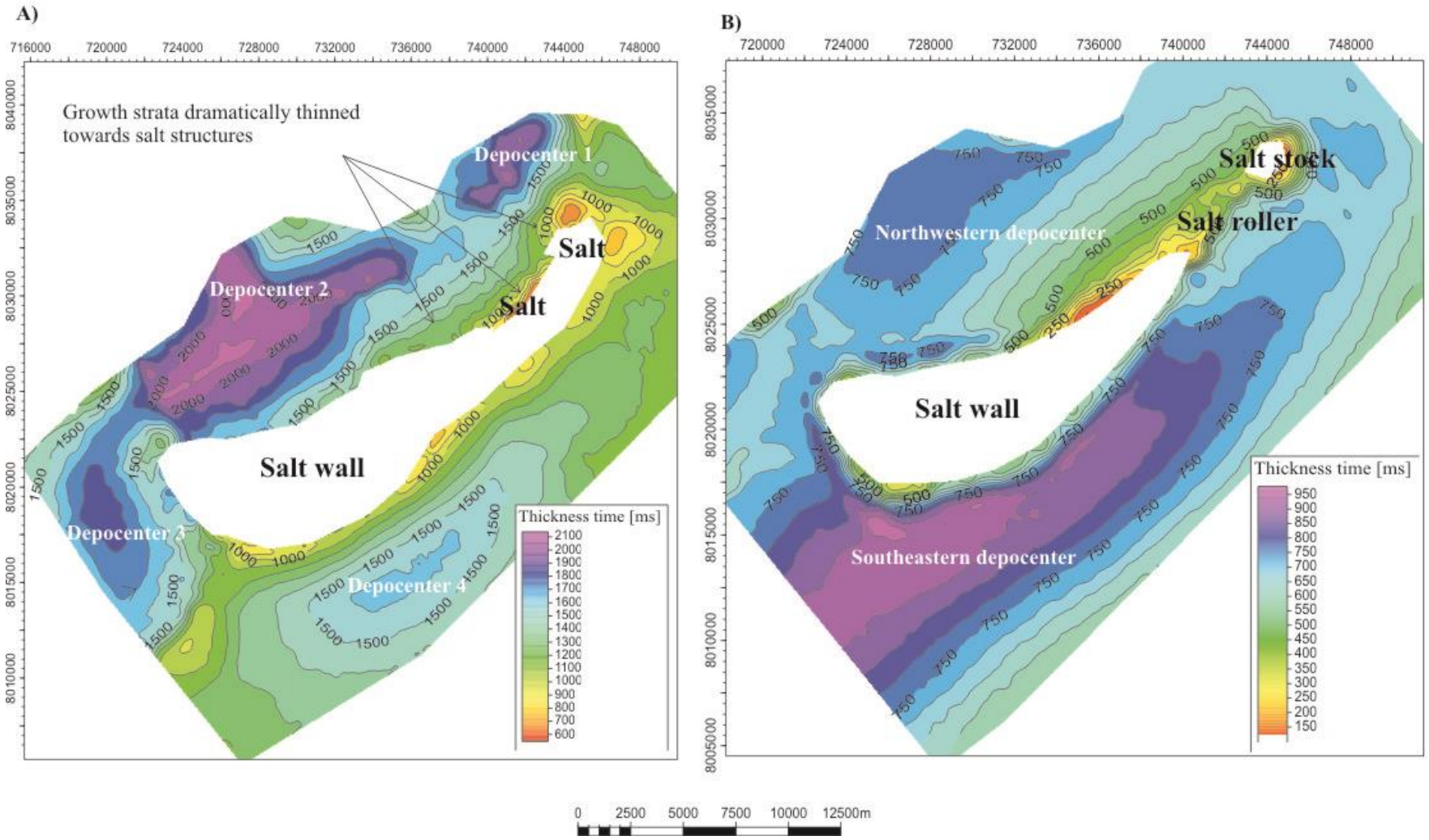

Figure 35. (A) Thickness map of Megasequence 2 (MS2). (B) Thickness map of Megasequence 3 (MS3).

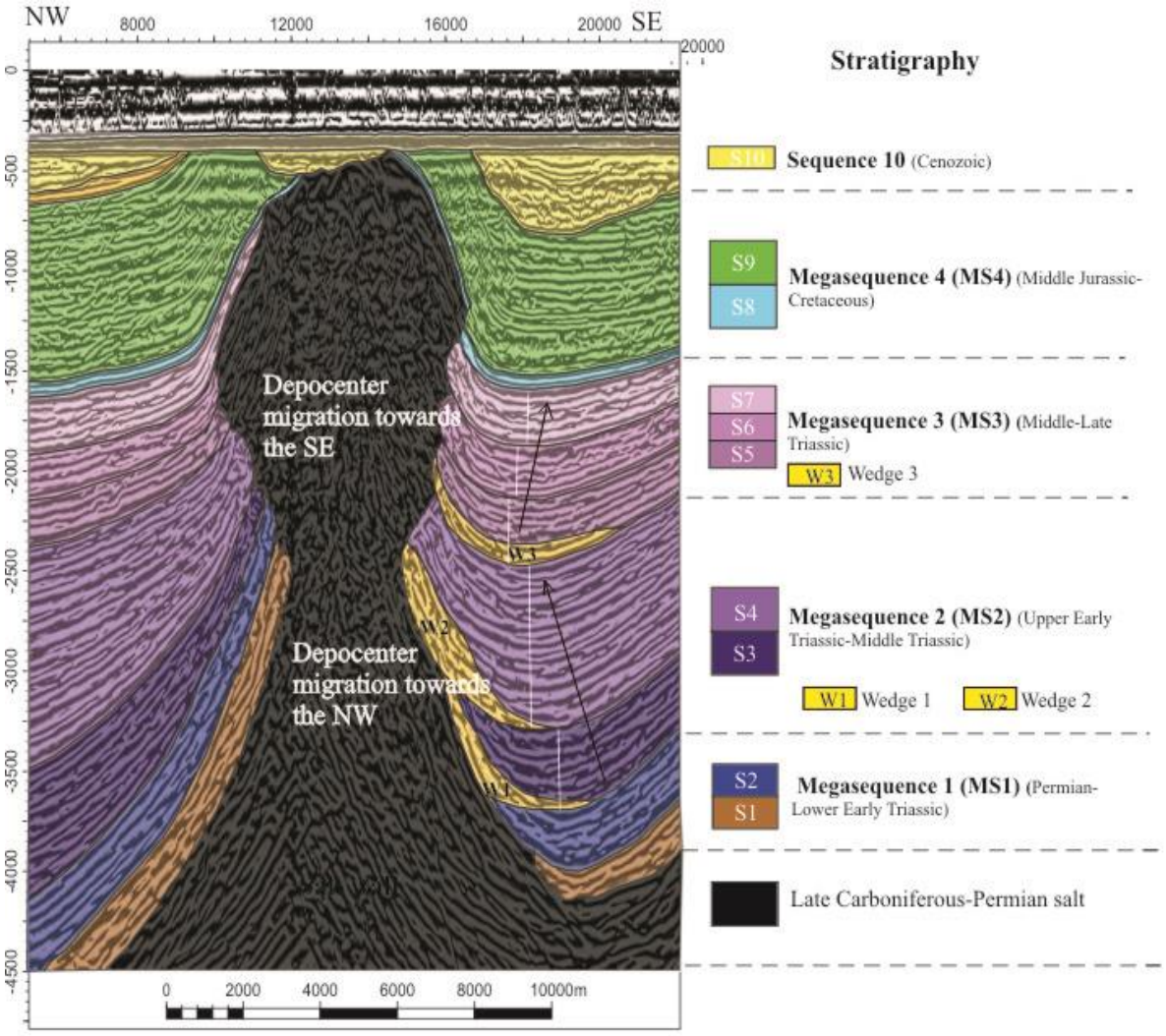

Figure 36. Vertical depocenter migration during the Triassic period.

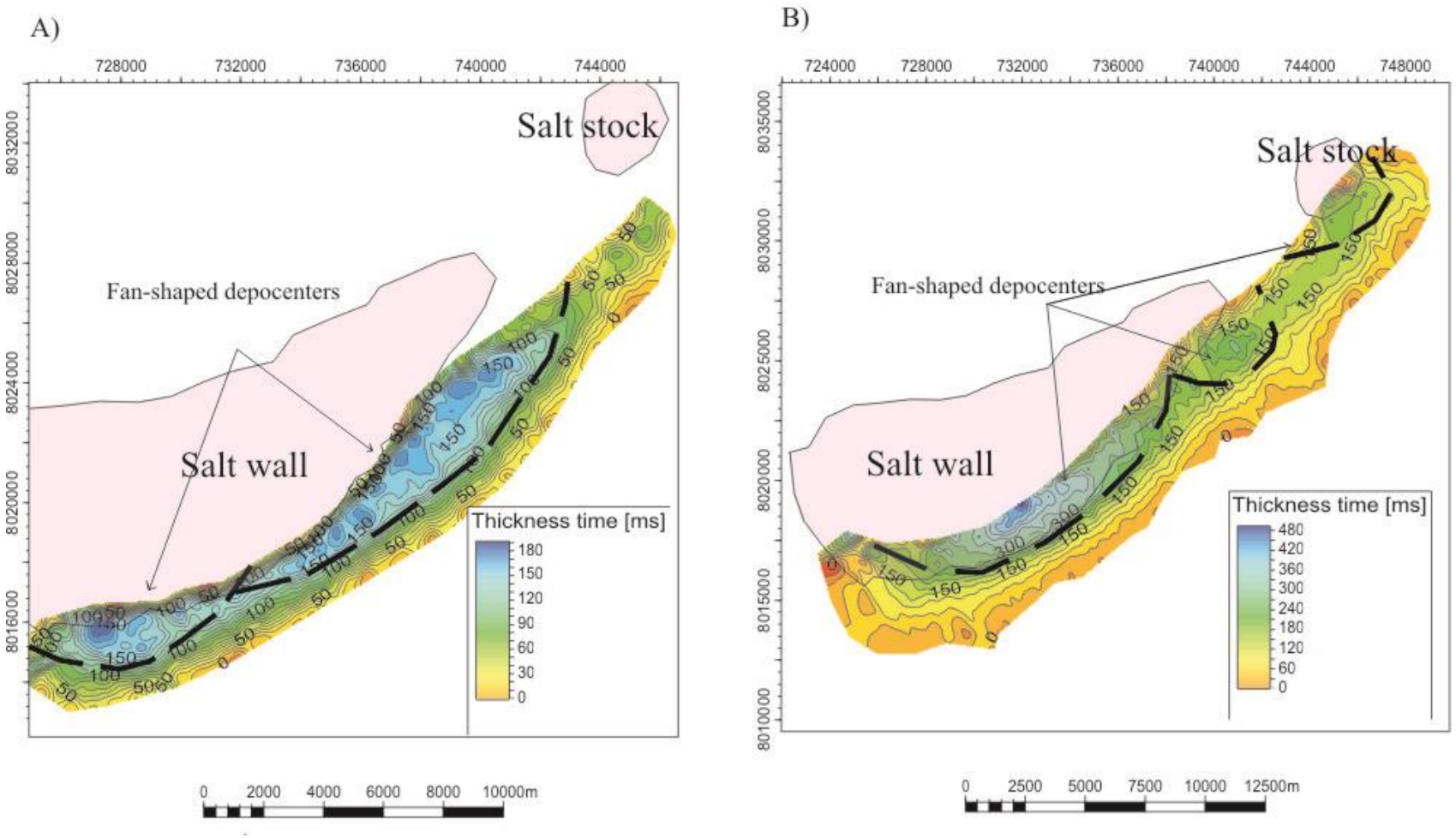

Figure 37. (A) Thickness map of sedimentary wedge 1. (B) Thickness of sedimentary wedge 2

Megasequence 3 (MS3) – Middle-Late Triassic

General

The Middle Triassic- Late Triassic megasequence is bounded by two high amplitude unconformities. The basal unconformity is represented by the previously discussed base Landinian (Middle Triassic) and, the top unconformity corresponds to the base of the Middle Jurassic. Three main sequences have been observed during the Middle Triassic-Late Triassic period. Each sequence is mainly characterized by the presence of truncations and growth strata indicating a possible salt-controlled sedimentation (Fig.30, 31, and 32).

Seismic analysis

- Sequence 5 (S5) (Fig.33). This sequence is mainly characterized by the presence of high-medium amplitude, semi-continuous, and irregular seismic events defined as fluvio-delatic environments of Facies 4. The frequency of high amplitude seismic events increases to the top, indicating shallower environments of deposition. On the other hand, the presence of high amplitude reflectors decreases towards outside areas from salt structures and becomes into low amplitude, semi-continuous, seismic events of Facies 1, indicating a more homogeneous sedimentation. In addition to Facies 1 and Facies 4, Facies 5 is also present at the base of this sequence and adjacent to salt structures. It is characterized by very high amplitude reflectors that develop downlaps at distal parts, being interpreted as wedge-shaped alluvial fans or fan deltas. Facies 5 is observed in the vicinity of the salt wall, but it is not present close to the salt stock and roller (Fig.31 and 32). Finally, growth strata located within 500 m distance from salt, is affected by an strong drape folding, developing 90 degrees and even overturned truncations.
- Sequence 6 (S6) (Fig.33). This sequence has similar seismic characteristics than the previous one. The presence of Facies 4 increases vertically and towards the salt structures. Facies 1 is mainly concentrated in distal areas from the salt. Facies 5 represented by wedge-shaped seismic features is encountered in the basal unconformity. This wedge located in this period, changes laterally very fast and it was not possible to map it for future thickness maps. Finally, areas located at 500 m from the diapir, display a dramatic drape folding of growth strata that generates truncations that might be overturned.
- Sequence 7 (S7) (Fig.33). This period is dominated by fluvio-deltaic of Facies 4 with more frequent high amplitude events to shallower areas. Truncations are present and growth strata are folded within an area of 500 m.

Thickness analysis

Horizontal distribution of depocenters

According thickness maps, MS3 displays smaller thickness variations compared to the previous MS2, ranging from 100 to 950 ms (Fig.35B):

- The northwestern depocenter extends along the salt wall, being approximately 6 km long and 4 km wide. The maximum thickness is 750 ms, decreasing gradually down to 250 ms towards the salt wall.

- The southeastern depocenter has an elongated shape, extending approximately 14 km along the salt wall and has a width of 4 km. Thickness variations occur gradually from 750 to 950 ms

Vertical distribution of depocenters.

During Megasequence 3, deponcenter migration occurs in the opposite direction with respect to the previous period. Depocenter migration toward the southeast is observed between sequences 5, 6, and 7, (Fig.36).

Sedimentary wedge 3

Previous seismic analyses demonstrate the presence of two seismic wedges located in sequences 5 and 6. However, the wedge located in sequence 6 changes rapidly laterally, being of minor interest for mapping because of its small size. However, wedge number 3 shows a larger extension and therefore, it has been mapped (Fig.38). This sedimentary wedge is just present in the southeastern flank of the salt wall. It extends up to 8km and has a width of 5 km. Furthermore, it exhibits a large fan-shaped depocenter with a maximum thickness of approximately 200 ms that reduces gradually towards outside areas from the diapir.

Structural analysis

The previously developed attribute workflow for detecting salt related structural elements has been run for each sequence within MS3 with the aim of detecting salt-induced structural elements (Fig.39)

- Sequence 5 (Fig.39A). This period does not show major structural elements. Some minor faults with unclear origin are located around the salt stock and salt wall.
- Sequence 6 (Fig.39B). Generally, areas adjacent to salt structures do not show distinctive features on the attribute time slices. Minor faults are located around the salt stock and the salt wall. However, it is unclear if these faults are related to halokinesis. Northeast striking faults are observed in the southwestern part, being probably associated with a diapir which is outside of the dataset.
- Sequence 7 (Fig.39C). As in previous sequences, areas adjacent to salt structures are poorly faulted. However in this period radial faults become easier to observe around salt structures.

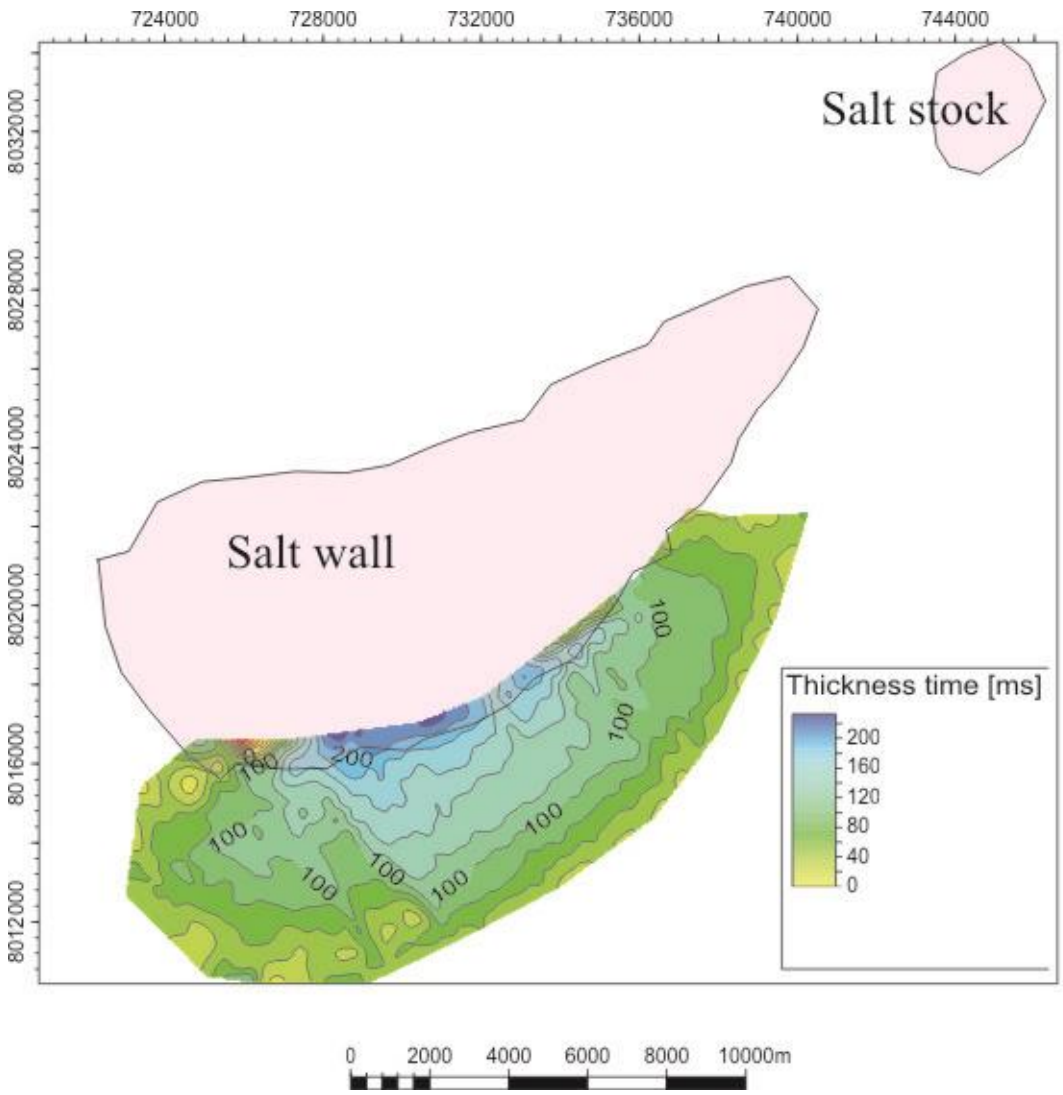

Figure 38. Thickness map of sedimentary wedge 3

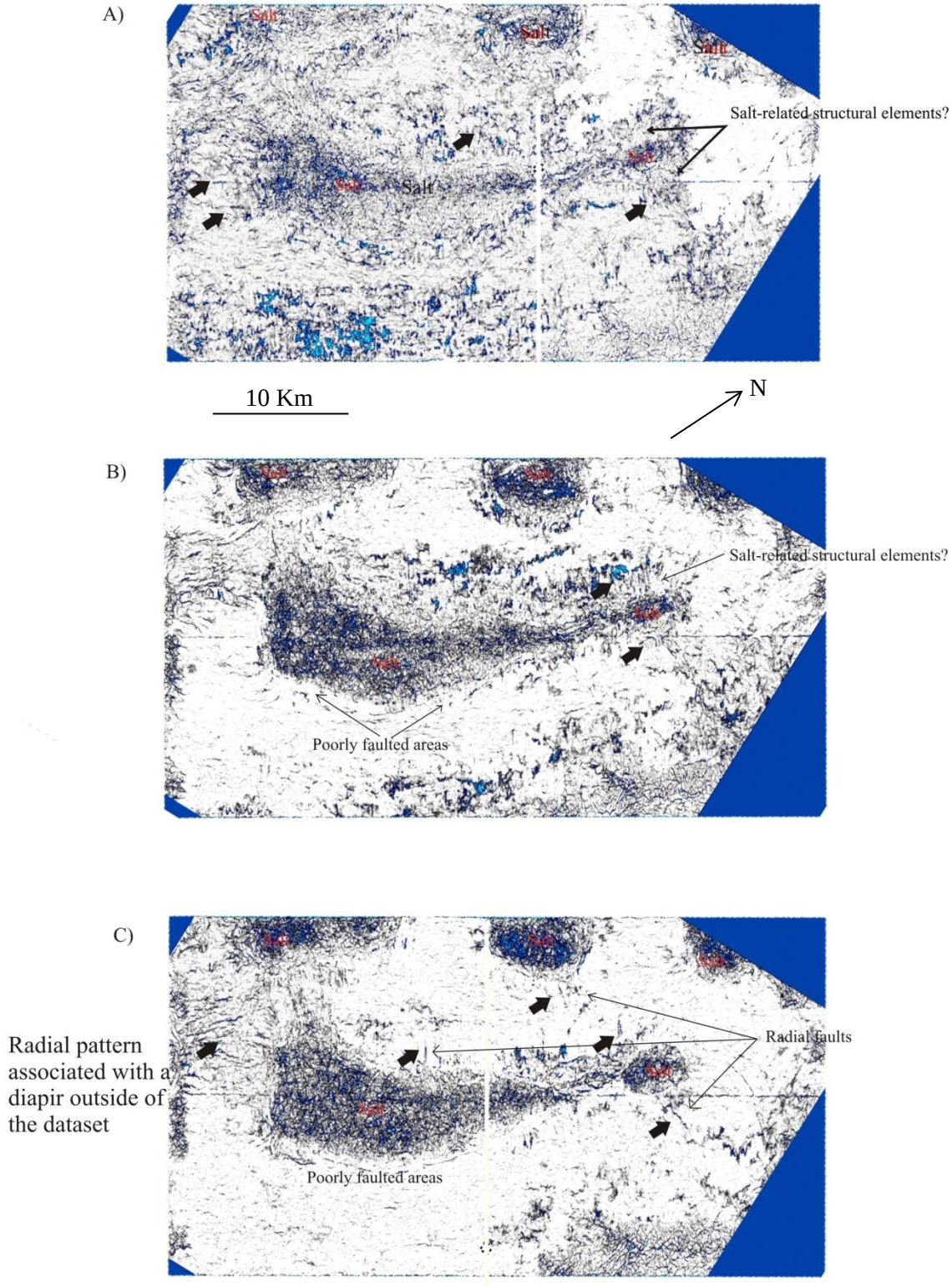

Figure 39. (A) Ant-track results of sequence 5 . (B) Ant- track results of sequence 6. (C) Ant-track results of sequence 7 displaying small evidences of radial faulting represented by black arrows.

Megasequence 4 (MS4) – Middle Jurassic - Cretaceous

General

Megasequence 4 (MS4) is encountered between the Middle Jurassic basal unconformity and the base Cenozoic unconformity. Contrary to the previous periods, this period does not show evidences of growth strata and is strongly truncated by the salt wall and salt stock (Fig. 30 and 32).

Seismic analysis

- Sequence 8 (S8) is bounded by very high amplitude events that correspond to the base Middle Jurassic unconformity at the bottom and the base Cretaceous unconformity at the top (Fig. 40). This period is characterized by very high amplitude, continuous, and parallel seismic events of Facies 6, defined as marine organic-rich shales. The Jurassic period does not show truncations beneath its top. However, due to diapirism, the Jurassic period is folded and truncated in areas adjacent to the salt wall and salt tock.
- Sequence 9 (S9) is bounded by two strong seismic events defined as unconformities. The basal unconformity represents the base Cretaceous and the top unconformity is represented by an erosional strong seismic event defined as the base of Cenozoic (Fig.40). This period is characterized by low-amplitude, semi-continuous, seismic events (Facies 1) interpreted as marine fine siliciclastics that change vertically to high-amplitude seismic events (Facies 4) defined as deltaic environments. No growth strata is observed in this period, however truncations are present beneath the base of Cenozoic towards the southwest.

Thickness analysis

The Middle Jurassic-Cretaceous megasequence exhibits generally slight thickness variations (Fig.41A) Maximum thickness is encountered in the northeastern areas, ranging between 1080 ms and 1140 ms. On the other hand, areas located towards the southeast are strongly truncated and display lower thickness, ranging from 660 to 750 ms.

Structural elements

Sequence 8 (S8) (Fig.42 A)**.** The Base Middle Jurassic has been flattened for this purpose. Generally, the Jurassic time interval is highly faulted, showing radial patterns embedded in high intensity faulted areas. As said before, radial patterns correspond to salt-induced stress fields. On the other hand, high faulted areas have been created by a different stress field.

Sequence 9 (S9) (Fig 42 B)**.** The Base Cretaceous has been flattened to obtain a time slice within this time interval. The time slice shows radial and circular fault pattern created by a salt-induced stress field. As in the previous time slice, the salt wall shows less abundance of radial features but still some are present. Other areas outside of the salt structures exhibit high distortions in the seismic events being caused by a different stress-regime.

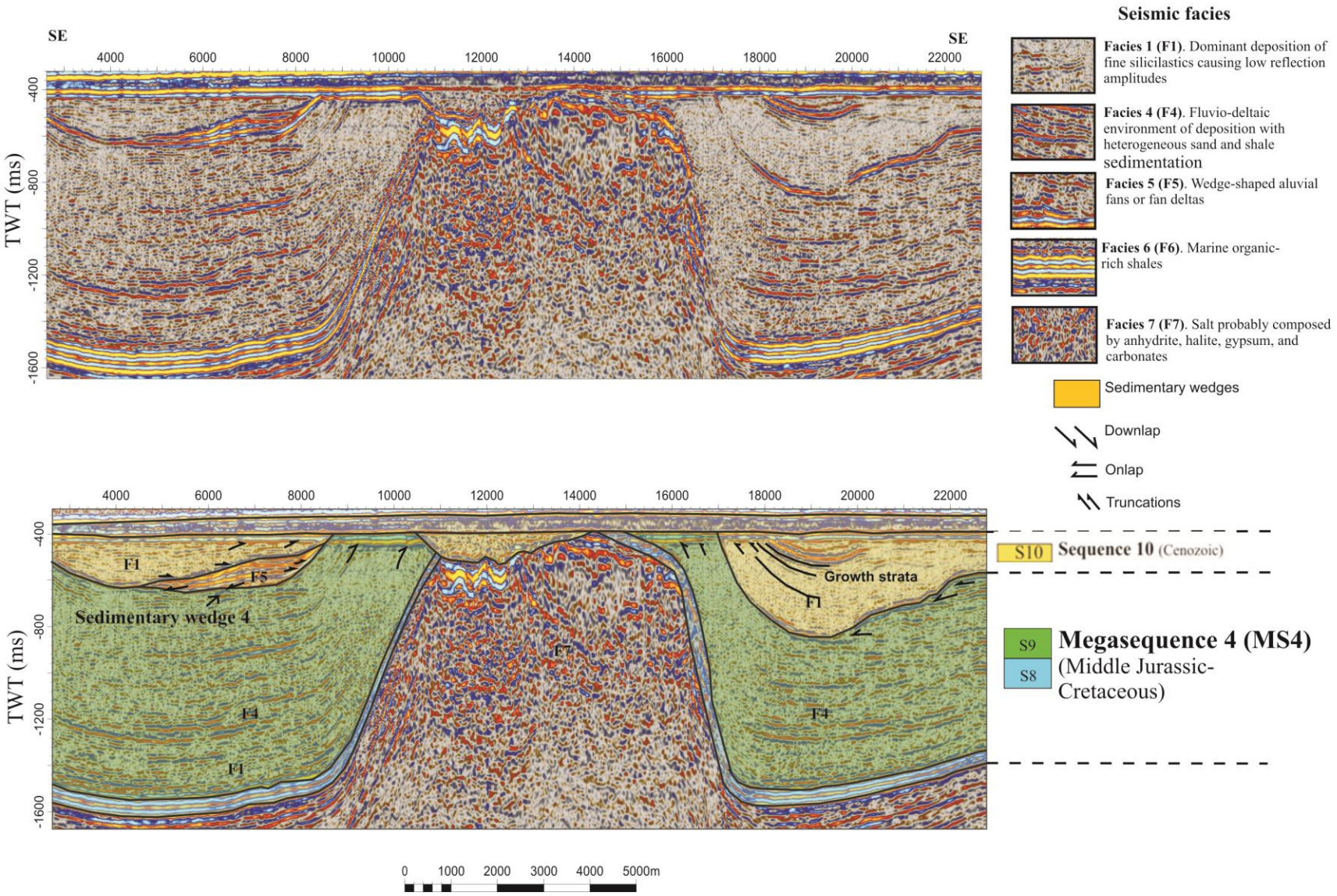

Figure 40. Seismic analysis of Megasequence 4 (MS4) (Middle Jurassic-Cretaceous) and Sequence 10 (Cenozoic)

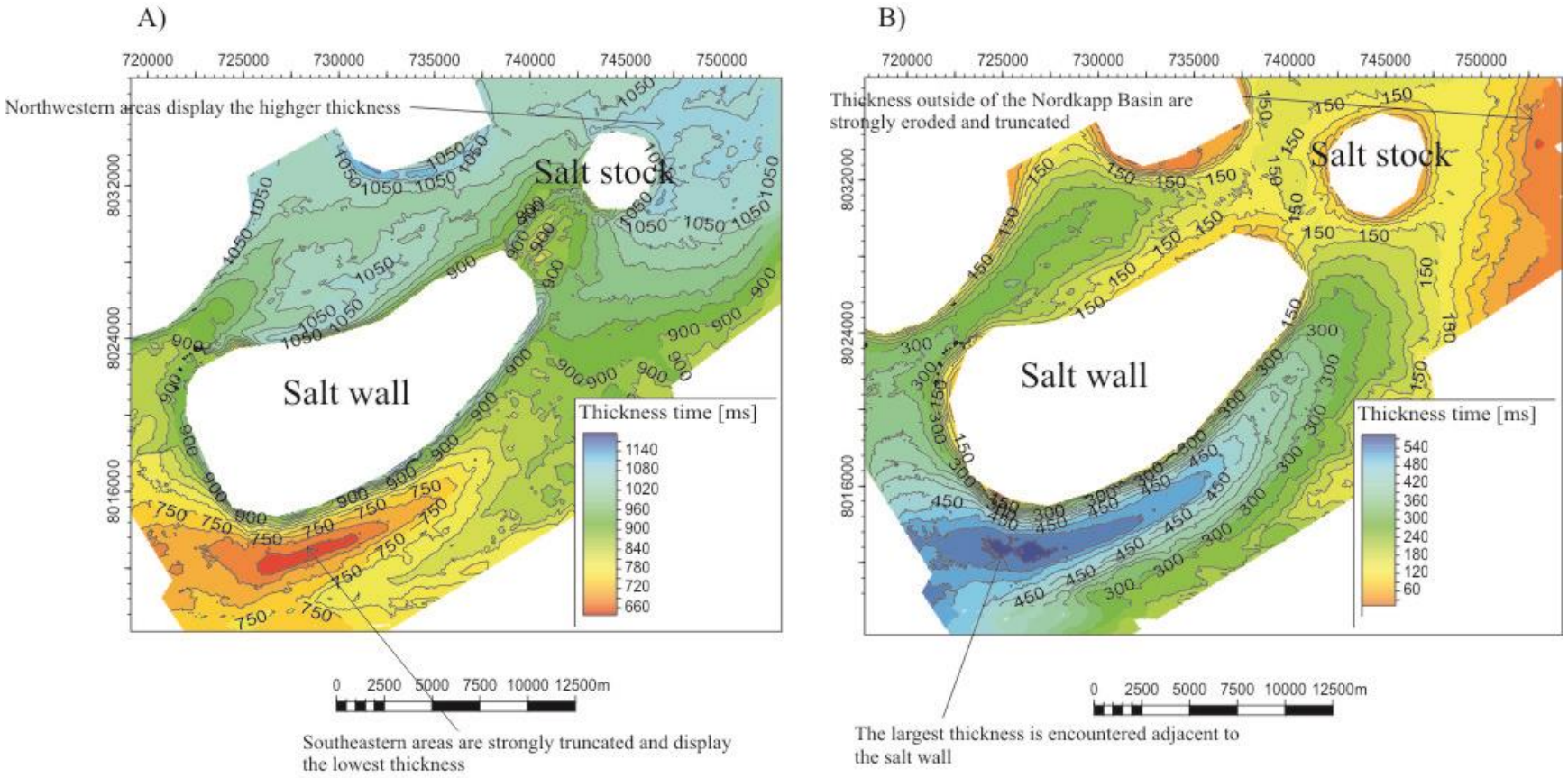

Figure 41. (A) Thickness map of Megasequence 4 (MS4)- (Middle Jurassic-Cretaceous) . (B) Thickness map of Sequence 10 (S10) – (Cenozoic).

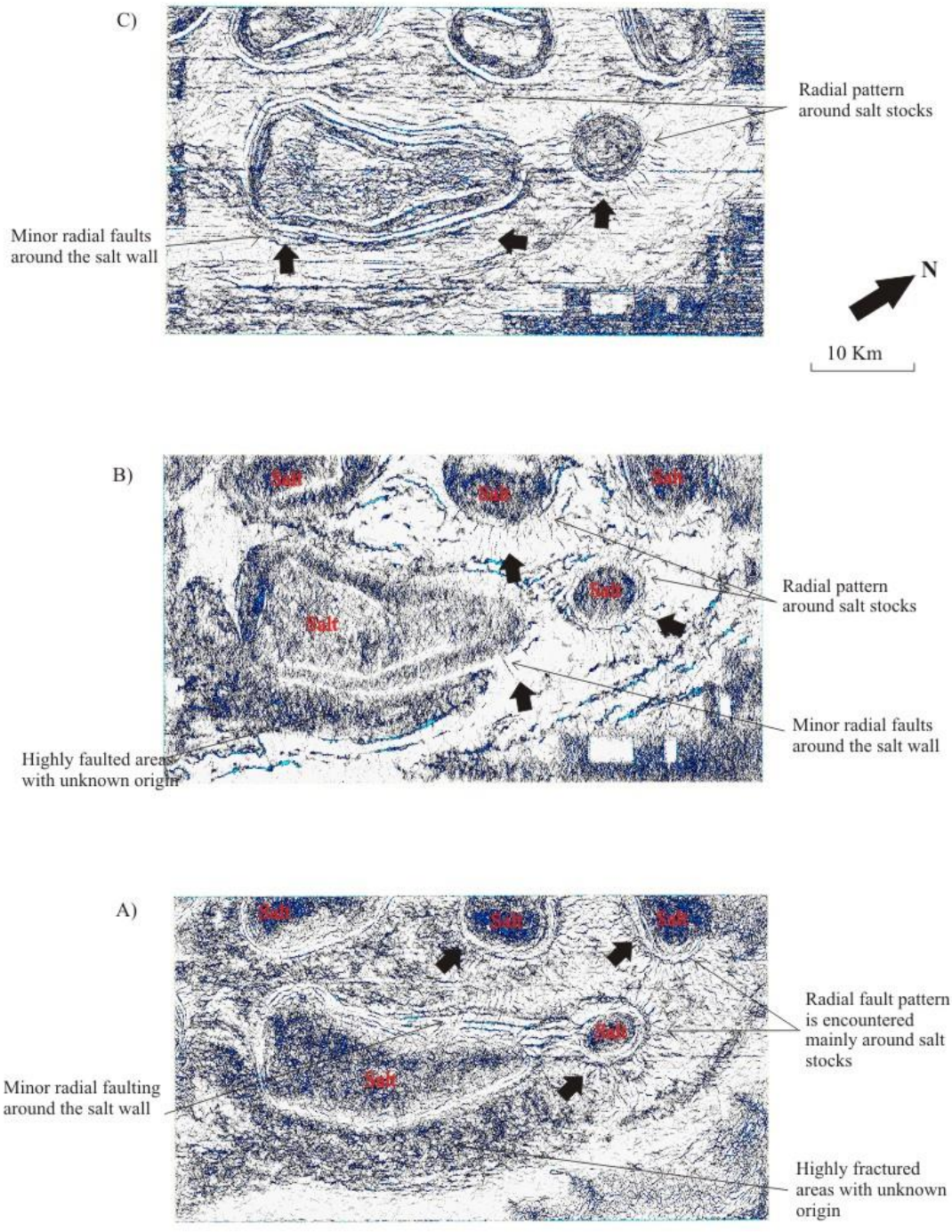

Figure 42. . (A) Ant-rack results for Sequence 8 (Jurassic). (B) Results for Sequence 9 (Cretaceous). (C) Results for Sequence 10 (Cenozoic). Salt-related structural elements are highlighted with black arrows.

Sequence 10 – Cenozoic

General

The Cenozoic period is bounded by the base Cenozoic unconformity and base Quaternary which disappears laterally, becoming the sea floor. This period is characterized by a markedly eroded growth strata, showing numerous truncations below the Quaternary sedimentary cover or directly beneath the sea floor (Fig.30, 31, and 32)

Seismic Analysis

The vertical variation of the seismic responses indicates a change in environment of deposition from very low semi-continuous amplitudes of Facies 1 defined as marine fine silicilastics , to medium-high amplitude continuous seismic events of Facies 4 interpreted as fluvial or fluvio-delataic (Fig.40). Facies 5 is also present adjacent to the salt wall, showing high continuous amplitude reflectors that develop downlaps at distal parts.

Thickness analysis

General

As an overview, the Cenozoic period exhibits large thickness variations. The largest thickness is encountered towards the southwest and in the vicinity of the salt wall, reaching a maximum of 540 ms and decreasing gradually towards the northeast where it is completely eroded (Fig.41B).

Wedge

Previous seismic analysis identified a wedge located in the northwestern flank of the salt wall (Fig.43). This wedge shows fan-shaped characteristics extending 10 km along the salt wall and 6 km in the perpendicular direction. The highest thickness ranges between 60 and 120 ms and is encountered adjacent to the salt wall. The thickness decreases gradually and radially towards outside areas from the salt wall.

Structural elements

Sequence 10 (S10) (Fig.42C)**.** For this time interval the Base Cenozoic has been flattened, showing excellent examples of radial faults around salt stocks. On the other hand, the salt wall exhibits less abundance of radial faults than the surrounding salt stocks .Areas further from the salt structures remains undisturbed, confirming that these faults have been induced by salt-induced stress.

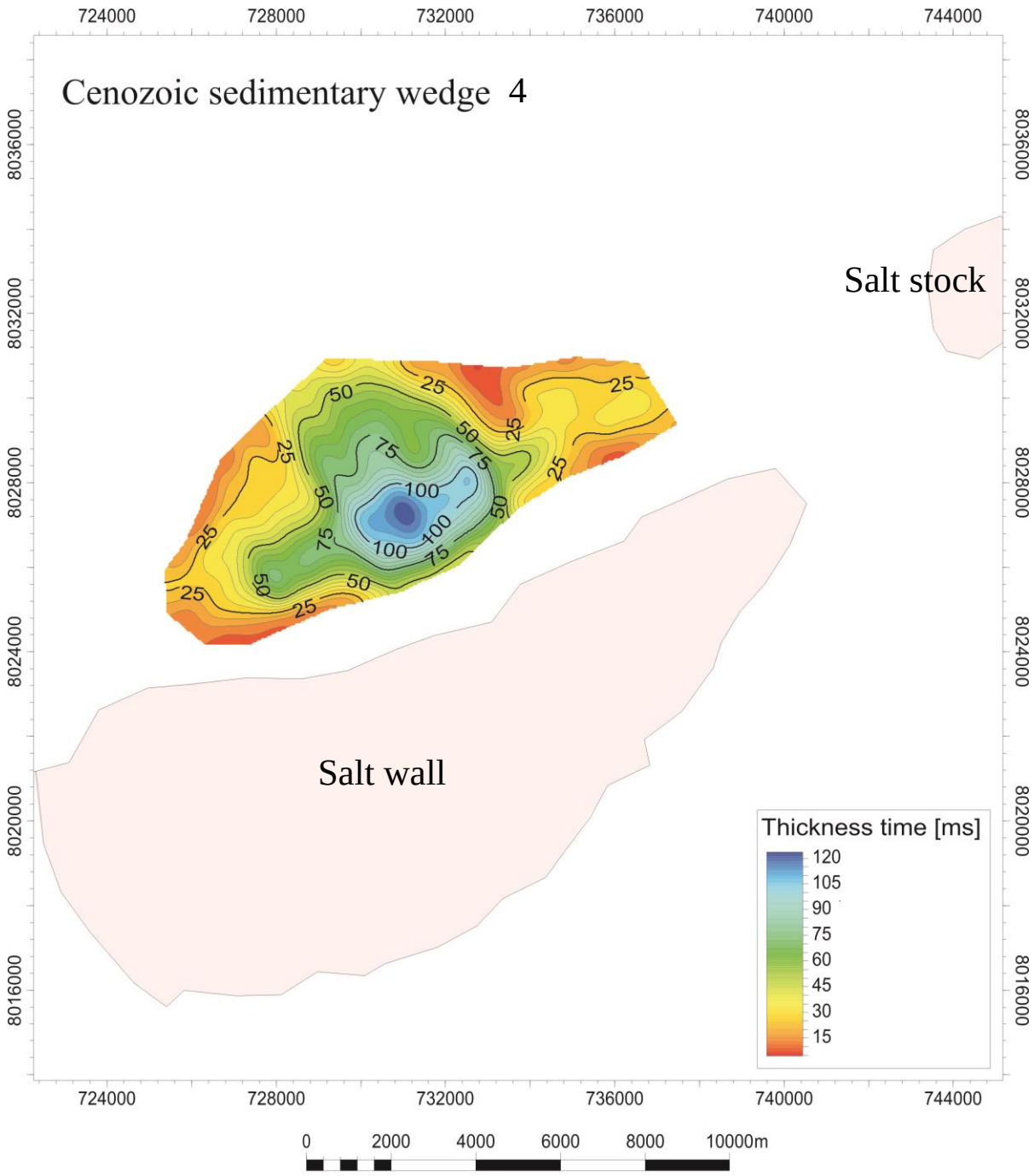

Figure 43. Thickness map of sedimentary wedge 4 (Cenozoic)

6. Salt modelling, depth conversion, and salt restoration

Observations in previous chapters were carried out using the 3D cube measured in two way travel time. However, there is still plenty of information unsolved such as sedimentation rates, salt movement through time etc… All of this new information can be extracted through the process of salt restoration. In order to restore a seismic profile, the seismic has to be converted to depth. However, to carry out depth conversion a 3D interval velocity model needs to be built that is based on structural interpretation (including salt modelling) and check shot data. Therefore, this chapter discusses the results of structural and velocity modelling followed by depth conversion and salt restoration, which will deliver additional information about halokinetic movements in the Nordkapp Basin.

6.1 Salt modelling

A very simple 3D model has been built for the present study area. The main modelling steps are cited as follows (Fig.44):

- **Structural modelling** (Fig.44A). The aim of this work is to create a structural 3D model including faults and salt structures described in previous chapters. The approximately shape of the salt structures has been modelled using curved faults. Each salt structure is composed by half-curved faults connected between each other. In total, 9 curved faults were necessary to model the different salt structures and related faults encountered in the dataset.
- **Pilar Gridding**. Pillar gridding offered by the modeling package used for this work (Petrel) is the process of building a skeleton grid that is guided by the modelled faults. Figure 44B displays the gridding results showing top, middle, and base skeleton.
- **Horizons and zones modelling** (Fig.44C). The purpose of this process is to generate horizons and zones in the skeleton grid which results in a 3D grid that can be used for modeling of the interval velocities. The input used in this study is the main surfaces interpreted within the 3D Cube.

-

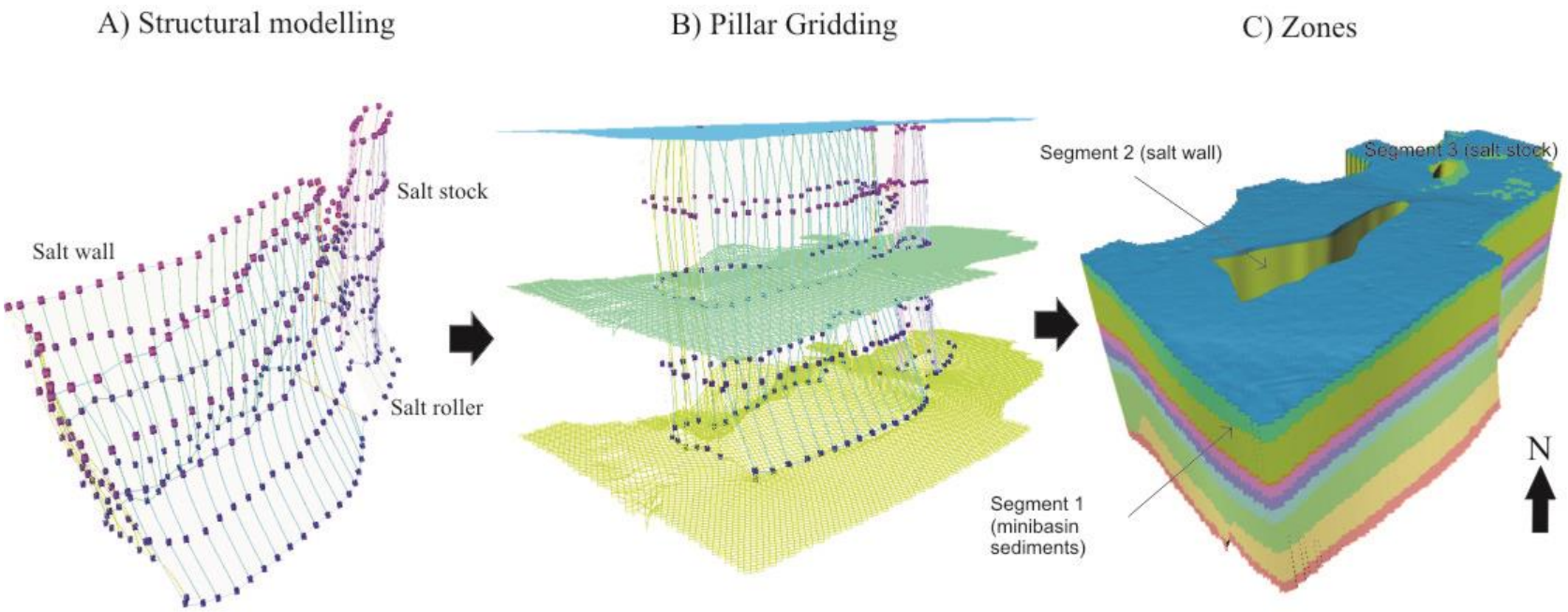

Figure 44. . (A) Structural modelling of the salt wall, roller, and stock using curved faults. (B) Pillar gridding process showing the creation of upper, middle, and lower skeleton. (C) Creation of 3 segments for future velocity model: segment 1 (minibasin sediments), segment 2 (salt wall) and segment 3 (salt stock).

6.2 Depth Conversion

In order to convert objects from two way travel time (TWT) into depth, it is essential to setup a velocity model. Velocity variations within the subsurface depend on many factors such as mineralogy, density, porosity and type of fluid within the pores. Generally, sediment compaction increases with depth, producing higher velocities towards deeper levels. However, with increasing complexity of the structure introduced for instance by faults, dipping layers, burial beneath hard rocks, and salt, the uncertainty of the depth conversion result increases (Lenkes, 2008). In this study, check-shot information from the only available well 7228/7-1A has been analyzed carefully to choose seismic velocities for this purpose. Figure 45 displays the check shot information as interval velocities versus depth. It is important to take into account that the maximum depth reached by this well is 2848 m and therefore does not provide velocity information for deeper levels, adding large depth uncertainty to the lower horizons. The depth conversion has been carried out through upscaling the check shot interval velocities into the 3D grid and interpolated the upscaled value. This operation resulted in a constant interval velocity for each model layer. The interval velocity of the lowest layer reached by the check shot survey was assigned to the remaining deep layers. As mentioned before, the salt structures have been modelled separately because they carry very high velocities. In this study, the well did not drill through salt and therefore an estimated salt velocity of 5000 m/s was assigned to the salt. The final interval velocity field was converted to average velocities that could be used by the depth conversion process of Petrel. It is important to note that the depth conversion uncertainty in this study is very large due to the lack of well data which results in simplistic velocity assumptions.

Figure 46 displays a depth converted seismic section that shows the salt roller. The section reaches a depth of 7 Km and shows the same characteristics as in the TWT section. Minor variations are mainly caused by velocity anomalies and corrected pull-up effect caused by salt pillows. For most of the layers the relative thickness in the time domain is comparable to the relative thickness in the depth domain. However, the Permian carbonates have a considerable smaller thickness in the depth domain compared to the time domain. This can be attributed to a relative low interval velocity assigned to this layer. This section shown in figure 46 has been chosen for the salt restoration for the following reasons:

- (1) There are not salt overhangs which might introduce artefacts in the depth conversion.
- (2) The complete stratigraphy of the Nordkapp Basin can be observed in this area. The areas located in the vicinity of the salt wall do not provide the complete stratigraphy because the seismic cube just covers a vertical TWT range of 4500 ms.
- (3) In this section, it is possible to estimate the position of the base salt which is observed in the southeastern flank and provides an idea about the depth of base salt for salt restoration.
- (4) The salt roller section is structurally not complex for salt restoration and it is possible to calculate sedimentation rates for each sequence.

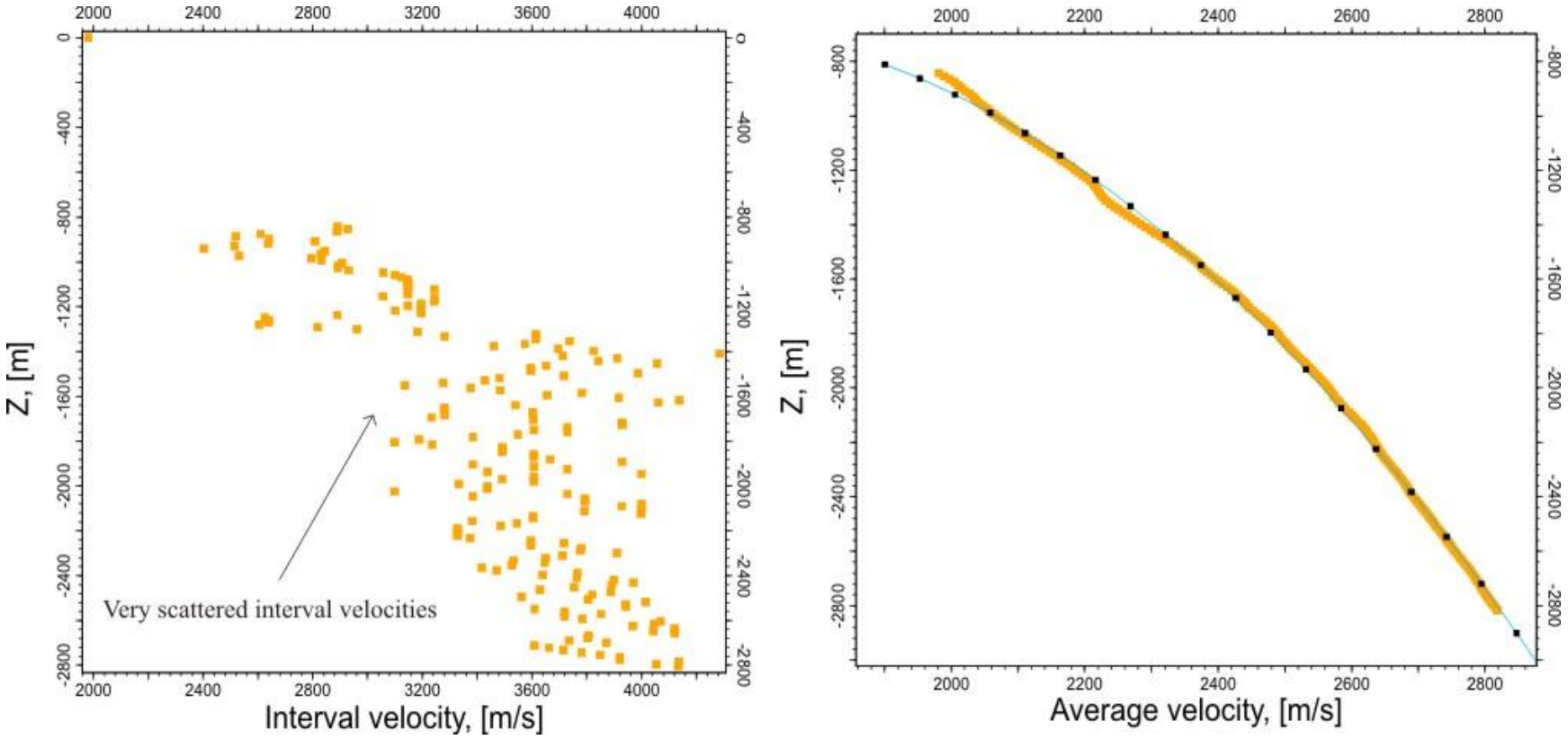

Figure 45. (Left) Interval velocities vs depth from the well 7228/7-1A. (Right) Average velocities vs depth from the well 7228/7-1A.

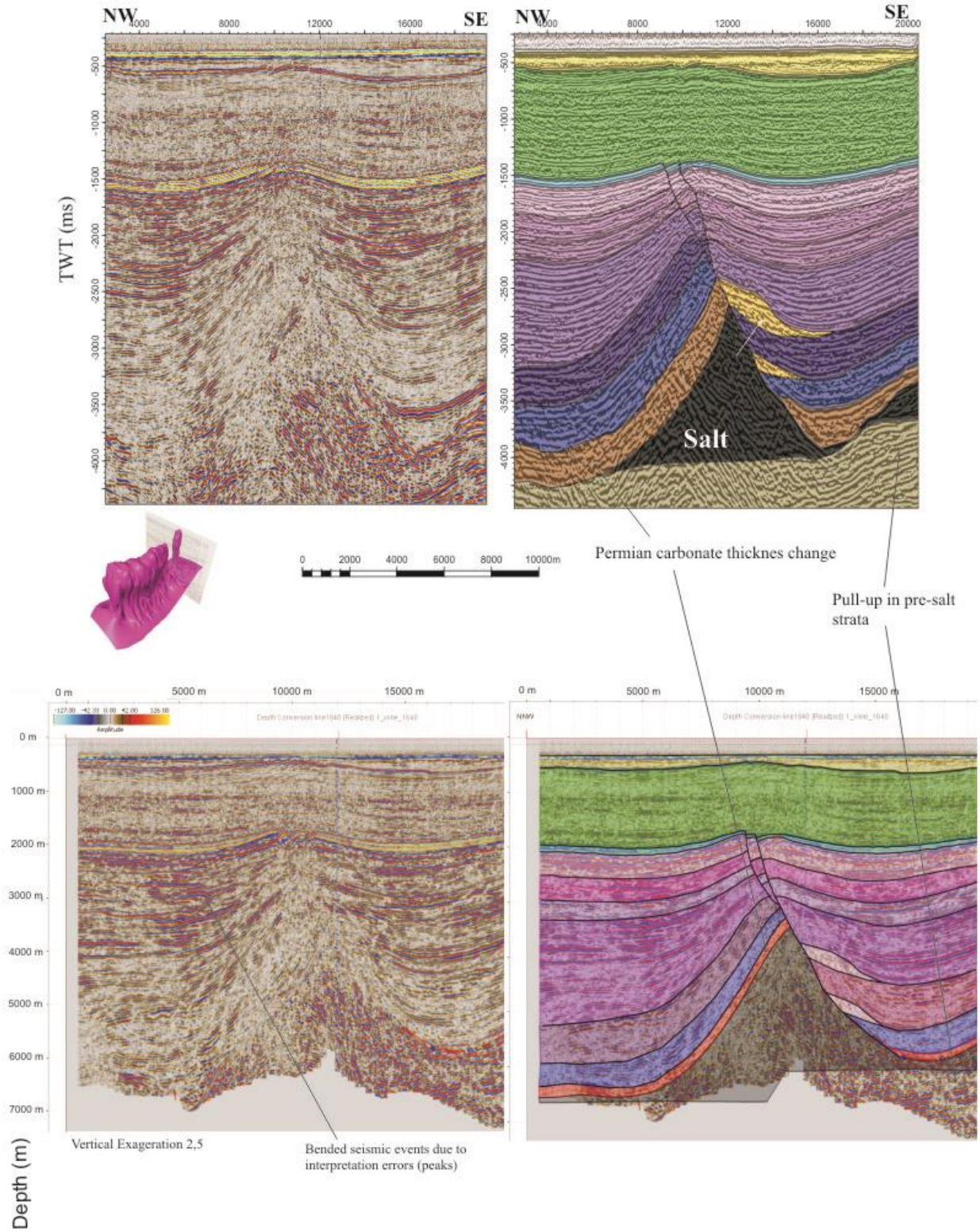

Figure 46. (Above) Salt roller interpretation in TWT (ms). (Below) Salt roller interpretation in depth (m)

6.3 Salt restoration

Restoration is the process in which the layers are transformed from deformed to depositional state using multiple increments, with the aim of showing the progressive evolution of the structures. Cross-section restoration normally assumes plain strain, meaning that there is no movement of material outwards or inwards from the section. Additionally, the area of each layer has to be conserved when the different restoration steps are applied (Rowan and Ratliff, 2012).

However, for salt restoration, these assumptions do not work. As previously mentioned salt behaves as a fluid and flows three-dimensionally inwards and outwards from the section (Rowan and Ratliff, 2012). In order to avoid these problems, the section as to be oriented in the direction of plane-strain deformation or salt flow, being in this study NW-SE approximately. Afterwards, the following structural geology techniques have been used to restore the profile:

- (1) Flexural slip used to unfold layers. The method preserves line length and bed thickness

- (2) Simple Shear has been used to remove the effect of faults. Beds are moved to the original position by selecting the same horizon in the hangingwall and footwall.

- (3) Block Restoration. Three different blocks bounded by faults have been identified in the cross-section. Each block is restored separately using flexural slip. Afterwards, all the blocks are joined together using simple shear.

- (4) Decompaction**.** Once the layers are restored by using the previous techniques, decompaction has been applied to remove the loss of porosity associated with increased burial depth, providing the original depositional thickness for sedimentation rate calculation. For this purpose, the Sclater and Christie equation has been used (Sclater and Christie, 1980)**.**

$$f = (f_o e^{-cy})$$

f is the present-day porosity at depth
fo is the porosity at the surface
c is the porosity-depth coefficient (Km^{-1})
y is depth (m)

Salt restoration results

Megasequence 4 (MS4) - Middle Jurassic–Cretaceous

- Sequence 9 (Base Early Cretaceous – Base Cenozoic) (Fig.47B). Generally, Cretaceous shows constant thicknesses and is folded and faulted by a later diapirism event. Salt source layer recovery has not been registered after removing Cenozoic strata. The estimated sedimentation rates for the Cretaceous are approximately 18,98 m/Ma.
- Sequence 8 (Base Middle Jurassic – Base Early Cretaceous) (Fig.47C). It is observed that salt source layers are slightly recovered after removing Cretaceous strata, indicating evidences of diapirism at the end of Cretaceous period. On the other hand, Jurassic strata display small thickness variations caused by normal faults. Estimated sedimentation rates for the Jurassic are approximately 6,78 m/Ma.

Megasequence 3 (MS3) – Middle-Late Triassic

- Sequence 7 (Top Norian – Base Middle Jurassic) (Fig.47D). Salt flow is still insignificant after removing Jurassic strata and salt source layers are not recovered. Sequence 7 displays thickness variations in the hangingwall caused by normal faults. Estimated sedimentation rates for Sequence 7 are approximately 19,43 m/Ma.
- Sequence 6 (Top Norian-IntraCarnian) (Fig. 48E). This period exhibits small thickness variations in the hangingwall caused by normal faults. Salt flow is still insignificant after removing Sequence 7 and salt recovery in salt source layers is not observed. Sedimentation rates are slightly higher than in the previous period, being approximately 30,60 m/Ma.
- Sequence 5 (Intra Carnian-Base Landinian) (Fig. 48F).Salt source layer recovery can be observed in both sides of the salt roller after Sequence 6 strata is removed. Additionally, thickness variations in the hangingwall start to become important respect to previous periods. Sedimentation rates are higher than previous periods, reaching 75 m/Ma.

Megasequence 2 (MS2) – Upper Early Triassic-Middle Triassic

- Sequence 4 (Base Ansian – Base Landinian) (Fig.48G). It is observed a significant salt recovery in the source layers after removing Sequence 5. According to salt restoration, salt was not exposed and the salt structure worked as salt roller with a faulted flank, causing a dramatic thinning of strata in the footwall, and thickening in the hanginwall. This sequence shows the highest sedimentary rates, being approximately 460m/Ma.
- Sequence 3 (Base Olenekian-Base Anisian) (Fig.48H). The main salt flow occurs when Sequence 4 is removed, showing a large recovery in salt source layers. The salt structure was not exposed during this period and worked as a salt roller, causing asymmetric infill. Estimated calculated rates are approximately 476m /Ma.

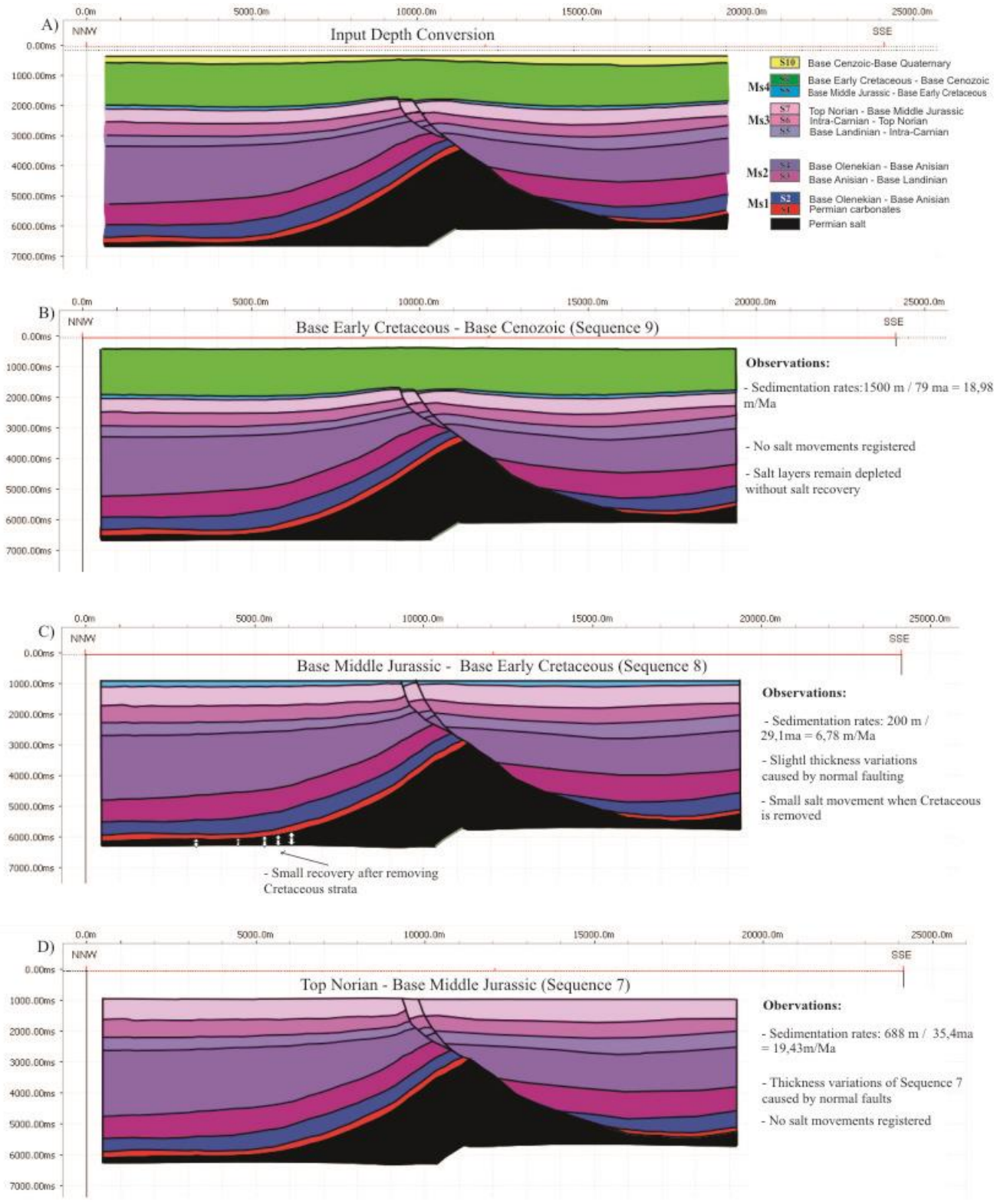

Figure 47. Retrodeformation of salt roller from Cenozoic to Base Middle Jurassic

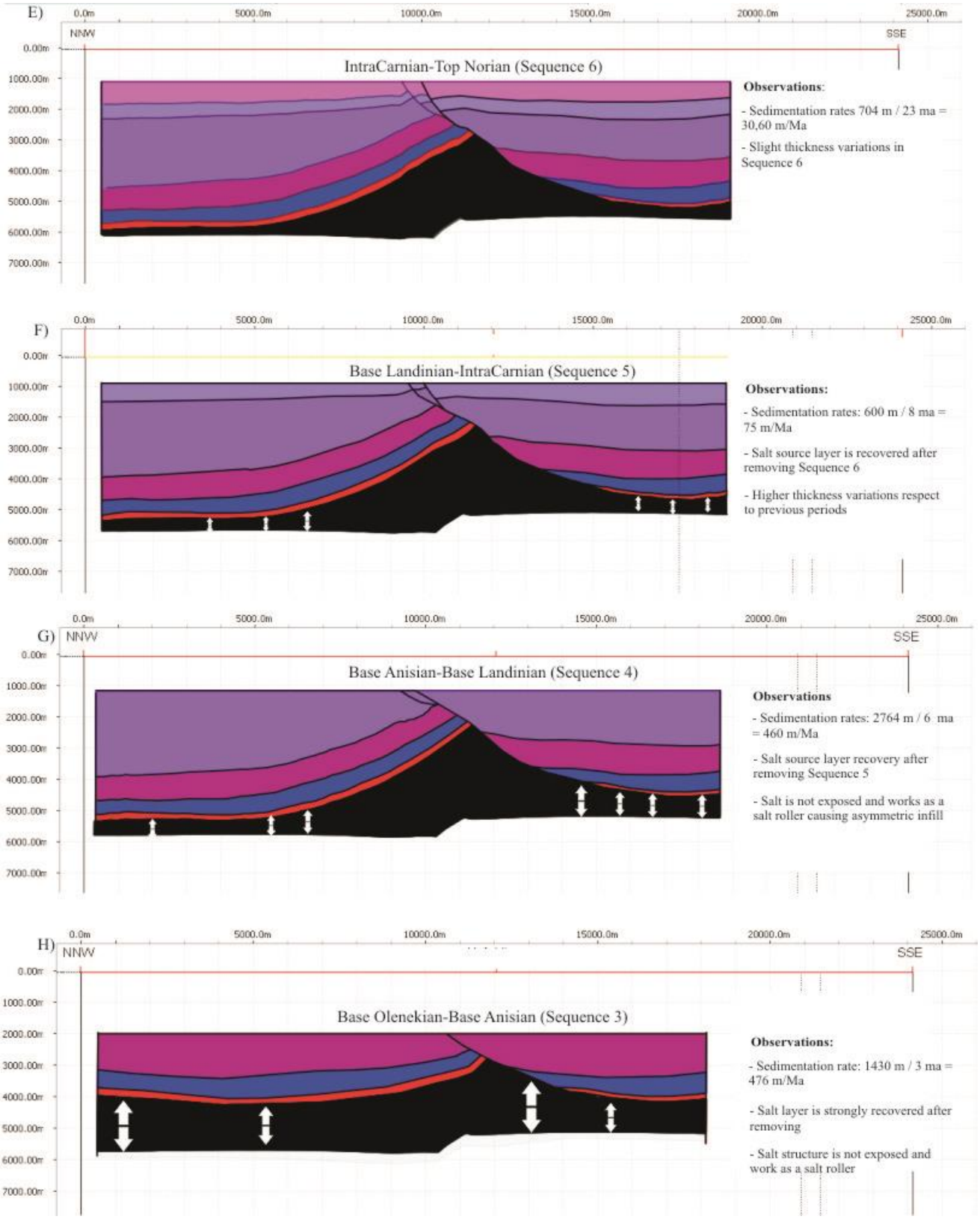

Figure 48. Retrodeformation of the salt roller from Base Middle Jurassic- Base Ansinian

Observations summary of the Nordkapp Basin

		Salt attribute workflow Dip-guided structural smoothing + Dip Ilumination + Variance	Minibasin stratigraphy attribute workflow Dip-guided structural smoothing + Frequency filters (40Hz, 50Hz, and 60 Hz) + Cosine of Phase			Salt-related structural elements attribute workflow Dip-guided structural smoothing + Chaos + Antrack	Salt restoration
PERIOD		**Salt Structures**	**Seismic Analysis**	**Thickness Analysis**	**Wedges**	**Structural analysis**	
Sequence 10 (Cenozoic)	S10	SALT WALL	- Fine marine siliclastics of Facies 1 grade vertically to fluvial or fluvio-deltaic Facies 4 - Presence of wedge-shaped aluvial fans or fan delta of Facies 5 located in the northwestern flank of the salt wall - Growth strata strongly truncated and coverd by Quaternary sediments	- Large thickness variations - The largest thickness is encountered towards the southeast and besides the salt wall	Yes	Radial faults mainly located around the salt stock and salt wall	- Small salt flow which creates folding and doming in underlying periods.
Ms4 (Base Middle Jurassic - Base Cenozoic)	S9	Widening	- Jurassic is characterized by the presence of organic-rich shales of Facies 6 - Cretaceous is represented by marine fine silicilastics (F1) chaging vertically to fluvio-deltaic environments (F4) - No growth strata - Truncations at the end of Cretaceous period	- Small thickness variations - Thickness decreases towards the southeast areas due to erosion	No	Radial faults mainly located around the salt stock and salt wall	- Cretaceous sedimentation rate: 18,98 m/Ma approx. - Jurassic sedimentation rate: 6,78 m/Ma approx. - Salt movement not registered
	S8				No		
Ms3 (Middle-Late Triassic)	S7		-Fluvio-deltaic environments characterized by Facies 3 - Facies 4 change gradually to Facies 1 towards outside areas from salt structures - Presence of facies 5 defined as wedge-shaped aluvial fans/fan deltas located close to salt structures - Growth strata is strongly folded within 800 m from the diapir, developing 90 degrees and overturned truncations	- Small thickness variations - Growth strata do not reduce its thickness drastically in the northwestern flank as in the previous period - Small depocenters - Depocenter migration towards the SE		Possible radial faults around salt stock at the end of S7	- Sedimentation rates decreases from 75 m/Ma in S7, to 19 m/Ma in S5 - Minor salt flow producing the total depletion of the source layer
	S6	SALT ROLLER			Yes		
	S5				Yes		
Ms2 (Lower Early Triassic- Middle Triassic)	S4		- Fine marine silicilastics during (Facies 1) grading vertically and towards the diapir to fluvio-deltaic environments (Facies 4) - Wedge-shaped deltaic wedges (Facies 3) adjacent to salt diapirs - Gradual drape folding of growth strata occur within 1,5 km	- Period of large thickness variations - Largest depocenters are encountered within this period - Growth strata thins considerably in the northwestern flank of salt structures	Yes	- Absence of salt-related structural elements.	- Salt structure was not exposed and worked as salt roller with a faulted flank - Approximately sedimentations rate: 460m /Ma - Main salt flow and source depletion occurs during this period - Large depocenters associated with source layer depletion
	S3		- Fine marine silicilastics during (F1) - Wedge-shaped marine gravity flows (Facies 2) - Gradual drape folding of growth strata occur within 1,5 km	- Main depocenters are encountered around the salt wall and salt stock - Vertical migration of depocenters towards the NW	Yes		
Ms1 (Permian-Lower Early) Triassic	S2	Triangular base	- Permian Carbonates (Facies 8) - Fine marine silicilastics during Lower Early Triassic (Facies 1) - Presence of truncations at the end of this period - Absence of growth strata	- Generally constant thicknesses - Small variations of thickness are encountered adjacent to salt diapirs mainly caused by erosion	No	- Absence of salt-related structural elements.	
	S1						

Figure 49. Observations summary of the Nordkapp Basin

7. Discussion

7.1 The role of seismic attributes in salt-related basins.

Previous observations indicated that the use of developed multi-trace seismic attributes workflows in salt-related basins improve the characterization of salt structures, salt-related structural elements, and halokinetic sequences. In terms of salt body characterization, the attribute workflow Dip-Structural Smoothing, Dip Illumination, and Variance has reduced the uncertainty in the interpretation from 2 km to approximately down to 200 m (Fig.21). This fact leads to a more accurate mapping of the edge of salt bodies at different depths and provide evidences of salt structure evolution during the basin infill of the basin. For example, the triangular basal shape of salt structures has been identified in all the salt structures and provides evidences of an early salt-roller stage as observed during the process of salt restoration (Fig.30, 31, 32 and 48G). It is of main importance to mention that the attributes used in this study provide an approximate location of the salt-sediment interface in a post-stack 3D Cube. Therefore the results highly depend on the quality of the processing close to salt structures and the amount of sub-vertical sedimentary layers dipping with the same angle as salt structures, which are not identified by dip-scans.

Salt-related structural elements identified by the attribute workflow Dip-Structural Smoothing, Chaos, and Ant-track provide information about diapir kinematics. Sequences with absence of structural elements indicate ductile deformation, especially produced during salt-controlled sedimentation periods along the Triassic characterized by the deposition of syn-kinematic halokinetic sequences around salt structures (Fig.39). On the other hand the presence of radial faults helps to identify sequences deposited under quiescence conditions identified mainly during Jurassic and Cretaceous periods. Such sequences acted as overburden that afterwards was faulted and folded by a late diapirism event, creating the characteristic radial fault pattern observed around salt structures (Fig.42).

In terms of minibasin characterization, the use of filters together with Cosine of Phase has been essential to improve the visualization of strata terminations and drape folding in uncertainty areas, being possible to identify the main types of composite halokinetic sequences and the presence of sedimentary wedges (Fig.50). Upper Early Triassic-Middle Triassic is characterized by the presence of Tapered composite halokinetic sequences, displaying drape folding of growth strata approximately within an area of 1-1,5 Km and developing truncations from 30 to almost 90 degrees in areas adjacent to salt structures. Due to the wide areas of drape folding, reservoirs might be more continuous without abrupt facies changes (Giles and Rowan, 2012). On the other hand, Middle-Late Triassic is characterized by the presence of tabular composite halokinetic sequences. Fast salt movement respect to low sedimentation rates, might have produce a strong drape folding of sequences 5,6 and 7, developing 90 degrees and overturned truncated growth strata in a very narrow area of 200 m. The presence of tabular composite halokinetic sequences plays an important role regarding reservoir development and trap geometry. The strong drape folding produce drastic facies changes in a very narrow area and might destroy the continuity of reservoirs adjacent to salt structures (Giles and Rowan, 2012).

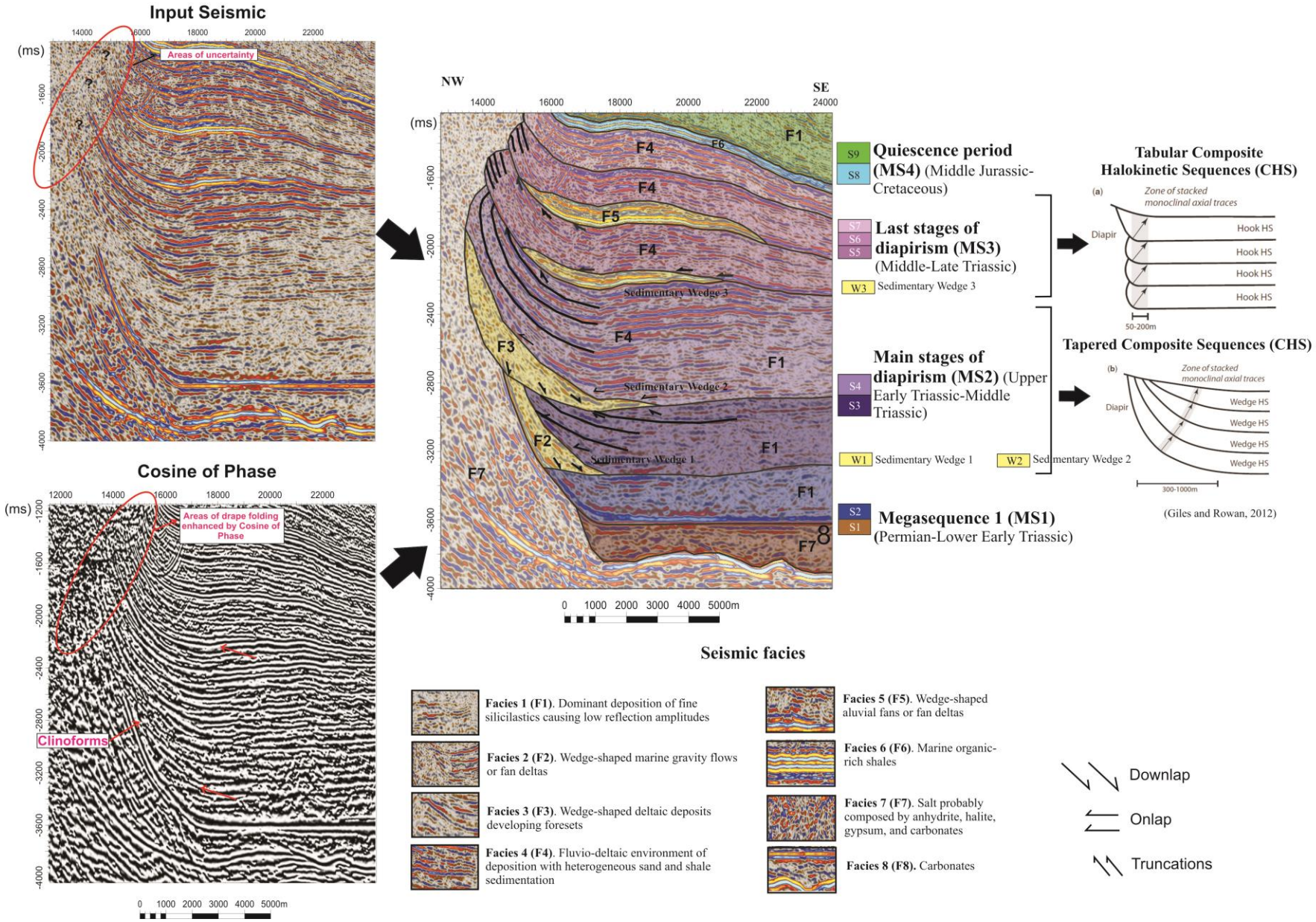

Figure 50. Characterization of halokinetic sequences based on input seismic and Cosine of Phase. Main stages of diapirism are characterized by the presence of Tapered composite halokinetic sequences. On the other hand , late stages of diapirism are characterized by Tabular composite halokinetic sequences.

7.2 Evolution

For the present discussion, previous halokinetic models together with previous publications, and observations provided by seismic attributes and salt restoration, have been revised to elaborate a conceptual model of the evolution of the study area (Fig.51).

Pre-kinematic Permian – Lower Early Triassic

Late Carboniferous-Early Permian salt was covered by late Permian carbonates (S1) with constant thickness unaffected by tectonic elements. No truncations were observed at the top of this succession, suggesting that the strong reflection coefficient is mainly caused by lithological differences between carbonates and Lower Early Triassic marine fine siliciclastics. Lower Early Triassic (S2) is characterized by constant thickness with small variations in areas adjacent to salt diapirs. The absence of growth strata and large thickness variations in these two periods support the pre-kinematic character described by previous studies (Jensen and Søresen, 1992; Koyi et al., 1995; Nilsen et al., 1995) (Fig.51A). Evidences of diapirism at the end of Lower Early Triassic are supported by the presence of truncations adjacent to salt structures. The triggering process of diapirism in the Nordkapp still remains unclear and, it has not been observed in the dataset. Previous hypothesis suggests that Permian-Lower Early Triassic overburden became strong enough to avoid halokinesis already driven by buoyancy inversion. However, the extensional event recorded in the Barents Sea during Early Triassic, might have faulted and thinned the overburden, producing extensional diapirism. (Gabrielsen et al., 1992; Jensen and Søresen, 1992; Koyi et al., 1995; Nilsen et al., 1995).

Main diapirism stage (Lower Early Triassic-Middle Triassic)

Salt Structures

During the Lower Early Triassic-Middle Triassic, salt tectonics is mainly driven by sedimentation due to high sedimentation rates reaching 480 m/Ma respect to salt supply. This salt-sediment relationship created salt structures with triangular shape such as pillows or rollers (McGuinness and Hossack, 1993)(Fig. 51B and C). Previous observation by Koyi et al. (1995) in the northeastern segment, suggested the existence of an early stage of diapirism dominated by asymmetric salt pillows or rollers generally obscured by salt overhangs. According to salt restoration in the southwestern segment, salt structures seemed to work as salt rollers with a faulted flank, causing asymmetric infill at both sides of salt structures (Fig.48G and H). Generally, in salt rollers, growth strata thin dramatically in the footwall and thicken against the salt structure in the hangingwall. Thus, the asymmetric infill together with the triangular basal shape observed in the salt wall, salt stock and salt roller (Fig. 30,31, and 32), support the hypothesis of salt roller-controlled sedimentation for this period.

Salt depletion

Lower Early Triassic-Middle Triassic was characterized by the largest salt mobilization that created peripheral sinks at both sides of salt rollers. This period started with the generation of primary rim-synclines allowing the deposition of Tapered CHS of Sequence 3 and depleting the source salt layer moderately (Fig.51B). The deposition of sequence 3 is followed by the deposition of Tapered CHS of

Sequence 4 in large secondary rim-synclines, producing the almost total depletion of the salt layer at the end of this period (Fig.51C).

Late Stages of Diapirism (Middle Triassic-Late Triassc)

Salt structures

Middle Triassic-Late Triassic is characterized by low sedimentation rates decreasing from 75 m/Ma in the S5 to 19,43 m/Ma in Halokinetic S7. As difference with the previous period, salt-supply rate was higher than sedimentation rate and salt structures developed from the salt roller stage to diapir stage, creating wider salt walls and stocks, and symmetric sedimentation at both sides of salt structures (Fig.51D, E, and F). Widening and exposure of salt diapirs is supported by the divergence vertical migration of depocenters observed in sequences S5, S6, and S7 (Fig.36), and by salt overhangs described in the northeastern segment of the Nordkapp Basin by Koyi et al. (1995); Nilsen et al. (1995).

Salt depletion

Previous studies suggested that the salt layer was totally depleted and passive diapirism was driven by basinwards-gravity gliding, which shortened salt structures and forced them to extrude and develop diapir overhangs (Nilsen et al., 1995). However, those processes have not been observed in the southwestern segment. According to the previous salt restoration, the source layer is not totally depleted during Middle-Late Triassic and there is still salt flow from the source layers to the salt roller (Fig.48F and G). However the thin remaining source layer, do not allow the further growing of the salt roller and just caused small doming, with the consequent thickness variations observed in this period. On the other hand, a thicker remaining source layer is predicted for the salt wall and salt stock, due to the further growth reaching the surface, and the development of third generation rim-synclines (Fig.51D, E, and F). The third generation of rim-synclines together with the low sedimentation rates allowed the symmetric deposition of Tabular CHS of S5, S6, and S7 at both sides of the structures.

Quiescence period (Middle Jurassic-Late Cretaceous)

The small thickness variations together with the no presence of growth strata indicate that Middle Jurassic – Late Cretaceous was a period of quiescence (Fig.51G). According to salt restoration, Middle Jurassic (S8) shows small variation of thicknesses caused by minor faults, which might be explained as salt-induced differential subsidence. However, salt restoration results do not show salt movement during this period and the source layer remained depleted, discarding the interpretation of salt-induced faults (Fig.47B). In another way, this study agrees with the hypothesis of Faleide et al. (1984); Jensen and Søresen (1992), proposing that these small thickness variations were formed by the Late Jurassic-Early Cretaceous extensional events in the Barents Sea. The deposition of Middle Jurassic is followed by approximately 1500 m of Cretaceous strata. According to salt restoration, no salt induced differential subsidence is registered during this period and minor subsidence is linked to the previously mentioned Late Jurassic-Early Cretaceous extensional event.

Reactivation (Cenozoic)

Cenozoic is a period mainly dominated by salt tectonics due to the presence of growth strata, large thickness variations. Evidences of salt diapirism during the late Cretaceous-Early Cenozoic described by Jensen and Søresen (1992); Koyi et al. (1995); Nilsen et al. (1995), is proved in the study area by truncations and larger Late Cretaceous erosional thickness variations adjacent to the main salt structures (Fig.40 and 41). The triggers of Late Cretaceous-Cenozoic diapir reactivation are still poorly understood. Jensen and Søresen (1992) proposed a combination of gravitational instability caused by post-Landinian sediments, together with a regional compressive episode during the Early Cenozoic. On the other hand, Nilsen et al. (1995) suggested that Late Cretaceous extensional event was caused basinwards-gravity glidding. This event caused reactivation of salt diapirs which faulted the Jurassic and Cretaceous thick cover. The present study agrees with the hypothesis of basinwards gravity glidding reactivation. The major salt-related structural elements are normal faults and no evidences of regional compression with linked folding and reverse faulting have been observed. It is interpreted that salt structures in the data set were squeezed in their upper parts by gravitational glidding (Fig.51H). According to results in salt roller restoration, lower parts do not seem to be squeezed and conserved the original triangular shape (Fig.47A and B).

A difference with previous salt-related sedimentation periods, Ant-track results shows that Cenozoic strata unexpectedly exhibit salt-related structural elements (Fig.42C). Generally during salt-controlled sedimentation, the deformation is ductil, forming drape folding of growth strata around diapir rims. Therefore, the presence of salt-related structural elements in Early Cenozoic indicates that halokinesis was not active along the whole period, providing evidences of quiescence period in between. Previous studies identified a new regional compressional event that forced the last diapirism event during Eocene-Oligocene (Nilsen et al., 1995). This last event of diapirism might have fractured the Cenozoic strata deposited under quiescence conditions, explaining the presence of structural elements in the Cenozoic period.

Finally, Late Cenozoic uplift episode eroded salt structures together with Cenozoic, Cretaceous and Jurassic strata, causing strong truncations covered by a thin succession of glacial Quaternary strata (Fig.51I).

UPLIFT AND EROSION (Cenozoic)

- Cenozoic, Cretaceous, and Jurassic strata strongly truncated
- Salt structures are covered by glacial Quaternary sediments

REACTIVATION (Cenozoic)

- Reactivation caused by regional contraction (Nilsen et al., 1995)
- Syn-kinematic deposition of S10
- Marine fine grain silicilastics to fluvial environments of deposition
- Presence of salt-sedimentary wedges
- S8 and S9 are affected by salt-related radial faults

QUIESCENCE (Middle Jurassic - Late Cretaceous)

- Deposition of S8 and S9
- Organic-rich shales to fine grain silicilastics

LATE STAGES OF DIAPIRISM (Middle Triassic - Late Triassic)

- Low sedimentation rates vs salt supply
- Exposure of salt structures
- Salt widening and divergent migration of depocenters
- Deposition of Tabular Composite Halokinetic Sequences (S5, S6, and S7)
- Third generation of rim-synclines
- Total depletion of salt source layer at the end of this period
- Fluvial environments of deposition

MAIN STAGE OF DIAPIRISM (Upper Early Triassic - Middle Triassic)

- High sedimentation rates vs salt supply
- Salt structures working as salt rollers
- Deposition of Tapered Composite Halokinetic Sequences (S3 and S4)
- Generation of primary and secondary rim synclines
- Major salt source layer depletion
- Inner shelf to fluvio-deltaic environments of deposition

PRE-KINEMATIC (Late Permian - Lower Early Triassic)

Deposition of Pre-kinematic strata:

- Late Permian (S1) and Lower Early Triassic (S2)

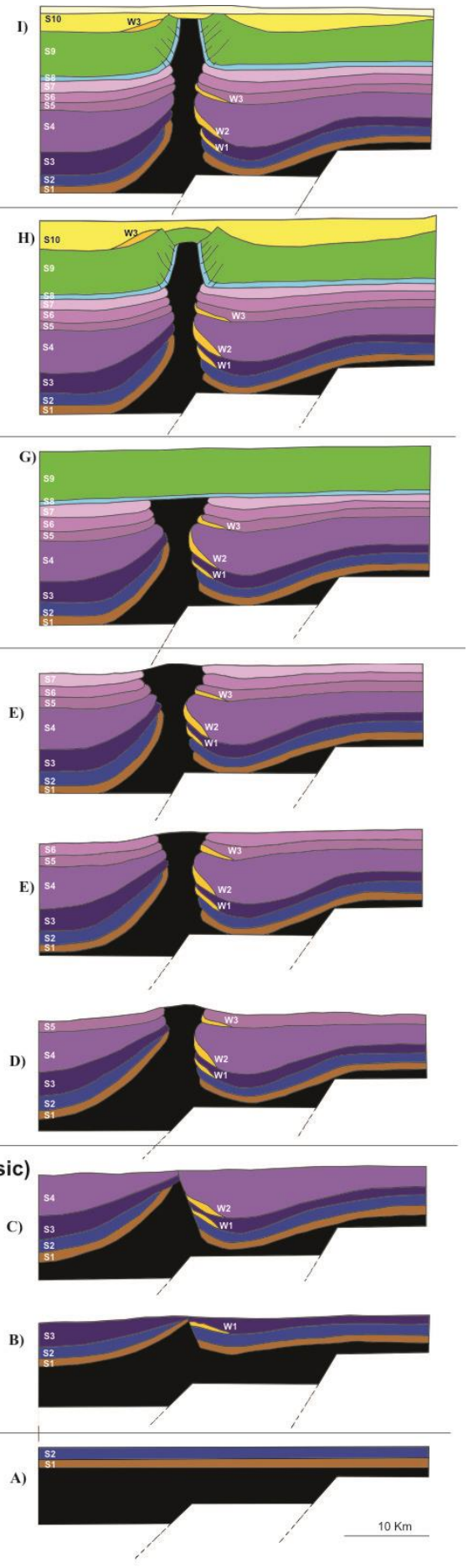

Figure 51. Halokinetic conceptual model for the study area in the Nordkapp basin

7.3 Implications of diapirism in the Triassic paleogeography

The Triassic paleogeography of the Nordkapp Basin is still poorly understood and continues to be debated. According to previous studies by Glørstad-Clark et al. (2010), the Early Triassic clinoforms prograde towards the west and northwest through the Nordkapp Basin, showing continental environments of deposition unaffected by salt tectonics. On the other hand, studies base on shallow stratigraphic drilling, suggested environment of depositions ranging from inner shelf to coastal plain environment. Therefore, uplifted areas formed by diapirism, might have acted as local sediment sources. On the contrary, depletion of salt might have caused restricted sub-basins, being favorable for organic-rich deposition (Bugge et al., 2002).

Main stages of diapirism

Base on seismic facies studies, the present study suggests a gradual change from inner shelf environments to fluvio-deltaic environments of deposition during this period. The generation of primary rim-synclines created restricted sub-basins, allowing the deposition of fine siliciclastics (Facies 1) of S3 (Fig.52). Areas close to salt rollers showed a more heterogeneous sedimentation characterized by the presence of sedimentary wedges (Facies 2) and small occurrences of high-amplitude seismic events. Most likely, footwall instabilities induced by large episodes of salt movements, might have created marine gravity flows at the beginning of this Tapered CHS, explaining the chaotic seismic response of sedimentary wedge 1 and its location just in the hangingwall. The presence of slumps induced by halokinesis is a common feature observed in deep waters of the Gulf of Mexico and provides an analog supporting the presence of these wedges in the Nordkapp Basin (Fig.52).

The deposition of S4 started with large diapirism event, causing the deposition of sedimentary wedge 2 (Facies 3). The origin of this wedge is controversial. Generally, it shows a chaotic seismic response and might be interpreted as marine gravity flows (Facies 2) as observed in Sequence 3. However, Cosine of Phase results display an internal organization composed by topsets, high angle foresets, and bottomsets (Fig.53).Additionally, sedimentary wedge 2 displays large dimensions being approximately 300 – 400 m thick and 3 km wide. These features provide evidences of deposition of Gilbert deltas developed in the hangingwall of the normal faults, as observed in several Gilbert delta analogs located in the Gulf of Corinth (Greece)(Gobo, 2014). The Evrostini Gilbert delta provides an analog for sedimentary wedge 2, displaying approximately the same dimensions and same internal architecture. It is believed that these salt-induced Gilbert deltas in the Nordkapp, may have been sourced from uplifted footwalls during salt roller diapirism. On the other hand, areas located further from the salt roller, displayed a homogeneous sedimentation characterized by fine grain silicilcastic (Facies 1) probably deposited in secondary rim-synclines.

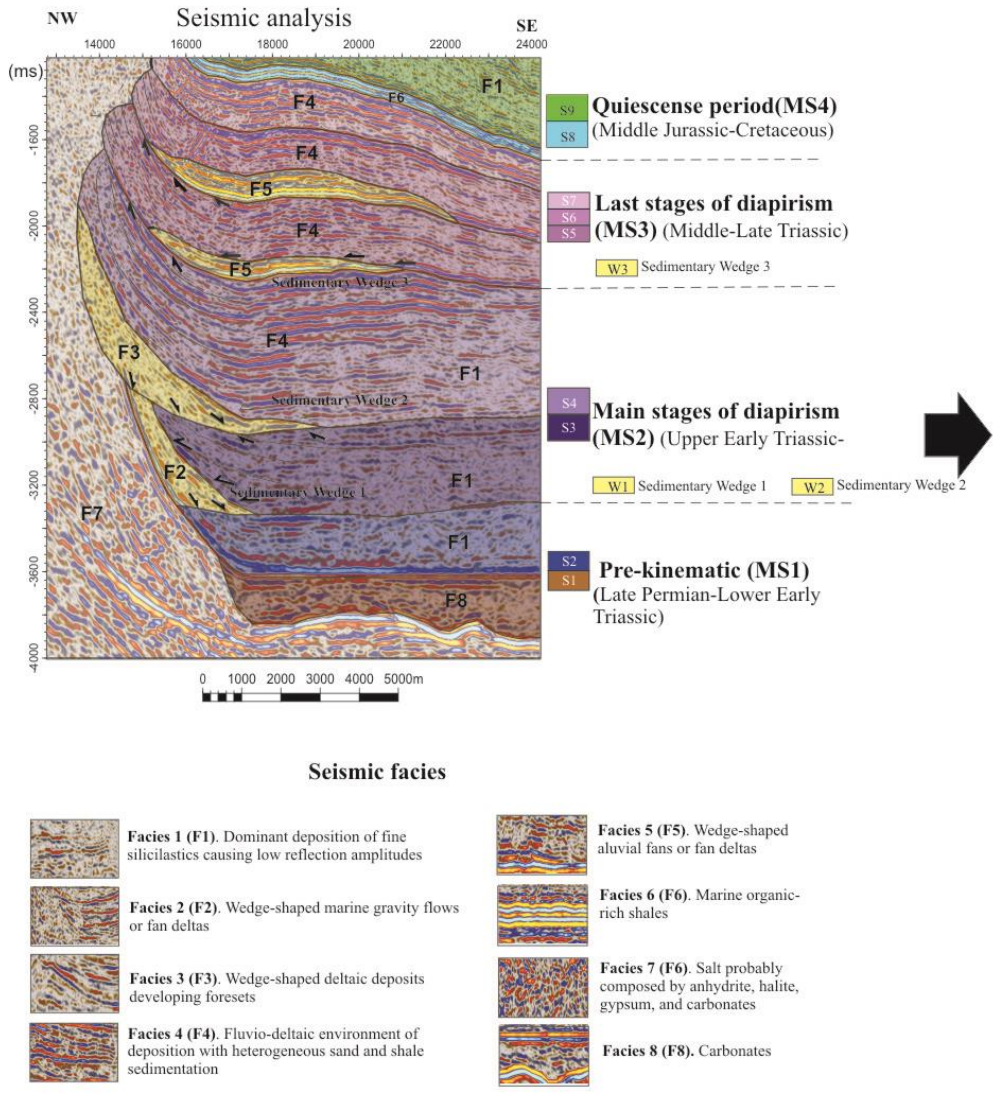

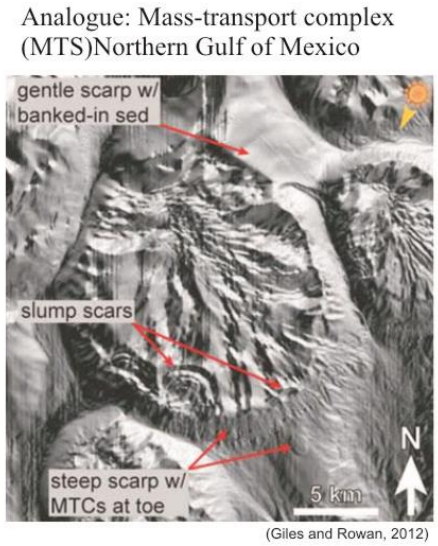

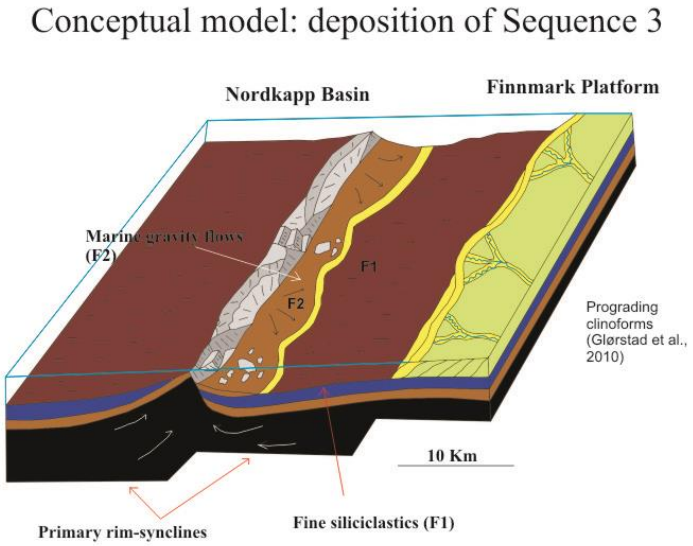

Figure 52.Conceptual model of depositional environments of sequence 3 (S3).

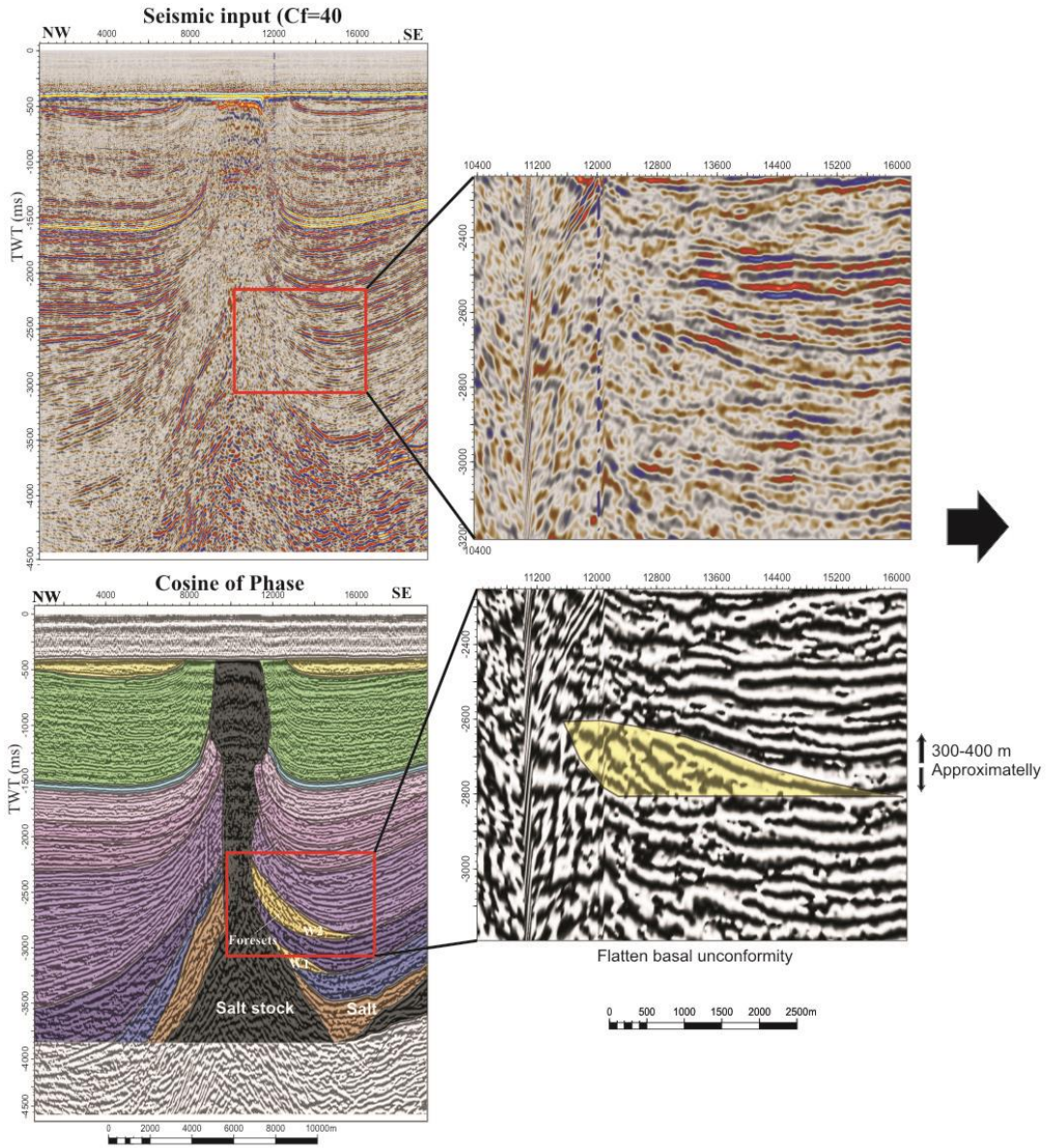

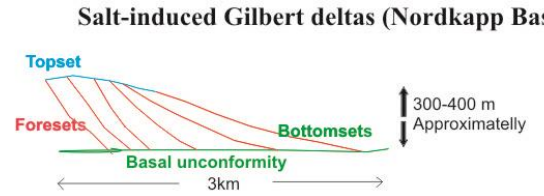

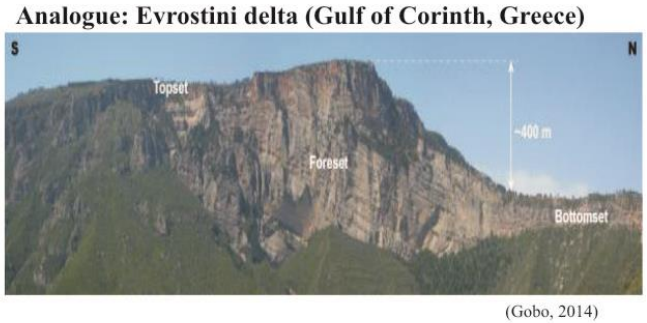

(Gobo, 2014)

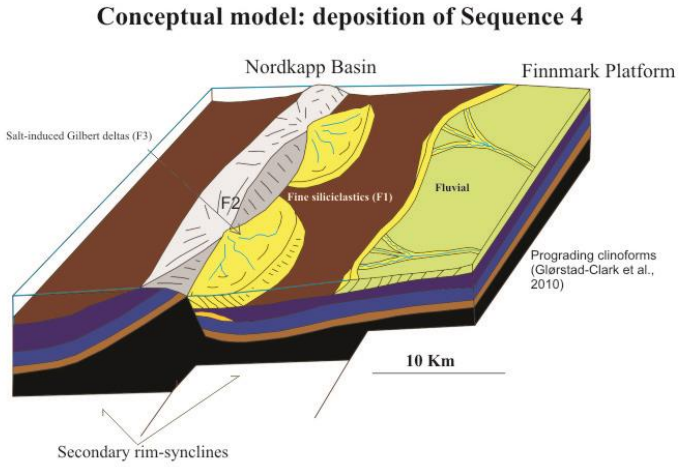

Figure 53. Conceptual model of depositional environments of sequence (S4).

Late stages of diapirism

The Paleogeography in the Nordkapp basin during this period is mainly dominated by fluvial environments of deposition (Glørstad-Clark et al., 2010). This fact is supported in this study by the presence of high-amplitude seismic events (Facies 4) defined as fluvial-fluviodeltaic sediments. However the distribution of fluvial environments of deposition around salt structures is still poorly understood. In addition, the presence of sedimentary wedges (Facies 5) indicates a complex fluvial paleogeography controlled by the late episodes of diapirism.

Wedges encountered in S5, and S6 have different characteristics and origin than previously discussed wedges. Continuous, parallel, high amplitude seismic events suggest a more stratiphied deposits interpreted as alluvial fans/fan deltas. These wedges are just encountered in the proximity of the salt wall, supporting evidences of exposure and erosion of this structure during Middle Triassic – Late Triassic (Fig.54).

The presence of diapir-related alluvial fans is currently observed in the Great Kavir diapirs located in Central Iran. Figure 54 displays Landsat 8 satellite images highlighting diapir-related alluvial fans locally sourced from uplifted diapirs (USGS, 2015). It is important to notice that diapir-induced alluvial fans are encountered just in one flank and probably this fact might indicate higher topography gradient in those areas. On the other hand, opposite flanks of salt diapirs show areas of embayment with clay deposition and evaporates that might be associated with salt depletion areas. This analog provides an example of complex fluvial arid environments of deposition controlled by exposed salt diapirs that support the presence of diapir related wedges encountered in the dataset. However, it is important to take into account that the arid climate conditions of Central Iran might not represent the climate conditions during Middle-Late Triassic in the Nordkapp basin.

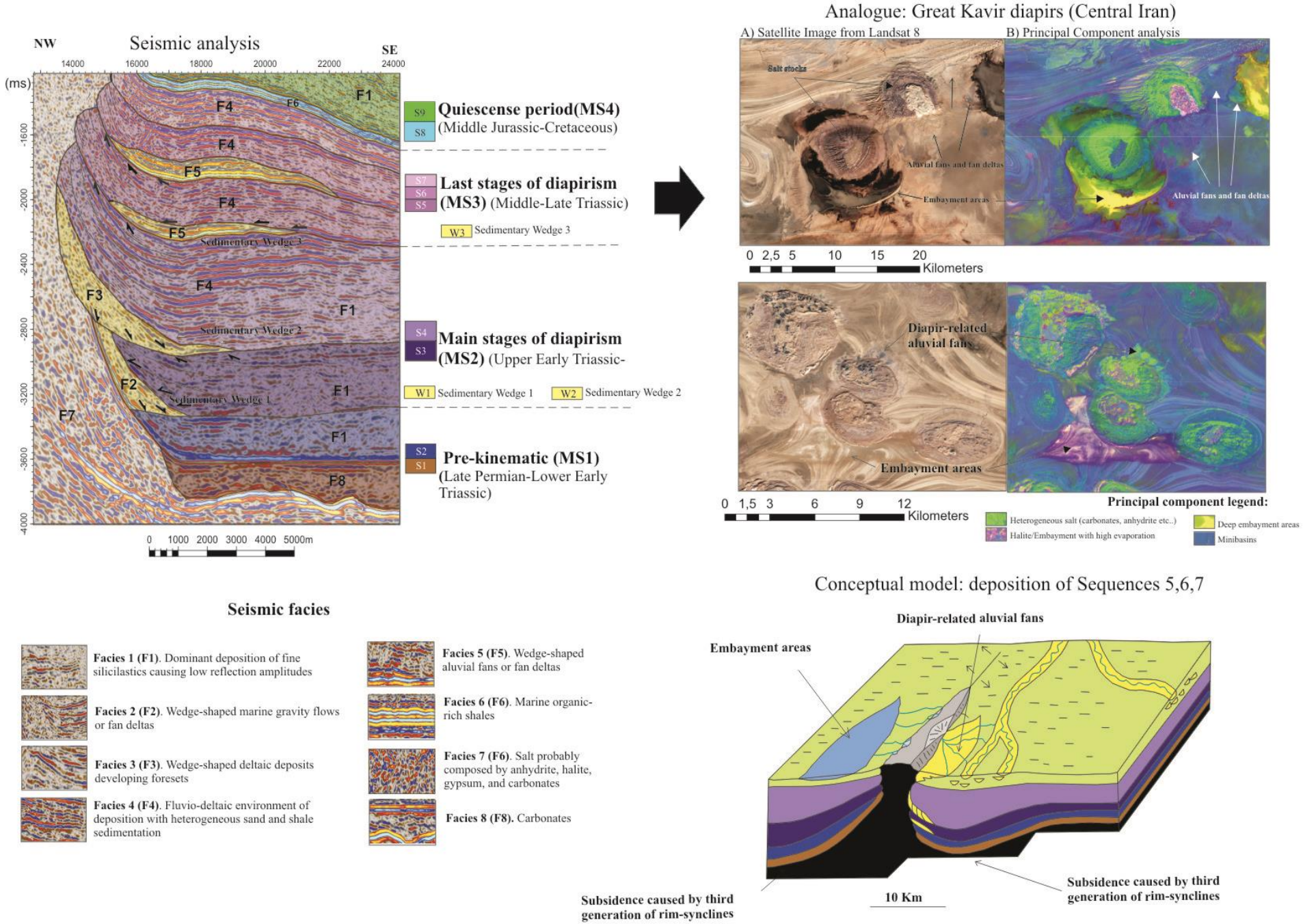

Figure 54. Conceptual model of depositional environments of sequences 5, 6, and 7.

8. Conclusions

The multi-trace seismic attribute workflows developed in this study are essential tools to improve the characterization and understanding of the Nordkapp Basin (southwestern Barents Sea). Salt characterization has been carried out using the workflow Dip Structural Smoothing, Dip Illumination, and Variance, which improves the salt body characterization at different depths and provides a more accurate mapping of diapir rims. The characterization of salt-related structural elements has been described by the attribute workflow Dip-Guided Structural Smoothing, Chaos, and Ant-track, and provides valuable information about diapir kinematics. Sequences with absence of structural elements are associated with periods of salt-controlled sedimentation around salt structures. On the other hand sequences with presence of salt-related structural elements indicate quiescence periods with not influence of salt tectonics that afterwards, were domed and faulted by a later diapirism event. Minibasin characterization has been carried out by the use of frequency filters and the attribute Cosine of Phase. The use of these attributes has improved the visualization of strata terminations and enhances the interpretation in areas of uncertainty adjacent to diapir rims, allowing identification of Tapered composite halokinetic sequences and Tabular composite halokinetic sequences.

Based on information obtained from the developed seismic attribute workflows and salt restoration results, the halokinetic evolution of the study area has been divided into 6 phases:

- (1) Pre-kinematic phase (Permian – Lower Early Triassic) defined as a period not influenced by salt tectonics.
- (2) Main stage of diapirism (Upper Early Triassic – Middle Triassic). This period is characterized by large halokinetic movements creating primary and secondary rim-synclines, which are filled by Tapered composite halokinetic sequences. Due to the high sedimentation rates, salt structures were not exposed and work as salt rollers, which controlled the distribution of environments of deposition in the Nordkapp Basin. Two sedimentary wedges have been encountered in the southeastern flank of salt structures. Sedimentary wedge 1 is interpreted as marine gravity flows formed by footwall instabilities in the salt roller. On the other hand, sedimentary wedge 2 is interpreted as Gilbert deltas sourced from salt roller footwalls.
- (3) Late stages of diapirism (Middle Triassic – Late Triassic). The total source layer depletion occurs during this period, creating the third generation of rim-synclines filled by Tabular composite halokinetic sequences. Due to the low sedimentation rates, salt structures were exposed during this period and influenced the paleodrainage of fluvial systems in the Nordkapp Basin. Sedimentary wedges encountered in this period are defined as alluvial fans sourced from exposed salt structures.
- (4) Quiescence period (Middle Jurassic – Late Cretaceous). Salt tectonics was not active during this period due to the total salt depletion of the previous period. Therefore, salt structures are covered by Jurassic and Cretaceous strata. The presence of radial faults affecting Jurassic and Cretaceous strata indicates a salt-reactivation at the end of this period.
- (5) Reactivation (Cenozoic). During this period salt structures were squeezed and reactivated, causing the deposition of growth strata around salt structures. Quiescence periods within the Cenozoic have been identified as well due to the presence of salt-related structural elements.

- (6) Uplift and erosion (Late Cenozoic). Late Cenozoic uplift eroded salt structures together with Cenozoic, Jurassic, and Cretaceous strata.

9. References

Aqrawi, A. A., T. H. Boe, and S. Barros, 2011, Detecting Salt Domes Using a Dip Guided 3D Sobel Seismic Attribute, SEG San Antonio Annual Meeting, Society of Exploration Geophysicists.

Aqrawi, A. A., W. Weinzierl, R. Daber, and T. H. Boe, 2012, Directional Guided Seismic Attributes and Their Use in Assisting Structural, Stratigraphic and Lithological Interpretation, SEG Las Vegas 2012 Annual Meeting, Society of Exploration Geophysicists.

Archer, S. G., G. I. Alsop, A. J. Hartley, N. T. Grant, and R. Hodgkinson, 2012, Salt tectonics, sediments and prospectivity: An introduction: Geological Society Special Publication, v. 363, p. 1-6.

Bergendhal, E., 1989, Halokinetisk utvikling av Nordkapp-bassengets sørvestre segment: Master's thesis, University of Oslo, Norway, 120 p.

Berthelot, A., A. H. S. Solberg, and L. J. Gelius, 2013, Texture attributes for detection of salt: J. Appl. Geophys., v. 88, p. 52-69.

Bornhauser, M., 1969, Geology of Day dome (Madison county, Texas); a study of salt emplacement: AAPG Bulletin, v. 53, p. 1411-1420.

Bugge, T., G. Elvebakk, S. Fanavoll, G. Mangerud, M. Smelror, H. M. Weiss, J. Gjelberg, S. E. Kristensen, and K. Nilsen, 2002, Shallow stratigraphic drilling applied in hydrocarbon exploration of the Nordkapp Basin, Barents Sea: Mar. Pet. Geol., v. 19, p. 13-37.

Davison, I., G. I. Alsop, N. G. Evans, and M. Safaricz, 2000a, Overburden deformation patterns and mechanisms of salt diapir penetration in the Central Graben, North Sea: Mar. Pet. Geol., v. 17, p. 601-618.

Davison, I., I. Alsop, P. Birch, C. Elders, N. Evans, H. Nicholson, P. Rorison, D. Wade, J. Woodward, and M. Young, 2000b, Geometry and late-stage structural evolution of Central Graben salt diapirs, North Sea: Mar. Pet. Geol., v. 17, p. 499-522.

Dengo, C. A., and K. G. Røssland, 1992, Extensional tectonic history of the western Barents Sea: in r.M. Larsen et al., eds., Structural and tectonic modelling and its application to petrolem geology: Norwegian Petroleum Society Special Publication, p. 91-107.

Escalona, A., and P. Mann, 2006, Sequence-stratigraphic analysis of Eocene clastic foreland basin deposits in central Lake Maracaibo using high-resolution well correlation and 3-D seismic data: AAPG Bulletin, v. 90, p. 581-623.

Faleide, J. I., S. T. Gudlaugsson, and G. Jacquart, 1984, Evolution of the western Barents Sea: Marine and Petroleum Geology, v. 1, p. 123-150.

Ferguson, C. J., A. Avu, N. Schofield, and G. S. Paton, 2010, Seismic analysis workflow for reservoir characterization in the vicinity of salt: First Break.

Fossen, H., 2010, Structural Geology: Published in the United States of America, Cambridge University Press, New York.

Gabrielsen, R. H., R. R. Faerseth, L. N. Jensen, J. E. Kalheim, and F. Riis, 1990, Structural elements of the Norwegian continental shelf, part I, the Barents Sea region: Norwegian Petroleum Directorate Bulletin No. 6, p. 33 p.

Gabrielsen, R. H., O. S. Kløvjan, and T. Stølan, 1992, Interaction between halokinesis and faulting: structuring of the margins of the Nordkapp Basin, Barents Sea region: in R.M. Larsen et al., eds., Structural and tectonic modelling and its application to petrolem geology: Norwegian Petroleum Society Special Publication, p. 121-131.

Giles, K. A., and T. F. Lawton, 2002, Halokinetic sequence stratigraphy adjacent to the El Papalote Diapir, northeastern Mexico: AAPG Bulletin, v. 86, p. 823-840.

Giles, K. A., and M. G. Rowan, 2012, Concepts in halokinetic-sequence deformation and stratigraphy: Geological Society Special Publication, v. 363, p. 7-31.

Glørstad-Clark, E., J. I. Faleide, J. P. Nystuen, and B. A. Lundschien, 2010, Triassic seismic sequence stratigraphy and paleogeography of the western Barents Sea area: Marine and Petroleum Geology, v. 27, p. 1448-1475.

Gobo, K., 2014, Development of Gilbert-type deltas:sedimentological case studies from the Plio-Pleistocene of Corinth Rift, Greece, University of Bergen (Norway).

Haugen, J. A., J. Mispel, and B. Arntsen, 2009, Seismic Imaging Below "Dirty" Salt: 71st Conference & Exhibition, EAGE, Expanded Abstract.

Henriksen, E., A. E. Ryseth, G. B. Larssen, T. Heide, K. Rønning, K. Sollid, and A. V. Stoupakova, 2011, Chapter 10 Tectonostratigraphy of the greater Barents Sea: implications for petroleum systems: Geological Society, London, Memoirs, v. 35, p. 163-195.

Hokstad, K., B. Fotland, G. Mackenzie, V. Antonsdottir, S.-K. Foss, C. Stadtler, C. Fichler, M. Haverl, M. Traub Waagan, E. A. Myrlund, L. Masnaghetti, F. Ceci, and P.-Y. Raya, 2011, Joint imaging of gephysical data: Case history from the Nordkapp Basin, Barents Sea: SEG San Antonio 2011 Annual Meeting, p. 1098-1101.

Hudec, M. R., and M. P. A. Jackson, 2007, Terra infirma: Understanding salt tectonics: Earth Science Reviews, v. 82, p. 1-28.

Jensen, L. N., and K. Søresen, 1992, Tectonic framework and halokinesis of the Nordkapp Basin, Barents Sea: Norwegian Petroleum Society (NPF) Special Publication 1, pp. 109-120. .

Jhonson, H. A., and D. H. Bredeson, 1971, Structural Development of Some Shallow Salt Domes in Louisiana Miocene Productive Belt: AAPG Bulletin, v. 55, p. 204 226.

Koyi, H., C. J. Talbot, and B. O. Tørudbakken, 1995, Salt tectonics in the northeastern Nordkapp Basin, southwestern Barents Sea: in M.P.A. Jackson, D.G. Roberts, and S.Snelson, eds., Salt tectonics: a global perspective: AAPG Memoir 65, p. 437-447.

Lemon, N. M., 1985, Physical Modeling of Sedimentation Adjacent to Diapirs and Comparison with the Late Precambrian Oratunga Breccia Body in Central Flinders Ranges, South Australia: aAPG Bulletin, p. 1327-1338.

Lenkes, L., 2008, 2D Modelling of the Cenozoic evolution in the southwestern Barents Sea with focus on the Pliocene and the Pleistocene glacial erosion: Master thesis, University of Stavanger (Norway).

Marin, D., A. Escalona, H. Nøhr-Hansen, K. Śliwińska Kasia, and A. Kayukova, 2015, Characterization of Lower Cretaceous seismic clinoforms in the SW Barents Sea: Implication for sand-prone bodies prediction: Deparment of Petroleum Engineering, University of Stavanger.

McGuinness, D., and J. Hossack, 1993, The development of allochthonous salt sheets as controlled by the rates of extension, sedimentation, and salt supply: Rates of geological processes: Gulf Coast Section SEPM 14th Annual Research Conference, p. 127-139.

Nilsen, K. T., C. Vendeville, and J.-T. Johansen, 1995, Influence of Regional Tectonics on Halokinesis in the Nordkapp Basin, Barents Sea: in M.P.A. Jackson, D.G. Roberts, and S.Snelson, eds., Salt tectonics: a global perspective: AAPG Memoir, v. 65, p. 413-436.

NPD, 2003, Factpages, exploration wellbore 7228/7-1A, http://factpages.npd.no/factpages/default.aspx?culture=en&nav1=wellbore (accesed January 28, 2015), Norwegian Petroleum Directorate.

Quintà, A., S. Tavani, and E. Roca, 2012, Fracture pattern analysis as a tool for constraining the interaction between regional and diapir-related stress fields: Poza de la Sal Diapir (Basque Pyrenees, Spain): Geological Society Special Publication, v. 363, p. 521-532.

Rowan, M. G., and R. A. Ratliff, 2012, Cross-section restoration of salt-related deformation: Best practices and potential pitfalls, p. 24-37.

Rønnevik, H. C., 1982, Structural and stratigraphic evolution of the Barents Sea: Norwegian Petroleum Directorate: Norwegian Petroleum Directorate Bulletin No. 1, p. 77.

Sclater, J. G., and P. A. F. Christie, 1980, Continental stretching: An explanation of the Post-Mid-Cretaceous subsidence of the central North Sea Basin: Journal of Geophysical Research: Solid Earth, v. 85, p. 3711-3739.

Stadtler, C., C. Fichler, K. Hokstad, E. A. Myrlund, S. Wienecke, and B. Fotland, 2014, Improved salt imaging in a basin context by high resolution potential field data: Nordkapp Basin, Barents Sea: Geophysical Prospecting, v. 62, p. 615-630.

Swanston, A. M., M. D. Mathias, and C. A. Barker, 2011, Wide-azimuth TTI imaging at Tahiti: Reducing structural uncertainty of a major deepwater subsalt field: Geophysics, v. 76, p. WB67-WB78.

Trusheim, F., 1960, Mechanism of salt migration in northern Germany: AAPG Bulletin, v. 44, p. 1519-1540.

USGS, 2015, Landsat 8 data Access, http://earthexplorer.usgs.gov (accesed March 2015), U.S. Department of the Interior and U.S. Geological Survey.

Van Bemmel, P. P., and R. E. F. Pepper, 2000, Seismic signal processing method and apparatus for generating a cube of variance values, Google Patents.

Worsley, D., 2008, The post-Caledonian development of Svalbard and the western Barents Sea: 2008, v. 27, p. 20.